AN IMPROVED NUMERICAL MODEL FOR FLOW COMPUTATIONS OF ELECTROTHERMAL ARCJET THRUSTERS

by

Guy B. Benson

B.S. Department of Mechanical and Aerospace Engineering, Rutgers University, 1990

SUBMITTED TO THE DEPARTMENT OF AERONAUTICS AND ASTRONAUTICS
IN PARTIAL FULFILLMENT OF THE REQUIREMENTS FOR THE DEGREE OF

Master of Science
in Aeronautics and Astronautics
at the
Massachusetts Institute of Technology

June 1996

Signature of Author _____
Department of Aeronautics and Astronautics
May 23, 1996

Certified by _____
Professor Manuel Martinez-Sanchez, Thesis Supervisor
Department of Aeronautics and Astronautics

Accepted by _____
Professor Harold Y. Wachman
Chairman, Department Graduate Committee

An Improved Numerical Model for Flow Computations of Electrothermal Arcjet Thrusters

by

Guy B. Benson

Submitted to the Department of Aeronautics and Astronautics on May 23,1996, in partial fulfillment of the requirements for the degree of Master of Science in Aeronautics and Astronautics

ABSTRACT

This research extends the work of Scott Miller begun at MIT's Space Power and Propulsion Laboratory. The fluid equations are rederived and discussed, with appropriately detailed discussions about the individual equations. In particular the formulation of the diffusive mass fluxes in a multi-species flow is expounded upon. In addition, new collision integrals are included within the calculation of the transport coefficients, and a reformulation of the transport coefficients is discussed.

In addition to the derivation of the fluid equations, a reformulation of MacCormack's method is discussed. In particular, a form of the numerical damping terms is presented which, it is believed, alleviates some of the difficulty in damping oscillations of the fluid equations in the context of a multi-species flow. Also, a discussion of newly generated grids in included.

Finally, the present work is compared to the previous work of Miller, and possibilities in the future of numerical modeling of arcjets are discussed.

Thesis Supervisor: Manuel Martinez-Sanchez

Title: Professor of Aeronautics and Astronautics

Acknowledgments

Let me just start off by saying that there are a lot of people that I want to thank, and that if I forget anyone, please forgive me. The hardest part about writing these acknowledgments is thanking all the right people without sounding too sappy. I've been here a good deal longer than I ever intended. Consequently I've seen many people come and go. The people worth mentioning are the ones who have had a profound difference on my being, whether through thinking, through feeling, or through acting. When I first arrived here, I had many doubts. Some have been overcome, while others have arisen. I have said it before, and I'll say it again. Life before and after MIT was and will be easy. It was easier before because I had never attempted anything so difficult before in my life. It will be easier after because I will never experience anything so difficult again. But it has been an incredible ride, and I knew from the moment that I arrived that it would be a turning point in my life. The move from Hamilton Square, NJ to Cambridge, MA on January 6, 1993 was the crucial step on the road to greater things. Today, I am not the same person that I was when I arrived. I still have more things to learn, more growing to do, more maturity and wisdom to gain, but I am definitely a better person. In the words of Belly, " I'm not the hero I could be, but not the dog I was."

The first person whom I'd like to thank is my advisor, Professor Manuel Martinez-Sanchez. He gave me a shot when no one else would. In the earlier days, I thought that I may have bitten off more than I could chew, but he thought that I could do the work. Over the years, he has been extremely patient with me, and I am grateful to him for not blowing up at me when I couldn't always deliver the goods as promised. I would also like to thank Professor Jaime Peraire, for his insights into the field of computational fluid dynamics. He is very approachable, and an all around good guy. In addition, I'd like to thank Professor David Gonzales, for providing me the lead to Professor Martinez-Sanchez.

I couldn't have made it through the last couple of years without the camaraderie of my friends and office mates here at MIT in general and in CASL/SPPL/SSL in particular. They have been the impetus and inspiration for many a drunken stupor. They have also kicked my butt when I needed it, and boosted my confidence when I was doubting. I couldn't have done this without them. So thanks to the old-timers Ray Sedwick, Sherri Oslick, Carmen Perez de la Cruz, Jim Soldi, Graeme Shaw, Mike Fife, Brian Nishida, Ed Piekos, Derek Plansky, David Oh, and Folusho Oyerokun; and thanks to the new kids Karen Willcox

and Tolulope Okusanya (RU Rah Rah...); and thanks to the newer kids (infants?) Greg Giffin and Angie Kelic. Along a similar vein, I'd like to thank the Thirsty Ear Pub and its bartenders and the MIT Rugby Football Club for many good times and bruises.

I have had many a roommate over the years, some have gotten married or engaged, some have dropped off the face of the earth (they still should be mentioned, in case the police should need to find anyone to identify the bodies...), and some are still my roommates. They tolerated, to a point, my messy tendencies, my idiot high school friends (to be mentioned later), and most of all, me. Lawren Wu was there in the beginning, and is still here in the end. Thanks, Lawren, for tolerating a lazy slob like me. I'd like to also thank Gregg Duthaler, Gustavo Arrizabalaga and his fiancé Aria, Chris and Kate Hamson, Bill York and his fiancé Robin, Ken Arndt, and Domingos Silva. Long live the many generations of 65 Belmont!

I have the extraordinary fortune of still beings friends with many people that I went to high school with. I have been told that this is uncommon, which makes me appreciate them all the more. "The Guys" have been a great source of inspiration, and most important of all, levity, in a lot of heavy situations. I'm not the most reliable person as far as staying in touch goes, I hope that they'll forgive me this indulgence. Thank you, Mike Dimarco, Ken Richards, Mike "Mosh" Baskiewicz, Len Contardo, Steve Bagley, Tim Oliver, Guy Poretti, Jerry Chmielewski, Joe Palma, and Mark Evans. I'd also like to thank their wives and girlfriends (I know what you're putting up with!): Denise Richards, Cynthia Baskiewicz, Renee Contardo, Beth Bagley, Beth Schneider, Sherrie Poretti, Deanna Chmielewski, and Sue Evans. Finally, I'd to give a special thanks to Nicholas Poretti. I only wish that I was around when you were born, Nick!

The list of people that I wish to thank would not be complete without my roommates and friends from good old Rutgers. If I hadn't persevered there, I wouldn't have been able to get here to begin with. My four years at Rutgers were difficult from an emotional standpoint, and I owe these people a great deal of gratitude for helping me grow and mature. Thanks, one and all, Rakesh Shah, Neel Vaidya, Tom Carroll, Robyn Risley, Andrew Platek, Thad Fisher, Ray Gibney, Sean "Stone" Wall, Jeff Ayers, Concetta Russo, Dori Ficarra, Debbie Paolino, Randy Young, Shalom Nelson, Dave Forrest, Joe Schumacher (Yo, Schumacher!) and his wife Erica, Rich Carrig and Diana Vondra Carrig, Don Elwell, Brant and Colin Brisson ("The Twins"), John McLaughlin, and lastly, but definitely not

lastly, Diana Bordon Elwell, who has always been and always will be a great friend.

Finally, I'd like to thank my family. My father, Guy T. "Tiberius" Benson deserves most of the credit of who I am today. He was my prototype, as it were. Thanks, Dad. My mother, Fran, deserves special note for giving me inspiration and determination, in her own unique way, to strive to be a better person. Thanks, Mom. My sister Kelly knows me better than perhaps anyone else. When I was little, I resented the fact that I had to give up my playroom so that my little sister could have a bedroom. Now, I am thankful that I have a little sister like her. Thanks, Kel. I'd also like to thank my future step-family, Pat and Kim Navatto. Their kindness and generosity (and great food) will always make me feel welcome in their house.

Well, there you have it. It's a bit long winded, but I only mentioned the people for whom I felt very strongly. But, there is one person for whom I feel the strongest. In the time that I have known her, she has changed my life in countless ways. The last stretch was hell, but she definitely made it more pleasant. In addition, her family welcomed me from the first time I met them. I can only begin to express my gratitude towards her. Thank you, Julie Buchheit, for being a true friend and loving companion.

So thank you, one and all.

This research was funded by AFOSR Grant 91-0256, the United States government (in the form of student loans), the Thirsty Ear Pub, MIT (student loans, again), and Mom and Dad. Brought to you by the letter P and the number 12.

" 'Twas a woman who drove me to drink,

and I never had the courtesy to thank her for it."

– W.C. Fields

" SPOON !! "

– The Tick

Contents

List of Figures

List of Tables

List of Symbols

c	Sound speed $[\mathrm{m\,s^{-1}}]$
$\hat{c}_{v,s}$	Constant volume specific heat of species s $[\mathrm{J\,mol^{-1}\,K^{-1}}]$
e	Electron charge [C]
e_d	Characteristic dissociation energy [J]
e_i	Characteristic ionization energy [J]
e_v	Characteristic vibrational energy [J]
$e_{s,int}$	Species internal energy per unit mass $[\mathrm{J\,kg^{-1}}]$
f_s	Distribution function of species s
g_e	Gravitational acceleration at earth's surface $[\mathrm{m\,s^{-1}}]$
g_l	Degeneracy of energy level l
h	Planck's constant [J s]
h_s	Enthalpy of particle of species s [J]
$\vec{j}$	Current Density $[\mathrm{A\,m^{-2}}]$
$\vec{j}_s$	Species current density $[\mathrm{A\,m^{-2}}]$
k	Boltzmann's constant $[\mathrm{J\,K^{-1}}]$
$\dot{m}$	Mass flow rate $[\mathrm{kg\,s^{-1}s}]$
m_s	Mass of particle of species s [kg]
m_{sr}	Reduced mass of species s and r
n_s	Species number density $[\mathrm{m^{-3}}]$
$\hat{n}_s$	Molar concentration $[\mathrm{mol\,m^{-3}}]$
p	Total scalar pressure [Pa]
p_s	Species scalar pressure [Pa]
$\overline{\overline{p}}$	Pressure tensor
q_a	Partition function of species a per unit volume

q_s	Charge of species s [C]
$\vec{q}_s$	Heat flux of species s $[\mathrm{J\,m^{-2}\,s^{-1}}]$
$\vec{u}$	Mass-averaged flow velocity $[\mathrm{m\,s^{-1}}]$
$\vec{u}_s$	Species velocity $[\mathrm{m\,s^{-1}}]$
$\vec{v}$	particle velocity $[\mathrm{m\,s^{-1}}]$
v_B	Bohm velocity $[\mathrm{m\,s^{-1}}]$
x_s	Species mole fraction
$\vec{B}$	Magnetic field [T]
D_a	Ambipolar diffusion coefficient $[\mathrm{m^2\,s^{-1}}]$
D_i	Effective diffusion coefficient $[\mathrm{m^2\,s^{-1}}]$
D_{ij}	Binary diffusion coefficient $[\mathrm{m^2\,s^{-1}}]$
$\overline{D}_{ij}$	Multicomponent diffusion coefficient $[\mathrm{m^2\,s^{-1}}]$
$\vec{E}$	Electric field $[\mathrm{V\,m^{-1}}]$
E_l	Elastic collisional energy transfer $[\mathrm{J\,s^{-1}\,m^{-3}}]$
E_s	Total species energy per unit mass $[\mathrm{J\,kg^{-1}}]$
$\mathbf{F}$	Flux vector in z direction
$\vec{F}_s$	External force [N]
$F^{(l,s)}$	Non-dimensional Coulomb collision integral
$\mathbf{G}$	Flux vector in r direction
H_s	Total species enthalpy per unit mass $[\mathrm{J\,kg^{-1}}]$
I	Current [A]
I_{sp}	Specific Impulse [s]
J	Jacobian of coordinate transformation
$\vec{J}$	Flux of a quantity
K_p, K_n, K_c	Equilibrium constants
N_A	Avogadro's number $[\mathrm{mol^{-1}}]$
Q_a	Partition function of species a
Q_{ij}	Collision cross section $\left[\mathrm{\overset{\circ}{A}^2}\right]$
$\hat{R}$	Universal gas constant $[\mathrm{kJ\,kmol^{-1}\,K^{-1}}]$
$\dot{R}$	Radiative energy transfer per unit volume $[\mathrm{J\,s^{-1}\,m^{-3}}]$
R_s	Species ordinary gas constant $[\mathrm{J\,kg^{-1}\,K^{-1}}]$

$\mathbf{S}$	Source vector
T	Thrust [N]
T_s	Species temperature [K]
$\mathbf{U}$	State vector
V	Volume $[\mathrm{m}^3]$
$\vec{V}_s$	Species diffusion velocity $[\mathrm{m\,s}^{-1}]$
Z_s	Charge magnitude of particles of species s
β	Hall parameter
β_0	Ratio of fluid pressure to magnetic pressure
δ_s	Inelastic correction factor of species s
ϵ_0	Permittivity of vacuum $[\mathrm{F\,m}^{-1}]$
κ_s	Species thermal conductivity $[\mathrm{J\,s}^{-1}\,\mathrm{m}^{-1}\,\mathrm{K}^{-1}]$
μ_a	Chemical potential of species a $[\mathrm{J\,mol}^{-1}]$
μ_0	Permeability of vacuum $[\mathrm{H\,m}^{-1}]$
μ_s	Species viscosity $[\mathrm{kg\,m}^{-1}\,\mathrm{s}^{-1}]$
ν_{ij}, ν'_{ij}	Stoichiometric coefficients
$\overline{\nu}_{sr}$	Average collision frequency between species s and r $[\mathrm{s}^{-1}]$
φ	Arbitrary quantity
ϕ	Electrical potential [V]
ρ	Total mass density $[\mathrm{kg\,m}^{-3}]$
ρ_c	Charge density $[\mathrm{C\,m}^{-3}]$
ρ_s	Species mass density $[\mathrm{kg\,m}^{-3}]$
ψ	Electron mobility $[\mathrm{m}^2\,\mathrm{ohm}^{-1}\,\mathrm{C}^{-1}]$
ψ_{ij}	Non-Dimensional parameter used in Coulomb collision integrals
σ	Electrical conductivity $[\mathrm{mho\,m}^{-1}]$, collision parameter $\left[\mathring{\mathrm{A}}^2\right]$
σ_{ij}	Effective hard sphere collision radius $\left[\mathring{\mathrm{A}}\right]$
$\overline{\overline{\tau}}$	Viscous stress tensor
θ_d	Characteristic dissociation temperature [K]
θ_r	Characteristic rotational temperature [K]
θ_v	Characteristic vibrational temperature [K]

χ	Collision deflection angle
ω_s	Species mass fraction
Φ	Viscous dissipation function $[\mathrm{J\,s^{-1}\,m^{-3}}]$
$\Omega_{ij}^{(l,s)}$	Collision integral $\left[\mathring{\mathrm{A}}^2\right]$
$\langle\Omega_{ij}^{(l,s)}\rangle$	Average effective collision integral $\left[\mathring{\mathrm{A}}^2\right]$
Δv	Change in velocity $[\mathrm{m\,s^{-1}}]$
∇	Gradient operator in coordinate space $[\mathrm{m^{-1}}]$
∇_v	Gradient operator in velocity space $[\mathrm{s\,m^{-1}}]$
$<>$	Average value of a quantity
$\ln\Lambda$	Spitzer logarithm

Chapter 1

Introduction

> *"The idea gradually dawned around the turn of the twentieth century that the rocket was the key to space travel. Only a few individuals grasped this concept, and no one paid much attention to them at first. But this discovery was a landmark in human thought. At last man had the answer to a problem that had intrigued and baffled him for centuries. The discovery opened the universe to human exploration...*
>
> *"What these three pioneers started, others were eager to finish. The impetus provided by their discoveries attracted dozens of eager engineers and scientists into rocketry and astronautical research. Major technical barriers still had to be overcome, but for the first time a sizable group of men had begun to take space travel seriously."*
>
> – excerpt from *Space Travel*, by Wernher von Braun and Frederick I. Ordway III

First dramatized by writers of science fiction such as Jules Verne, space travel was thought as an impossibility until the latter half of the nineteenth century. Konstantin Tsiolkovsky, a Russian schoolteacher and scientist, was the first to realize that Newton's Third Law: *"Every action is accompanied by an equal and opposite reaction,"* is valid even in the vacuum of space. Rockets provided the key to propulsion in a vacuum, since, by their very nature, rockets carry their propellant with them. Tsiolkovsky first opened the door to rocket propulsion by formulating the mathematics behind it in the 1890's. Robert Goddard, born in Worcester, Massachusetts, realized the implications of Newton as well, albeit later. Goddard stuck his foot in the door by modernizing rocketry through exhaustive experimentation, being rightfully dubbed the "Father of Modern Rocketry." Hermann Oberth, a Hungarian born German, threw the door wide open by expanding on the theoretical work of Tsiolkovsky, and by promoting rocketry whenever he could [54].

These three pioneers paved the way for the first ballistic missile, the German V2, the prototype for both American and Soviet space launch vehicles.

The Soviet Union launched earth's first man-made satellite, Sputnik, in October of 1957. This event opened up a veritable Pandora's Box of applications. Spacecraft now are used for communication, observation, and transportation in the form of communications satellites, weather satellites, space probes, and manned orbiters such as the Space Shuttle. A spacecraft in motion, however, is subject to a myriad of forces which tend to pull it out of its desired trajectory, whether in orbit about the earth or bound for interstellar space. To keep the spacecraft in its desired trajectory, rockets or thrusters of some sort must be used for adjustment.

The thrust of a simple quasi-one-dimensional thruster is given by Hill and Peterson [18] as

$$T = \dot{m} u_{eq}, \tag{1.1}$$

where

$$u_{eq} = u_e + \left(\frac{p_e - p_a}{\dot{m}} \right) A_e \tag{1.2}$$

is an equivalent exhaust velocity, p_a being the ambient pressure, p_e being the pressure of the flow at the nozzle exit, $\dot{m}$ being the mass flow rate, u_e being the nozzle exit velocity, and A_e being the area of the nozzle exit. In the near vacuum of space, $p_a \approx 0$. In addition, if the flow is expanded ideally to near vacuum, $p_e \approx 0$. Therefore, the equivalent velocity is very nearly the exhaust velocity, $u_{eq} \approx u_e$, and $T = \dot{m} u_e$.

An effective measure of rocket performance is specific impulse, which is defined as

$$I_{sp} = \frac{T}{\dot{m} g_e} = \frac{u_{eq}}{g_e}, \tag{1.3}$$

where g_e is the acceleration of gravity at the earth's surface. The gravitational acceleration is used to make the specific impulse in units of seconds, so that specific impulse is independent of the system of units used. The specific impulse is, basically, a measure how well a rocket's propellant is converted to kinetic thrust. Typically, the higher the specific impulse, the more desirable the thruster, since more thrust is achieved from a smaller amount of mass, enabling a satellite or other spacecraft to carry more payload, or enabling the spacecraft to operate in a certain orbit for a longer period of time. Figure 1-1 shows a plot of I_{sp} versus

vehicle thrust-to-weight, for a number of different propulsion systems (Derived from data in Sutton [50]).

As can be seen, chemical propellant systems offer a higher thrust to vehicle weight ratio than electric propulsion systems such as arcjets. The reasoning behind this is that electric propulsion systems typically need power generation and conditioning equipment to produce and regulate the current and voltage of the device. As a consequence, electric propulsion is not suitable for earth to orbit launches, since the thrust necessary to achieve earth orbit requires a prohibitively large weight in the form of power generation equipment. However, electric propulsion devices can be used for orbital transfer and station-keeping, since higher thrust is not necessary, and the required Δv can be obtained through longer firing times as necessary.

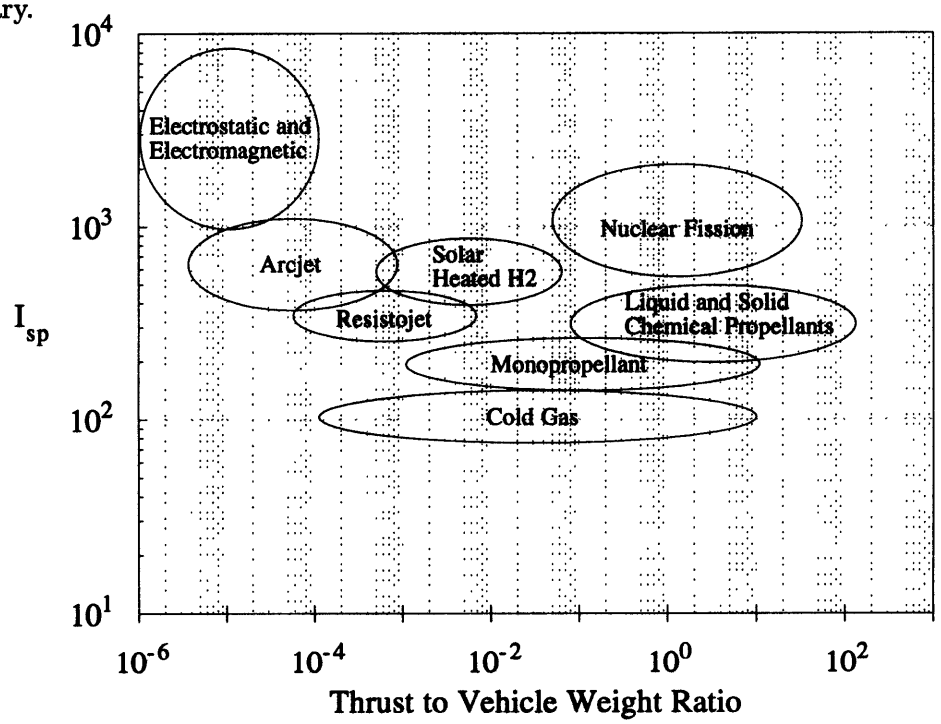

Figure 1-1: *Specific Impulse versus Thrust-to-Weight Ratio of Various Propulsion Systems*

1.1 Electric Propulsion Systems

Under the category electric propulsion systems, there are a variety of different kinds, using different physical laws. All of the devices have the characteristics of low thrust and high specific impulse. Resistojets, arcjet thrusters, magnetoplasmadynamic (MPD) thrusters, stationary plasma thrusters (SPT's or Hall thrusters), and ion engines are all examples of

electric propulsion devices; ion engines falling under the category electrostatic and MPD and Hall thrusters falling under the category electromagnetic in Figure 1-1. The various mission applications for which electric propulsion systems are approximately suited can be seen in Figure 1-2 (from Sutton [50]). As can be seen, MPD thrusters generate the highest I_{sp}, but with the highest cost in power. The practical upper limit for power at present is about 15 kilowatts, for reasons of spacecraft-environment interaction, which will be discussed shortly.

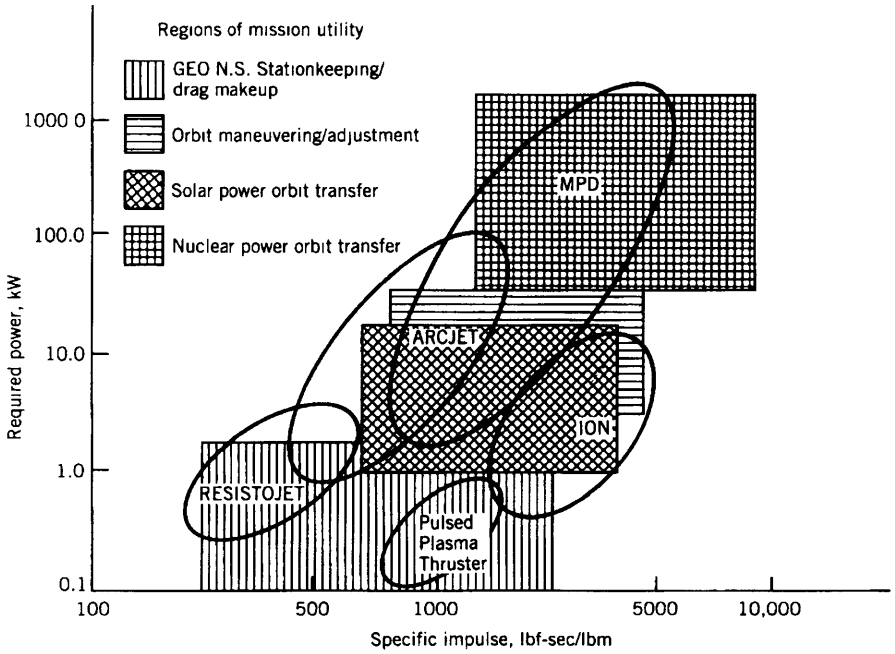

Figure 1-2: *Approximate Regions of Application of Various Electric Propulsion Systems (from Sutton)*

Resistojets and arcjet thrusters (to be discussed in greater detail in Section 1.2) are of a class of devices known as electrothermal. Basically, the propellant is heated through some electrical means and then expanded through a nozzle to produce thrust. In resistojets, the propellant is simply passed over an electrically heated surface to increase its temperature. In arcjets, an electrical arc burns through the constrictor region of the nozzle, as current passes from an axially mounted cathode to the nozzle wall, which acts as the anode. The induced magnetic field of the constricted arc is negligible, as the flow is collision dominated. Depending on the type of propellant used, core temperatures in the arcjet can be on the order of 30,000 K. However, frozen flow losses limit the conversion of thermal energy to kinetic thrust, resulting in efficiencies of a maximum of between 30-50% .

The device with perhaps the most interesting history is the stationary plasma thruster. Scientists in the United States abandoned research into the SPT in the 1960's, feeling that the plasma instabilities present within the thruster were too much to overcome. Soviet scientists persevered, and as a consequence, produced a series of very successful thrusters that were not known to exist until the fall of the Soviet Union. Presently, the Russian SPT-70 and SPT-100 are being considered for a variety of satellite missions. In an SPT, a magnetic field is set up so that the $\vec{B}$ field lines point radially outward from the axis, through an annular ionization chamber. Electrons emitted by a cathode follow an applied electric field into the chamber where they ionize a neutral propellant gas. The electrons are confined about the magnetic field lines, with the $\vec{E} \times \vec{B}$ drift in the azimuthal direction. Since the mass of the ions (typically Xe+) is relatively high, the ions are not confined by the magnetic field, and are accelerated out of the thruster by the electric field. Typically operated at lower pressures, the SPT can obtain specific impulses of from 2,000 to 10,000 seconds.

Magnetoplasmadynamic thrusters operate along the same lines as an arcjet, but at lower pressures and higher powers. Consequently, the flow in an MPD is not as collision dominated as the flow through an arcjet, and the induced magnetic field of the arc becomes a factor in the acceleration of the flow. The radial current provides a $\vec{j} \times \vec{B}$ force along the axial direction, and further collisions result in a bulk acceleration of the flow through the nozzle, augmenting the acceleration obtained by nozzle expansion. As a result, the specific impulse of MPD thruster can be as high as 5000 seconds. As mentioned previously, MPD and Hall thrusters are of a class of propulsion systems known as electromagnetic. Other electromagnetic propulsion devices include electromagnetic rail guns and pulsed plasma thrusters.

By definition, all of these propulsion systems are powered through electrical means. Therefore, the power limitations of satellites and other spacecraft dictate which propulsion systems can be used. For the range of powers indicated in Figure 1-2, photovoltaic (solar) or nuclear power generation is required. Nuclear power generation for satellites is still being developed and debated for political as well as environmental reasons. Therefore, photovoltaic power generation is the most viable. High power systems ($>$ 10 kW) can be operated in one of two regimes, high voltage and low current or high current and low voltage. Operation at high voltages is preferred over high currents for two reasons. The first reason

is due to the resistive power loss during transmission being lower for high voltage power systems than high current systems. The second reason is that the mass of the cables and wiring needed to distribute the power is lower for high voltage systems than high current systems [40]. Because of this, high voltage solar arrays are necessary. These arrays, which can be quite large, interact with the ambient plasma around the spacecraft. The small mass the electron and, hence, the higher electron mobility, causes a majority of the array to float negative with respect to the ambient plasma, and electric arc discharges between different portions of the array and between the array and the plasma can occur. These discharges can cause electromagnetic interference and sputtering of the array material, resulting in disruption of spacecraft systems and loss in efficiency of power generation of the array. In addition, a large solar array may cause a significant drag on the spacecraft if orbiting in low earth orbit (LEO).

For the reasons stated above, MPD thrusters are as yet impractical. Electrothermal arcjets, ion engines and SPT's are practical, however. Of the three practical types just mentioned, the arcjet provides the highest thrust. Because of the arcjet thruster's higher specific impulse over chemical systems and higher thrust over other electrical systems, there may be missions for which the arcjet is solely suited. In addition, a greater understanding of the internal physics of arcjets may aid in the understanding of the physics of its lower pressure, higher power cousin, the MPD thruster.

1.2 Electrothermal Arcjet Thrusters

1.2.1 Basics of Arcjet Operation

The cross section of an arcjet nozzle is shown with a typical length scale in Figure 1-3. As can be seen, the thrust producing portion of an arcjet is small, on the order of centimeters long. The cathode lies along the axis of the thruster. The nozzle and constrictor walls of the thruster act as the anode. The propellant is injected into the annulus surrounding the cathode with some azimuthal swirl. The swirl is thought to stabilize the arc during startup. A high voltage spike is used to break down the dielectric (propellant gas) and produce charge carriers (electrons and ions) which carry the current from the cathode to the anode. Once a current is started, the voltage or current is brought to its desired value. The current heats the gas to temperatures of up to 30,000 K in the core, depending upon the propellant

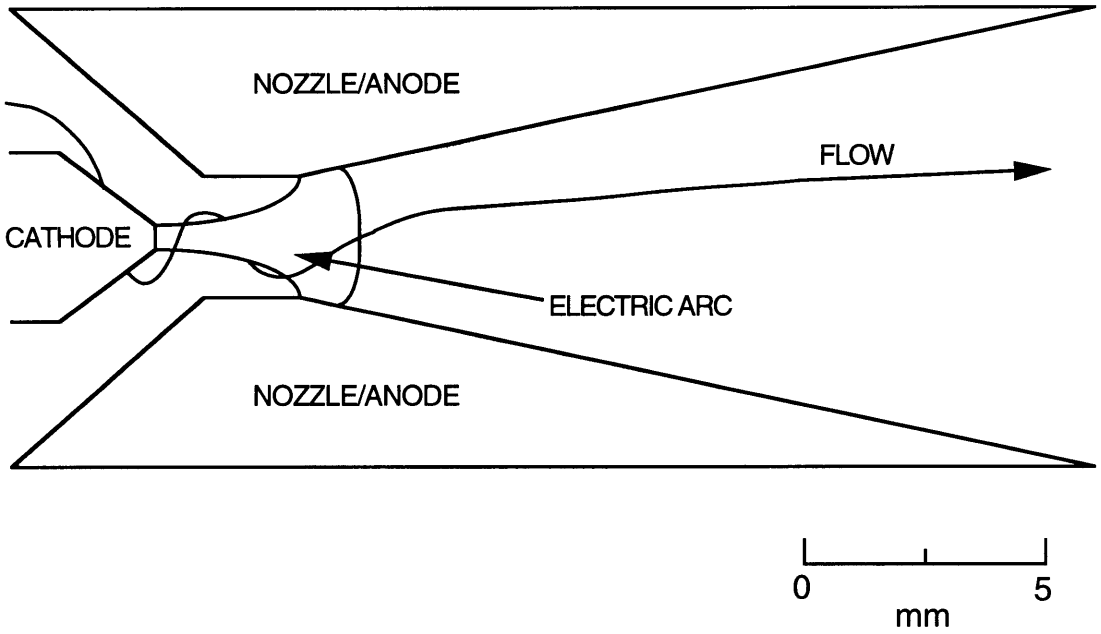

Figure 1-3: *Basic Arcjet Thruster Diagram*

used. This hot gas is then expanded through the nozzle to produce thrust. As mentioned previously, the arcjet system requires a large amount of peripheral equipment, such as a propellant feed system, power conditioning equipment, and so forth. Consequently, the thrust producing portion of the thruster is very small portion of the whole assembly. Figure 1-4 shows the entire assembly of the Olin Aerospace MR-508 1.8 kW hydrazine thruster. As can be seen (lower left corner of picture), the nozzle portion of the thruster assembly is quite small.

1.2.2 Internal Physics of Arcjets

The workings of the arcjet thruster are, at a first glance, rather simple. An arc burns through a propellant gas, dissociates and ionizes the gas, increasing its temperature. The high temperature flow is then accelerated through a nozzle, producing thrust. When looked at in detail, however, the arcjet thruster is a complicated device. The shape of the cathode, the shape of the nozzle, the type of propellant used, and the mass flow rate all have an effect on the performance characteristics of an arcjet. In addition, the fact that the flow is at least partially ionized can have a large effect on the voltage and current characteristics, since the charged particles produce sheath regions near the electrodes. In these sheath regions, large potential drops can exist, resulting in loss of efficiency of the device.

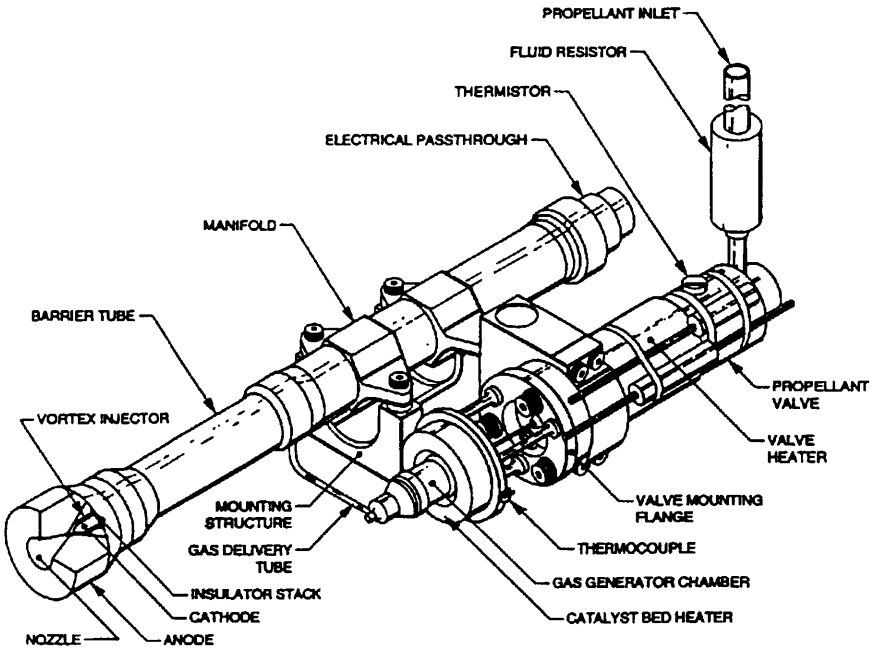

Figure 1-4: *Olin Aerospace MR-508 1.8kW Hydrazine Thruster*

All gases are good electrical insulators at room temperature. To initiate an arc in arcjet thrusters, a large electric field is produced between the electrodes to break down the gas and produce charge carriers, thus creating an arc discharge. Once the arc is established, the current is ramped up to its desired value. A typical arc discharge, with characteristic voltage drops, is shown in Figure 1-5. This figure is a simplified representation of what happens inside an arcjet thruster, but the basic ideas are essentially the same.

Regions *I* and *V* define the sheath regions of the cathode and anode, respectively. In these sheath regions, a net space charge and high gradients in electrical potential exist, and conduction transitions from one of metallic conduction to one of gaseous conduction. In other words, the sheath regions define the transition regions from areas where electrons flow through a relatively stationary background of ions to areas where both ions and electrons contribute to the current [41]. In atmospheric plasmas, d_A and d_C are on the order of 10^{-4} to 10^{-6} m, which is comparable to the electron mean free path. The voltage drop in the sheath regions can be very high, leading to very high electric fields. These large electric fields can have a large effect on the current attachment regions. Regions *II* and *IV* define transition regions, where large gradients in plasma properties are present, but quasi-neutrality prevails [34]. The lengths of these transition regions, d'_A and d'_C, are usually on the order of millimeters for atmospheric plasmas. Region *III* constitutes the bulk of the

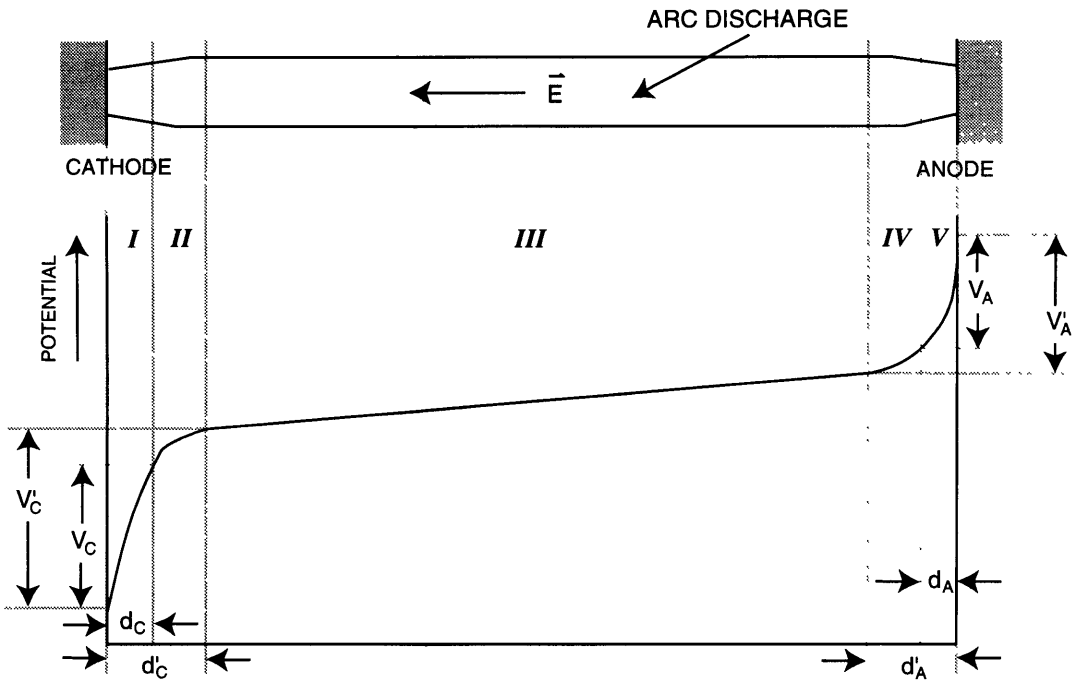

Figure 1-5: *Potential Drops Within an Arc Discharge*

arc column. In this region, the gradients in plasma properties along the direction of the arc are small. However, the gradients in plasma properties near the edge of the arc tend to cause heat conduction and ambipolar diffusion of ions and electrons outward. To maintain the mass balance, neutrals must diffuse inward. In the steady state, a net ionization rate must exist within the arc core to balance the loss of charged species through diffusion and subsequent recombination outside of the main arc region.

The current attachment at the cathode tip can be either a diffuse attachment or a spot attachment. Spot attachments are characterized by high $(10^9 - 10^{12}\,\mathrm{A/m^2})$ current densities and, sometimes, fast motion of the arc foot. In arcjets, the attachments at the cathode are typically of the spot kind, and are enhanced by the shape of the cathode tip, which is conical. The cathode, being a conductor, is an equipotential surface. As such, the electric field near the tip is intensified, since the field lines must remain at all times perpendicular to the surface. The tip acts like a focus, through which the current flows. This focusing results in heating of the cathode tip. Since the dominant mode in liberation of electrons from the cathode tip is thermionic emission, the enhanced electric field due to the shape of the cathode acts to increase the local temperature and, thus, increase the thermionic emission. In addition, the electric fields in the area of the cathode tip accelerate the electrons away from the tip as well. Since the flow is conserved, this acceleration acts

to constrict the current flow, further heating the cathode tip. In general, some of the tip boils away during startup, reducing the electric field intensity and creating a stable arc attachment condition.

The current at the cathode tip is due to both thermionic emission and field emission of electrons, as just mentioned. In addition, ions contribute to the current as well, providing about 15-20% of the total current. Most cathodes within arcjet thrusters are made of alloys of tungsten, which is observed to be a good thermionic emitter, due to its relatively low surface work function ($\phi_W \approx 4.5V$). The alloying material is typically thorium ($\phi_{Th} = 3.35\text{V}$), which helps reduce the work function further. The Richardson-Dushman equation for thermionic emission as modified by Schottky to account for field enhanced emission [41],

$$j_S = 6 \times 10^5 \, T_C^2 \exp\left[-\frac{1}{kT_C}\left(e\phi_C - \sqrt{\frac{e^3 E}{4\pi\epsilon_0}}\right)\right], \quad \left[\text{A/m}^2\right] \tag{1.4}$$

provides an estimate of the enhanced field thermionic emission, where E is the electric field strength in V/m, T_C is the temperature of the cathode in K, and ϕ_C is the work function of the cathode material, in volts. The magnitude of the current due to pure field emission is given by the Fowler-Nordheim equation [41]

$$j_{FN} = 1.54 \times 10^{-6} \, \frac{E^2}{e\phi_C} \exp\left[-\frac{6.83 \times 10^9 \, (e\phi_C)^{\frac{3}{2}}}{E} f\left(\frac{3.79\sqrt{E}}{e\phi_C} \times 10^{-5}\right)\right], \quad \left[\text{A/m}^2\right] \tag{1.5}$$

where E is in units of V/m, $e\phi_C$ is in eV, and f is a function which decreases from $f(0) = 1$ to $f(1) = 0$.

The anode within an arcjet is just a passive collector of current. The current attachment at the anode can be of either the spot kind or diffuse kind. The diffuse attachment can be the result of a constant low current density discharge, while the spot kind of attachment can come in the form of a sporadic high current density discharge. It has been postulated that the current attachment at the anode may be a 3-dimensional effect, as current "spokes" may appear, with rotation of the spokes occurring due to the applied swirl velocity and due to motion of the high temperature area of the arc discharge with respect to the gas [31, 32]. This phenomenon has some theoretical basis, but, at this time, it is difficult if not impossible to prove this phenomenon experimentally. The anode sheath region is very

similar to the cathode sheath region, with the notable exception that the current is carried almost exclusively by the electrons, resulting in a net negative space charge. The voltage drop in the anode sheath, V_C, can positive or negative, depending on the magnitude of the collected current.

The propellant used within an arcjet can have a dramatic effect on the performance characteristics. The best propellant to use in arcjets is hydrogen, due to its small mass and low dissociation energy. Presently, carrying hydrogen for space missions is impractical, since the propellant must be cryogenically cooled to liquid form. However, work on better insulation and refrigeration techniques is underway, and hydrogen may soon be a viable propellant option. For present missions, hydrazine (N_2H_4) is the fuel of choice, since it exists as a liquid at room temperatures. In addition, hydrazine is very volatile. Therefore, the hydrazine used in arcjets is probably dissociated into molecular hydrogen and nitrogen before it reaches the arc discharge region.

The major loss in efficiency of arcjets is due to frozen flow losses. The energy is tied up in ionization, dissociation, and excited rotational and vibrational states of molecules, rather than translational modes. As a result, the efficiency of arcjets hovers in the 30% to 40% range. A number of different methods have been devised to decrease frozen flow losses. Oyerokun and Martinez [36] have proposed seeding hydrogen with a small fraction of an alkali metal such as cesium. The cesium atoms, having a lower ionization energy than hydrogen atoms, ionize first, and then carry the current. The hydrogen atoms remain neutral, thereby reducing ionization losses. Foutter [15] proposes an interesting approach to reducing frozen flow losses in the nozzle expansion region. By shaping the nozzle appropriately, shock waves would be produced, thereby inducing recombination mechanically. However, in his thesis, Foutter assumed inviscid flow. In the viscous nozzle expansion of an arcjet, the nozzle contour must be more dramatic to achieve the same results. Since it is unclear how these nozzle contours affect I_{sp}, it is not yet known whether this method would provide the desired result of an increase in efficiency.

1.3 Thesis Overview

The work in this thesis is an extension of the work done by Scott Miller at MIT's Space Power and Propulsion Laboratory, which has now become part of MIT's Space Systems Laboratory.

The original focus of this research was to extend the work of Miller [34] in the field of numerical modeling of electrothermal arcjet thrusters to other cases and other propellants. It is a difficult topic, encompassing elements of plasma physics, chemical kinetics, kinetic theory of gases, and computational fluid dynamics. The governing equations are a complex set of coupled, non-linear equations, and are not easy to solve. It was soon discovered after the work towards this thesis was begun that these goals might be a little lofty, considering the amount of work necessary in achieving them. The numerical code, as inherited, was very lengthy. It took a good deal of time to decipher and learn the script. In the end, the goals achieved hardly resembled the goals sought after. Nonetheless, much was learned along the way. Although this thesis will not serve as a destination along the road in the field of the numerical simulation of electrothermal arcjet thrusters, it is hoped that this thesis will provide a smoother path in the field, a path filled with less pitfalls and pot holes.

Chapter 2 details the derivation of the governing equations to be used in acquiring a numerical solution. This chapter very closely mirrors the third chapter of Miller's thesis. It differs in areas where the author felt that more elaboration was necessary. There are many fine points hidden within the equations, and the author has done his best to see that most of these fine points, if not discussed in detail, are at least mentioned. It starts with the derivation of the fluid equations by taking the moments of the Boltzmann equation. From there it progresses to the description of the source terms in the species mass conservation equations, in particular the finite rate chemistry used in finding a functional form for these terms. Lastly, a brief discussion of the Chapman-Enskog solution to the Boltzmann equation is given. It sets the stage for the derivation of the transport coefficients which are needed in the momentum and energy conservation equations. A short summary of the final form of the governing equations is given on pp. 56-58.

Chapter 3 details the numerical methods used and developed within this work. A modified form of MacCormack's method is presented which can be used in finding a numerical solution to the fluid equations. In particular, a formulation of the numerical smoothing terms is presented which, it is believed, alleviates some of the difficulty in damping numerical oscillations which inevitably occur in the numerical solution to the fluid equations, particularly multi-species flows. The Successive Over-relaxation (SOR) scheme, used in the solution of the electrical potential equation, is discussed as well. In addition, the techniques used in generating grid meshes is discussed. The chapter ends with a discussion of the

boundary value calculations needed on the grid boundaries and initial value calculations needed on startup.

As mentioned above, the goals sought in this thesis bear little resemblance to the goals that were achieved. Since this thesis is an extension of previous work, it is only fair to compare the work of this thesis to the previously accomplished work. Chapter 4 discusses the differences in the formulations as developed in this thesis with the formulations of previous work. It begins with a discussion of the differences in the physics between this work and the work of Miller. In particular, the transport properties as calculated by the methods of this thesis are compared to the calculations of Miller. Also discussed is the reformulation of MacCormack's method, and the ramifications of this new formulation. The chapter ends with a discussion of the methods as developed, including some recommendations for the progression of the work in the field of numerical calculation of electrothermal arcjets.

Chapter 2

Governing Equations

2.1 Basic Equations

The governing equations of the flow through an axisymmetric arcjet thruster are typical of most fluid flows. In the this chapter, the methodology of Miller [34] and Bittencourt [4] is closely followed in deriving these governing equations.

The fluid equations are derived from taking moments of Boltzmann's Equation, including, as appropriate, Lorentz force terms. The results are, not surprisingly, equations for species and global mass conservation, momentum conservation, and energy conservation. This set of equations is closed by Maxwell's equations and an appropriate equation of state.

2.1.1 Maxwell's Equations

For the application at hand, Maxwell's equations for a vacuum are most applicable:

$$\nabla \cdot \vec{E} = \frac{\rho_c}{\epsilon_0} \tag{2.1}$$

$$\nabla \times \vec{E} = -\frac{\partial \vec{B}}{\partial t} \tag{2.2}$$

$$\nabla \cdot \vec{B} = 0, \tag{2.3}$$

$$\nabla \times \vec{B} = \mu_0 \left(\vec{j} + \epsilon_0 \frac{\partial \vec{E}}{\partial t} \right) \tag{2.4}$$

where ρ_c is the charge density, ϵ_0 is the permittivity of free space, μ_0 is the permeability of free space, $\vec{j}$ is the current density, and $\vec{E}$ and $\vec{B}$ are the vector electric and magnetic fields,

respectively. In ionized gases, Maxwell's equations for a medium are impractical to use, since the complicated motion of the charges makes it difficult to lump their effects into an equivalent ϵ and μ, which are used in finding the displacement field $\vec{D}$ and magnetic field strength $\vec{H}$ [9].

2.1.2 Conservation Equations

In the rigorous kinetic theory of gases, the dynamical state of N particles can be characterized by N distribution functions describing the behavior of each particle in generalized coordinates. Fortunately, this amount of detail is unnecessary, as we are able to glean enough information from a lower order distribution function, $f_s(\vec{x}, \vec{v}, t)$, which describes the behavior of a species s of particles in six-dimensional $(\vec{x}, \vec{v})$ phase space and in time. The equation which describes the total time rate of change of this distribution function is the Boltzmann equation:

$$\frac{\partial f_s}{\partial t} + \vec{v} \cdot \nabla f_s + \frac{\vec{F}_s}{m_s} \cdot \nabla_v f_s = \left(\frac{\partial f_s}{\partial t}\right)_{coll}, \tag{2.5}$$

where $\vec{F}_s$ is a vector of applied body forces and ∇_v is the gradient operator in velocity space. The term on the right hand side of the equation represents the time rate of change of the distribution function due to collisions, and can be a complicated function of the distribution functions of the various species present, their relative velocities, and collision cross-sections.

The macroscopic conservation equations can be derived by taking the appropriate moments of the Boltzmann equation. We begin by multiplying Equation 2.5 by some quantity $\varphi_s(\vec{x}, \vec{v}, t)$ which, as indicated, may vary with position, velocity, and time. By integrating over all velocity space, the general transport equation is obtained:

$$\frac{\partial}{\partial t}\left(n_s < \varphi_s >\right) - n_s < \frac{\partial \varphi_s}{\partial t} > + \nabla \cdot \left(n_s < \varphi_s \vec{v} >\right) - n_s < \vec{v} \cdot \nabla \varphi_s >$$

$$- n_s < \frac{\vec{F}_s}{m_s} \cdot \nabla_v \varphi_s > = \int \varphi_s \left(\frac{\partial f_s}{\partial t}\right)_{coll} d^3v; \tag{2.6}$$

where the definition of the average value of a quantity in velocity space ($< >$) has been used. The integration reduces the problem from one in six-dimensional phase space and time to one in three-dimensional coordinate space and time. The species conservation equations can be obtained by taking φ_s as the correct quantity associated with mass, momentum,

and energy. The global equations can then be easily obtained through summation over all species. As mentioned above, the collisional term on the right hand side of the equation can be quite complicated. For pressures below about 10^3 atmospheres, binary collisions dominate, thereby simplifying the collisional term.

With the aid of Equation 2.6, the species mass conservation equation can be obtained by taking $\varphi_s = m_s$. Taking the averages in the necessary quantities results in

$$\frac{\partial \rho_s}{\partial t} + \nabla \cdot (\rho_s \vec{u}_s) = S_s = m_s \int \left(\frac{\partial f_s}{\partial t}\right)_{coll} d^3v, \tag{2.7}$$

where $\vec{u}_s$ represents the species flow velocity in coordinate space, and S_s is a volumetric source term representing the rate of production of mass of species s due to collisions.

By taking $\varphi_s = m_s \vec{v}$, the species momentum equation can be obtained:

$$\frac{\partial \rho_s \vec{u}_s}{\partial t} + \nabla \cdot (\rho_s \vec{u}_s \vec{u}_s) + \nabla \cdot \bar{\bar{p}}_s - n_s < \vec{F}_s >= \vec{A}_s = m_s \int \vec{v} \left(\frac{\partial f_s}{\partial t}\right)_{coll} d^3v. \tag{2.8}$$

By expanding the momentum flow dyad and upon substituting Equation 2.7, an alternate form of the species momentum equation may be obtained:

$$\rho_s \left[\frac{\partial \vec{u}_s}{\partial t} + (\vec{u}_s \cdot \nabla)\, \vec{u}_s\right] + \nabla \cdot \bar{\bar{p}}_s - n_s < \vec{F}_s >= \vec{A}_s - \vec{u}_s S_s. \tag{2.9}$$

The term $\bar{\bar{p}}_s$ is the kinetic pressure tensor, representing the scalar pressure, p_s, and other normal and shear stresses. The quantity $\vec{A}_s$ represents the collisional change of momentum of species s. The body force, for the purposes of this research, is the Lorentz force:

$$< \vec{F}_s >= q_s \left(\vec{E} + \vec{u}_s \times \vec{B}\right). \tag{2.10}$$

The collisional momentum term can be thought of as the average rate of loss of momentum between particles, and can be approximated as

$$\vec{A}_s = \rho_s \sum_s \bar{\nu}_{sr} \frac{m_{sr}}{m_s} \left(\vec{u}_r - \vec{u}_s\right), \tag{2.11}$$

where $\bar{\nu}_{sr}$ is an average collision frequency between species s and species r, and m_{sr} is the reduced mass of species s and species r. Inserting Equations 2.10 and 2.11 into Equations

2.8 and 2.9 yields two forms of the species momentum equation,

$$\frac{\partial \rho_s \vec{u}_s}{\partial t} + \nabla \cdot (\rho_s \vec{u}_s \vec{u}_s) + \nabla \cdot \bar{\bar{p}}_s = n_s q_s \left(\vec{E} + \vec{u}_s \times \vec{B} \right) + \rho_s \sum_s \overline{\nu}_{sr} \left(\vec{u}_r - \vec{u}_s \right), \tag{2.12}$$

which is in conservative form, and

$$\rho_s \left[\frac{\partial \vec{u}_s}{\partial t} + (\vec{u}_s \cdot \nabla) \vec{u}_s \right] + \nabla \cdot \bar{\bar{p}}_s = n_s q_s \left(\vec{E} + \vec{u}_s \times \vec{B} \right) + \rho_s \sum_s \overline{\nu}_{sr} \left(\vec{u}_r - \vec{u}_s \right) - \vec{u}_s S_s. \tag{2.13}$$

Finally, by substituting $\varphi_s = m_s v^2$ into the general transport equation, the species energy conservation equation can be found. By separating the components of $\vec{v}$ into a mean species velocity and a random species velocity, and after appropriate averaging the following equation results:

$$\frac{\partial}{\partial t} \left(\frac{3}{2} p_s + \frac{1}{2} \rho_s u_s^2 \right) + \nabla \cdot \left[\left(\frac{3}{2} p_s + \frac{1}{2} \rho_s u_s^2 \right) \vec{u}_s \right] + \nabla \cdot (\bar{\bar{p}}_s \cdot \vec{u}_s)$$

$$+ \nabla \cdot \vec{q}_s - n_s < \vec{F}_s \cdot \vec{v} >= M_s, \tag{2.14}$$

where

$$M_s = \frac{1}{2} m_s \int v^2 \left(\frac{\partial f_s}{\partial t} \right)_{coll} d^3 v \tag{2.15}$$

represents the rate of energy transfer per unit volume due to collisions and $\vec{q}_s = -\kappa_s \nabla T_s$ is the heat flux vector for species s. M_s can be thought of as an average rate of energy loss, and can be approximated as

$$M_s = \sum_r \frac{\rho_s \overline{\nu}_{sr}}{m_s + m_r} \left[3k \left(T_r - T_s \right) + m_r \left| \vec{u}_r - \vec{u}_s \right|^2 \right]. \tag{2.16}$$

where k is Boltzmann's constant.

As written, Equation 2.14 only applies to simple particles with translational energy only, and doesn't apply to particles with additional energy, such as molecules, which possess energy in internal vibrational and rotational modes. The rigorous derivation of the energy equation for particles with internal degrees of freedom is quite involved, and will not be discussed here (see Chapter 11 of Chapman and Cowling [7]). As it turns out, however, the species energy equation for particles with internal energy is not much more complicated

than the equation for simple particles:

$$\frac{\partial}{\partial t}\left(\frac{3}{2}p_s + \frac{1}{2}\rho_s u_s^2 + \rho_s e_{s,int}\right) + \nabla \cdot \left[\left(\frac{3}{2}p_s + \frac{1}{2}\rho_s u_s^2 + \rho_s e_{s,int}\right)\vec{u}_s\right] + \nabla \cdot (\bar{\bar{p}}_s \cdot \vec{u}_s)$$

$$+ \nabla \cdot \vec{q}_s - n_s < \vec{F}_s \cdot \vec{v} >= \sum_r \frac{\rho_s \overline{\nu}_{sr}}{m_s + m_r}\left[3k\left(T_r - T_s\right) + m_r\left|\vec{u}_r - \vec{u}_s\right|^2\right]. \tag{2.17}$$

Here $e_{s,int}$ represents the average internal energy per unit mass of species s, and includes vibrational, rotational, dissociation, and ionization energies where necessary. When the Lorentz force (Equation 2.10) is substituted into Equation 2.17, the terms including the magnetic field vanish, and the species energy equation becomes:

$$\frac{\partial}{\partial t}\left(\frac{3}{2}p_s + \frac{1}{2}\rho_s u_s^2 + \rho_s e_{s,int}\right) + \nabla \cdot \left[\left(\frac{3}{2}p_s + \frac{1}{2}\rho_s u_s^2 + \rho_s e_{s,int}\right)\vec{u}_s\right] + \nabla \cdot (\bar{\bar{p}}_s \cdot \vec{u}_s)$$

$$+ \nabla \cdot \vec{q}_s = \vec{j}_s \cdot \vec{E} + \sum_r \frac{\rho_s \overline{\nu}_{sr}}{m_s + m_r}\left[3k\left(T_r - T_s\right) + m_r\left|\vec{u}_r - \vec{u}_s\right|^2\right], \tag{2.18}$$

where $\vec{j}_s = n_s q_s \vec{u}_s$ is the current density carried by species s.

This equation may be further simplified by defining a total energy per unit mass:

$$E_s = \frac{3}{2}\frac{p_s}{\rho_s} + \frac{1}{2}u_s^2 + e_{s,int}, \tag{2.19}$$

where $\frac{3}{2}\frac{p_s}{\rho_s}$ is the energy per unit mass due to random motion of the particles, $\frac{1}{2}u_s^2$ represents the kinetic energy per unit mass due to directed motion, and $e_{s,int}$ is the internal energy per unit mass, as stated previously. Inserting Equation 2.19 into Equation 2.18 results in a simpler form of the species energy equation:

$$\frac{\partial}{\partial t}\left(\rho_s E_s\right) + \nabla \cdot \left(\rho_s \vec{u}_s E_s\right) + \nabla \cdot \left(\bar{\bar{p}}_s \cdot \vec{u}_s\right) - \nabla \cdot \left(\kappa_s \nabla T_s\right) = \vec{j}_s \cdot \vec{E} + M_s \tag{2.20}$$

2.1.3 Equation of State

In this research, each species is assumed to behave as an ideal gas. For the range of temperatures and pressures expected in this research, this is a good assumption. Given this, the equation of state for a species is

$$p_s = n_s k T_s = \rho_s R_s T_s, \tag{2.21}$$

where $R_s = \frac{k}{m_s}$ is the gas constant specific to species s in units of $\frac{J}{kg \cdot K}$.

2.2 Arcjet Flow Model

The macroscopic conservation equations and the equation of state as derived in the previous section are a closed set on coupled nonlinear differential equations which can be tailored to solve the flow within an electrothermal arcjet. In general, the equations are a modified form of the Navier-Stokes equations as applied to a multi-species chemically reacting flow.

The model as originally derived by Miller takes into account viscous effects, heat conduction, ambipolar diffusion, Ohmic heating, and collisional energy transfer between electrons and heavy species. In this work, the diffusion formulation of Miller has been improved so as to better predict the heat conduction characteristics of the flow, especially in the transition region between the hot inner arc core and the cooler outer flow.

2.2.1 Simplifying Assumptions

Although three-dimensional effects probably do occur within arcjets, the set of equations makes the numerical solution in three dimensions very computationally intensive, for any numerical scheme. Fortunately, a great deal of information can be obtained by restricting the physics to a two-dimensional axisymmetric flow. In other words, the azimuthal derivatives (or the $\frac{\partial}{\partial \theta}$ terms) are negligible, and can be removed from the governing equations. The terms which are constant in θ but vary in z and r are retained. In particular, an azimuthal or swirl velocity component is retained, since, in most experimental arcjets, the propellant is injected into the plenum with some swirl velocity. It is believed that this swirl component stabilizes the arc during startup.

As is true with any partially ionized gas in contact with a solid wall, electrically non-neutral sheaths form close to the solid surfaces. As discussed in Section 1.2.2, these sheath regions within an arcjet thruster are typically very small for the range of temperatures and pressures usually found. Due to this fact, the sheath regions are neglected, and the grid boundaries are treated as sheath boundaries. Within the flow, quasi-neutrality ($n_e \approx n_i$) is assumed. The assumption of quasi-neutrality not only makes the calculation of some physical quantities much simpler, but it also reduces the number of necessary mass conservation equations by one.

Another major assumption that is used within this research concerns the temperatures of the various species. Each species within the internal flow of an arcjet can, possibly, have its own translational temperature. In other words, each species can have a different temperature corresponding to its own random thermal motions. In addition, molecules and other complex particles can have temperatures associated with internal degrees of freedom (such as vibrational or rotational modes) which are not in thermal equilibrium with the particles' translational temperature. For simplicity, all the heavy species in this work are assumed to be in translational thermal equilibrium with one another. In addition, the temperatures of the various internal modes are assumed to be in equilibrium with this translational temperature. The exception to this is the electron temperature. An electron temperature which is different from the other temperatures is important in the non-equilibrium production of charge carriers, which is important in self-consistent arc attachment on the anode.

The final major assumption within this research concerns the self-induced magnetic field. Within an arcjet, the self-induced magnetic field is negligible. This assumption can be quantified by relating the fluid pressure to the magnetic field pressure, defined as [9]

$$p_B = \frac{B_0^2}{2\mu_0}. \tag{2.22}$$

The ratio of the fluid pressure to the magnetic pressure is denoted by a factor, β_0 (not to be confused with the Hall parameter, β, defined in Section 2.2.3),

$$\beta_0 = \frac{\sum_j n_j k T_j}{B_0^2/2\mu_0}, \tag{2.23}$$

which provides a measure of the importance of the self-induced magnetic field. Assuming a coaxial current flow through an area of radius R_0, β_0 becomes

$$\beta_0 = \frac{8\pi^2 R_0^2 \sum_j n_j k T_j}{\mu_0 I^2}. \tag{2.24}$$

For arcjets, β_0 is typically large, which means that the induced magnetic field has little effect on the flow. For example, the German TT1 thruster, which operates at $p \approx 1.5$ atmospheres, for a current flow of 100 amperes and $R_0 = 2mm$ (the cathode radius), $\beta_0 = 3.8 \times 10^3$. For comparison, a typical MPD thruster may have a current flow within the

arc of $I = 30,000$ A, operating at a pressure of about 10^{-2} atm. If we take $R_0 = 5.2$ cm, as is the case in the MPD thruster of Heimerdinger [17], $\beta_0 = 0.2$.

2.2.2 Definitions

In deriving the global equations, it is advantageous to define global quantities. The global density is simply the sum of the species densities

$$\rho = \sum_s \rho_s. \tag{2.25}$$

We next define a mass averaged flow velocity

$$\vec{u} = \frac{1}{\rho} \sum_s \rho_s \vec{u}_s, \tag{2.26}$$

where $\vec{u}_s$ is the species velocity relative to the laboratory reference frame. Using the definition above (Equation 2.26) we can decompose the species velocity into components:

$$\vec{u}_s = \vec{u} + \vec{V}_s, \tag{2.27}$$

where $\vec{V}_s$ is the species slip velocity, relative to the mass averaged velocity. From Equations 2.26 and 2.27, it can be easily shown that the slip velocities obey the relation:

$$\sum_s \rho_s \vec{V}_s = 0. \tag{2.28}$$

For the purposes of this research, the slip velocity is the velocity of mass diffusion. Therefore, the terms species slip velocity and species diffusion velocity can be used interchangeably without ambiguity.

The global pressure is simply the sum of the partial pressures of the various species,

$$p = \sum_s p_s = \sum_s \rho_s R_s T_s. \tag{2.29}$$

In terms of the species pressure tensor, $\bar{\bar{p}}_s$, the scalar pressure, p_s, is defined as one third of the trace of the pressure tensor, or, in other words, the mean value of the diagonal elements

of the pressure tensor:

$$p_s = \frac{1}{3}\left(p_{s11} + p_{s22} + p_{s33}\right). \tag{2.30}$$

Using this definition, the pressure tensor can be separated into two parts:

$$\overline{\overline{p}}_s = p_s\overline{\overline{I}} - \overline{\overline{\tau}}_s, \tag{2.31}$$

where $\overline{\overline{I}}$ is an identity matrix, and $\overline{\overline{\tau}}_s$ is the viscous stress tensor for species s. As its name suggests, the viscous stress tensor contains the viscous stresses present within the fluid. As with the other global quantities, the global pressure tensor can be defined as the sum of the species pressure tensor:

$$\overline{\overline{p}} = \sum_s \overline{\overline{p}}_s = \sum_s \left(p_s\overline{\overline{I}} - \overline{\overline{\tau}}_s\right) = p\overline{\overline{I}} - \overline{\overline{\tau}}. \tag{2.32}$$

With the aid of Equation 2.27, the total current density can be written as

$$\vec{j} = \vec{u}\sum_s n_s q_s + \sum_s n_s q_s \vec{V}_s. \tag{2.33}$$

The first term on the right hand side is the convection current density, which is due to convection of net space charge. The second term is the conduction current density, which occurs because of differing slip velocities. For a quasi-neutral plasma, the first term vanishes, leaving

$$\vec{j} = \sum_s n_s q_s \vec{V}_s. \tag{2.34}$$

2.2.3 Electric Potential Equation

The electric potential equation can be derived utilizing the species momentum equation, Equation 2.13, and Maxwell's equations. By summing over all species and using the definition of current density (Equation 2.34) and electrical conductivity (cf. Section 2.4.5), the generalized Ohm's law for a partially ionized, collision-dominated gas may be obtained [35]:

$$\sigma\left(\vec{E} + \vec{u}\times\vec{B} + \frac{\nabla p_e}{en_e}\right) = \vec{j} + \beta_e\vec{j}\times\vec{b} + s\vec{b}\times\left(\vec{j}\times\vec{b}\right), \tag{2.35}$$

where $\vec{b} = \frac{\vec{B}}{B}$ and ∇p_e is the electron pressure gradient. In this equation, the definitions of electron Hall parameter,

$$\beta_e = \frac{eB}{m_e \sum_r \overline{\nu}_{er}}, \tag{2.36}$$

ion Hall parameter,

$$\beta_i = \frac{q_i B}{m_{in} \sum_r \overline{\nu}_{ir}}, \tag{2.37}$$

and ion slip factor,

$$s = \left(\frac{\rho_n}{\rho}\right)^2 \beta_e \beta_i, \tag{2.38}$$

have been used; where q_i is the ion charge magnitude, $m_{in} = \frac{m_i m_n}{m_i + m_n}$ is the reduced mass of an ion and a neutral, and ρ_n is the total density of the neutral species. Neglecting the magnetic field, and assuming that only electrons carry the current (a good assumption in collision-dominated plasmas), the generalized Ohm's law simplifies to:

$$\vec{j} = \sigma \vec{E} + \psi \nabla p_e, \tag{2.39}$$

where

$$\psi = \frac{\sigma}{e n_e} = \frac{e}{m_e \sum_r \overline{\nu}_{er}} \tag{2.40}$$

is the electron mobility.

Since the plasma is macroscopically neutral and the self-induced magnetic field is negligible, Maxwell's equations reduce to $\nabla \cdot \vec{E} = 0$ and $\nabla \times \vec{E} = 0$. Therefore, the electric field vector may be written as the gradient of a scalar potential:

$$\vec{E} = -\nabla \phi. \tag{2.41}$$

In addition, $\nabla \cdot \vec{j} = 0$ due to charge conservation. Inserting Equation 2.41 into Equation 2.39, and noting that the divergence of the current density is zero, we obtain the electric potential equation:

$$\nabla \cdot (\sigma \nabla \phi - \psi \nabla p_e) = 0. \tag{2.42}$$

Written in a cylindrical coordinate system, and neglecting azimuthal gradients, the potential

equation is found to be

$$\frac{1}{r}\frac{\partial}{\partial r}\left(r\sigma\frac{\partial\phi}{\partial r}\right)+\frac{\partial}{\partial z}\left(\sigma\frac{\partial\phi}{\partial z}\right)=\frac{1}{r}\frac{\partial}{\partial r}\left(r\psi\frac{\partial p_e}{\partial r}\right)+\frac{\partial}{\partial z}\left(\psi\frac{\partial p_e}{\partial z}\right). \tag{2.43}$$

2.2.4 Mass Conservation Equations

Using Equation 2.7, the species mass conservation equation can be written as

$$\frac{\partial\rho_s}{\partial t}+\nabla\cdot(\rho_s\vec{u}_s)=m_s\dot{n}_s \tag{2.44}$$

where $\dot{n}_s$ represents the net rate of production of species s per unit volume. In axisymmetric coordinates, the species mass conservation equation becomes

$$\frac{\partial\rho_s}{\partial t}+\frac{\partial\rho_s u_{sr}}{\partial r}+\frac{\rho_s u_{sr}}{r}+\frac{\partial\rho_s u_{sz}}{\partial z}=m_s\dot{n}_s, \tag{2.45}$$

where $u_{sr}=u_r+V_{sr}$ and $u_{sz}=u_z+V_{sz}$. The diffusion velocities are calculated by the means of Section 2.4.2.

Throughout this thesis, the propellant, for simplicity, is assumed to be diatomic, such as hydrogen or nitrogen. If dissociation and ionization are taken into account, there are four dominant species: diatomic molecules, atoms, ions, and electrons. The set of species mass conservation equations which characterize the flow are then

$$\frac{\partial\rho_{S_2}}{\partial t}+\nabla\cdot(\rho_{S_2}\vec{u})+\nabla\cdot\left(\rho_{S_2}\vec{V}_{S_2}\right)=-m_S\left(\dot{n}_S+k_d^e n_e n_{S_2}\right) \tag{2.46}$$

$$\frac{\partial\rho_S}{\partial t}+\nabla\cdot(\rho_S\vec{u})+\nabla\cdot\left(\rho_S\vec{V}_S\right)=m_S\left(\dot{n}_S+k_d^e n_e n_{S_2}-\dot{n}_e\right) \tag{2.47}$$

$$\frac{\partial\rho_{S_+}}{\partial t}+\nabla\cdot(\rho_{S_+}\vec{u})+\nabla\cdot\left(\rho_{S_+}\vec{V}_{S_+}\right)=m_S\dot{n}_e \tag{2.48}$$

$$\frac{\partial\rho_e}{\partial t}+\nabla\cdot(\rho_e\vec{u})+\nabla\cdot\left(\rho_e\vec{V}_{S_+}\right)=m_e\dot{n}_e \tag{2.49}$$

where S_2 denotes the diatomic species, S denotes the atomic species, $S+$ applies to the atomic ions, and e applies to electrons. The current density does not appear in the electron equation, since $\nabla\cdot\vec{j}=0$. In the above equations, $\dot{n}_S$ represents the net rate of production of monatomic neutrals per unit volume by heavy species dissociating collisions, $k_d^e n_e n_{S_2}$ represents the rate of production of atomic species per unit volume by electron impact

dissociation, and $\dot{n}_e$ represents the net production of electrons (and ions) per unit volume through inelastic collisions. Throughout this research, it is assumed that the production of molecular ions, S_2^+ is negligible, so no corresponding mass conservation equation is needed. The dissociation process, as can be seen, is modeled by including electron impact dissociation of the molecules in addition to dissociation and recombination due to collisions between the heavy species. In addition, the probability of an electron colliding with a molecule, dissociating it, and further ionizing one or both of the atoms is assumed to be much smaller than the probability of two separate collisions causing the same outcome.

Adding over all species, the source terms of the species equations cancel, giving the global mass conservation equation,

$$\frac{\partial \rho}{\partial t} + \nabla \cdot (\rho \vec{u}) = 0, \tag{2.50}$$

or, in axisymmetric coordinates,

$$\frac{\partial \rho}{\partial t} + \frac{\partial \rho u_r}{\partial r} + \frac{\rho u_r}{r} + \frac{\partial \rho u_z}{\partial z} = 0. \tag{2.51}$$

Since quasi-neutrality is assumed, only the global and two of the species mass conservation equations are needed to fully determine the composition of the flow of a diatomic propellant.

2.2.5 Momentum Conservation Equations

By utilizing Equation 2.12, summing over all species, and utilizing the definitions of the global density, mass averaged velocity, and pressure, the global momentum conservation equation can be found. After separating out the viscous stress tensor (cf. Equation 2.32) and summing over all species, the collisional momentum transfer and electric field terms cancel, and the global momentum conservation equations, in component form, are found to be

$$\frac{\partial}{\partial t}(\rho u_r) + \frac{\partial}{\partial r}\left(\rho u_r^2 + p - \tau_{rr}\right) + \frac{\partial}{\partial z}(\rho u_r u_z - \tau_{rz}) + \frac{1}{r}\left(\rho u_r^2 - \rho u_\theta^2 - \tau_{rr} + \tau_{\theta\theta}\right) = 0 \tag{2.52}$$

$$\frac{\partial}{\partial t}(\rho u_\theta) + \frac{\partial}{\partial r}(\rho u_r u_\theta - \tau_{r\theta}) + \frac{\partial}{\partial z}(\rho u_\theta u_z - \tau_{\theta z}) + \frac{2}{r}(\rho u_r u_\theta - \tau_{r\theta}) = 0 \tag{2.53}$$

$$\frac{\partial}{\partial t}(\rho u_z) + \frac{\partial}{\partial r}(\rho u_r u_z - \tau_{rz}) + \frac{\partial}{\partial z}\left(\rho u_z^2 + p - \tau_{zz}\right) + \frac{1}{r}(\rho u_r u_z - \tau_{rz}) = 0, \tag{2.54}$$

where

$$\tau_{rr} = \frac{2}{3}\mu_g \left(2\frac{\partial u_r}{\partial r} - \frac{\partial u_z}{\partial z} - \frac{u_r}{r}\right) \tag{2.55}$$

$$\tau_{\theta\theta} = \frac{2}{3}\mu_g \left(2\frac{u_r}{r} - \frac{\partial u_r}{\partial r} - \frac{\partial u_z}{\partial z}\right) \tag{2.56}$$

$$\tau_{zz} = \frac{2}{3}\mu_g \left(2\frac{\partial u_z}{\partial z} - \frac{\partial u_r}{\partial r} - \frac{u_r}{r}\right) \tag{2.57}$$

$$\tau_{r\theta} = \mu_g \left(\frac{\partial u_\theta}{\partial r} - \frac{u_\theta}{r}\right) \tag{2.58}$$

$$\tau_{rz} = \mu_g \left(\frac{\partial u_r}{\partial z} + \frac{\partial u_z}{\partial r}\right) \tag{2.59}$$

and

$$\tau_{\theta z} = \mu_g \frac{\partial u_\theta}{\partial z}. \tag{2.60}$$

The heavy species viscosity coefficient, μ_g, will be derived later in Section 2.4.3 as a function of the species viscosities. As with the mass conservation equation, the azimuthal gradient terms have been neglected due to axisymmetry. In calculating the viscosity coefficient, the effect of the electrons is neglected. It can be shown that neglecting the electrons in the calculation of viscosity is a valid assumption [11, 35].

2.2.6 Energy Conservation Equations

It is assumed throughout this research that, since the gas within an arcjet is collision dominated, all of the heavy species (molecules, atoms, ions) have a common translational temperature, and that the molecular vibrational and rotational temperatures are in thermal equilibrium with this translational temperature. In addition, it is assumed that the electrons may have a temperature different from that of the heavy species. Therefore, two energy equations must be found, one for the heavy species, another for the electrons.

Heavy Species

The conservation equations for the heavy species are found using Equation 2.20. Again, after separating out the viscous stress tensor, the species energy conservation equations can be written as

$$\frac{\partial}{\partial t}\left(\rho_{S_2} E_{S_2}\right) + \nabla \cdot \left(\rho_{S_2} H_{S_2} \vec{u}_{S_2}\right) + \nabla \cdot \left(\overline{\overline{\tau}}_{S_2} \cdot \vec{u}_{S_2}\right) - \nabla \cdot \left(\kappa_{S_2} \nabla T_g\right) = M_{S_2} \tag{2.61}$$

$$\frac{\partial}{\partial t}(\rho_S E_S) + \nabla \cdot (\rho_S H_S \vec{u}_S) + \nabla \cdot (\overline{\overline{\tau}}_S \cdot \vec{u}_S) - \nabla \cdot (\kappa_S \nabla T_g) = M_S \tag{2.62}$$

$$\frac{\partial}{\partial t}(\rho_{S+} E_{S+}) + \nabla \cdot (\rho_{S+} H_{S+} \vec{u}_{S+}) + \nabla \cdot (\overline{\overline{\tau}}_{S+} \cdot \vec{u}_{S+}) - \nabla \cdot (\kappa_{S+} \nabla T_g) = \vec{j}_{S+} \cdot \vec{E} + M_{S+}, \tag{2.63}$$

where T_g is the temperature which is common to all heavy species, and the definition of total enthalpy per unit mass, $H_s = E_s + \frac{p_s}{\rho_s}$, has been used.

The total enthalpy H_s, of each species, and therefore, the total energy, is obtained through consideration of both the internal energy based on molecular degrees of freedom and the energies associated with dissociation and ionization. For the problem at hand, the energy of dissociation is bound to the atoms and ions, while the ionization energy is arbitrarily bound to the electrons. The enthalpy per particle for the heavy species may be written as

$$h_{S_2} = \frac{7}{2} k T_g - e_d + \frac{e_v}{e^{\frac{e_v}{kT_g}} - 1} + \Delta \tag{2.64}$$

for molecules, and

$$h_S = h_{S+} = \frac{5}{2} k T_g + \frac{\Delta}{2} \tag{2.65}$$

for atoms and ions, where e_d and e_v are characteristic energies of dissociation and vibration, respectively, and Δ is a constant chosen to make the enthalpy of the S_2 molecule vanish at the common reference temperature, $T_f = 298.15^o\text{K}$. The $\frac{7}{2}$ fraction for the diatomic species accounts for translation ($\frac{3}{2}kT$), rotation (kT), and pressure work (kT). There is no rotational energy associated with the atomic species and the ions, hence the $\frac{5}{2}$ coefficient (translation and pressure work only) in Equation 2.65. For the present application, the vibrational energy is negligible at the reference temperature, so $\Delta = e_d - \frac{7}{2} k T_f$. With this the heavy species enthalpies become

$$h_{S_2} = \frac{7}{2} k \left(T_g - T_f\right) + \frac{e_v}{e^{\frac{e_v}{kT_g}} - 1} \tag{2.66}$$

for molecules, and

$$h_S = h_{S+} = \frac{5}{2} k T_g + \frac{1}{2} e_d - \frac{7}{4} k T_f \tag{2.67}$$

for atoms and ions. The total enthalpy and energy per unit volume can then be written as

$$\rho H = \sum_s n_s h_s + \sum_s \frac{1}{2} \rho_s u_s^2$$

$$= \frac{5}{2}\left(\rho_S + \rho_{S+}\right) R_S T_g + \frac{7}{2}\rho_{S_2} R_{S_2} T_g + \frac{1}{2}\left(\rho_S + \rho_{S+}\right) R_S \theta_d + \frac{\rho_{S_2} R_{S_2} \theta_v}{e^{\frac{\theta_v}{T_g}} - 1}$$

$$- \frac{7}{2}\rho_{S_2} R_{S_2} T_f - \frac{7}{4}\left(\rho_S + \rho_{S+}\right) R_S T_f + \frac{1}{2}\rho_{S_2} u_{S_2}^2 + \frac{1}{2}\rho_S u_S^2 + \frac{1}{2}\rho_{S+} u_{S+}^2 \tag{2.68}$$

and

$$\rho E = \rho H - \rho_{S_2} R_{S_2} T_g - \left(\rho_S + \rho_{S+}\right) R_S T_g, \tag{2.69}$$

where $\theta_d = \frac{e_d}{k}$ and $\theta_v = \frac{e_v}{k}$ are the characteristic temperatures of dissociation and vibration, respectively.

Summing Equations 2.61-2.63 and utilizing the definition of slip velocity (Equation 2.27), the heavy species energy equation becomes

$$\frac{\partial \rho E}{\partial t} + \nabla \cdot (\rho H \vec{u}) - \nabla \cdot (\bar{\bar{\tau}} \cdot \vec{u}) + \nabla \cdot \left(\rho_{S_2} H_{S_2} \vec{V}_{S_2} + \rho_S H_S \vec{V}_S + \rho_{S+} H_{S+} \vec{V}_{S+}\right) - \nabla \cdot \left(\bar{\bar{\tau}}_{S_2} \cdot \vec{V}_{S_2}\right)$$

$$- \nabla \cdot \left(\bar{\bar{\tau}}_S \cdot \vec{V}_S\right) - \nabla \cdot \left(\bar{\bar{\tau}}_{S+} \cdot \vec{V}_{S+}\right) - \nabla \cdot (\kappa_g \nabla T_g) = M_{S_2} + M_S + M_{S+}, \tag{2.70}$$

where κ_g is an overall heavy species conductivity, to be derived in Section 2.4.4. In addition, the ion current density, $\vec{j}_{S+}$ is neglected, as the electrons carry the current. In Miller's work, the axial slip velocities were neglected, as it was assumed that they were negligible with respect to energy transport. In this thesis, however, the axial slip velocities are retained, as they may be important when used in conjunction with the diffusion velocity formulation of Section 2.4.2, especially in the region of the cathode tip. In addition, retaining these terms causes minimal extra computational effort. Therefore, Equation 2.70, in axisymmetric coordinates, may be rewritten as

$$\frac{\partial}{\partial t}(\rho E) + \frac{\partial}{\partial r}\left(\rho H u_r + q_{gr} - \tau_{rr} u_r - \tau_{r\theta} u_\theta - \tau_{rz} u_z\right) + \frac{1}{r}\left(\rho H u_r + q_{gr} - \tau_{rr} u_r - \tau_{r\theta} u_\theta - \tau_{rz} u_z\right)$$

$$+ \frac{\partial}{\partial z}\left(\rho H u_z + q_{gz} - \tau_{rz} u_r - \tau_{\theta z} u_\theta - \tau_{zz} u_z\right) + \frac{\partial}{\partial r}\left(\rho_{S_2} H_{S_2} V_{S_2 r} + \rho_S H_S V_{Sr} + \rho_{S+} H_{S+} V_{S+r}\right)$$

$$+ \frac{1}{r}\left(\rho_{S_2} H_{S_2} V_{S_2 r} + \rho_S H_S V_{Sr} + \rho_{S+} H_{S+} V_{S+r}\right)$$

$$+ \frac{\partial}{\partial z}\left(\rho_{S_2} H_{S_2} V_{S_2 z} + \rho_S H_S V_{Sz} + \rho_{S+} H_{S+} V_{S+z}\right) = E_l, \tag{2.71}$$

where

$$q_{gr} = -\kappa_g \frac{\partial T_g}{\partial r} \quad \text{and} \quad q_{gz} = -\kappa_g \frac{\partial T_g}{\partial z} \tag{2.72}$$

and

$$E_l = 3\frac{\rho_e}{m_S}\left(\overline{\nu}_{eS+} + \overline{\nu}_{eS} + \delta_{S_2}\overline{\nu}_{eS_2}\right) k\left(T_e - T_g\right). \tag{2.73}$$

The only term to remain after the summation of the M_s is the collisional energy transfer from the electrons to the heavy species, represented by E_l. In addition, the species diffusive viscous dissipation terms $(\nabla \cdot (\overline{\overline{\tau}}_s \cdot \vec{V}_s))$ were assumed to be negligible. The factor preceding the electron-molecule collision frequency, δ_{S_2}, the inelastic correction factor, is needed to compensate for the fact that not all of the electron-molecule collisions are elastic, as some energy may be transferred to internal modes, such as vibrational or rotational modes. The value of this correction factor over a range of electron temperatures is shown in Figure 2-1 for hydrogen and nitrogen (from Sutton and Sherman [49]).

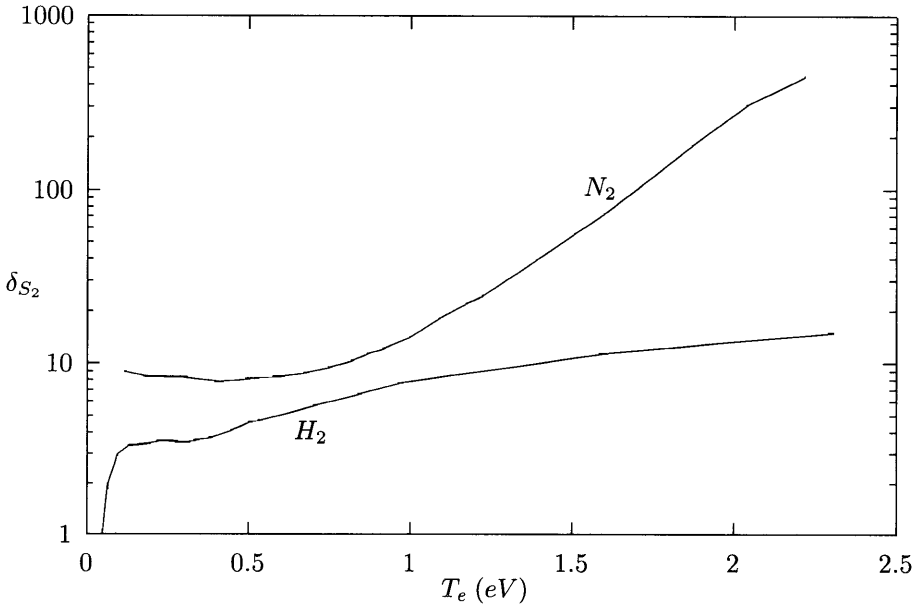

Figure 2-1: *Inelastic Correction Factor for Energy Transfer Between Electrons and Hydrogen and Nitrogen Molecules*

As stated by Miller [34], the strong conservative form of the energy equation, Equation 2.71, is not appropriate for the arcjet simulation. In certain regions of the flow, the dissociation energy dominates the total energy, while in other regions the kinetic energy dominates. The combined effect leads to a situation where the gas temperature is indeterminate or becomes negative in certain regions of the flow. To overcome this difficulty, Miller uses the internal energy form of the energy equation. In this form, the kinetic energy terms are eliminated by utilizing the species mass and momentum conservation equations. The terms

which include the dissociation energy can be moved to the right hand side of the equation as a single source term. This modified heavy species energy equation is not strongly conservative, but is accurate as long as the flow is free of shocks and other discontinuities:

$$\frac{\partial}{\partial t}(\rho e_g) + \frac{\partial}{\partial r}(\rho h_g u_r + q_{gr}) + \frac{1}{r}(\rho h_g u_r + q_{gr}) + \frac{\partial}{\partial z}(\rho h_g u_z + q_{gz}) - u_r \frac{\partial p_g}{\partial r} - u_z \frac{\partial p_g}{\partial z}$$

$$+\frac{\partial}{\partial r}(\rho_{S_2} h_{S_2} V_{S_2 r} + \rho_S h_S V_{Sr} + \rho_{S+} h_{S+} V_{S+r}) + \frac{1}{r}(\rho_{S_2} h_{S_2} V_{S_2 r} + \rho_S h_S V_{Sr} + \rho_{S+} h_{S+} V_{S+r})$$

$$+\frac{\partial}{\partial z}(\rho_{S_2} h_{S_2} V_{S_2 z} + \rho_S h_S V_{Sz} + \rho_{S+} h_{S+} V_{S+z}) - V_{S_2 r}\frac{\partial p_{S_2}}{\partial r} - V_{Sr}\frac{\partial p_S}{\partial r} - V_{S+r}\frac{\partial p_{S+}}{\partial r}$$

$$- V_{S_2 z}\frac{\partial p_{S_2}}{\partial z} - V_{Sz}\frac{\partial p_S}{\partial z} - V_{S+z}\frac{\partial p_{S+}}{\partial z} = \Phi + E_l - \frac{1}{2} e_d (\dot{n}_S + k_d^e n_e n_{S_2}), \tag{2.74}$$

where

$$\Phi = \mu_g \left[2\left(\frac{\partial u_r}{\partial r}\right)^2 + 2\left(\frac{\partial u_z}{\partial z}\right)^2 + 2\left(\frac{u_r}{r}\right)^2 + \left(\frac{\partial u_r}{\partial z} + \frac{\partial u_z}{\partial r}\right)^2 \right.$$

$$\left. + \left(\frac{\partial u_\theta}{\partial r} - \frac{u_\theta}{r}\right)^2 + \left(\frac{\partial u_\theta}{\partial z}\right)^2 - \frac{2}{3}\left(\frac{\partial u_r}{\partial r} + \frac{\partial u_z}{\partial z} + \frac{u_r}{r}\right)^2 \right] \tag{2.75}$$

is the viscous dissipation term,

$$\rho h_g = \frac{5}{2}(\rho_S + \rho_{S+}) R_S T_g + \frac{7}{2}\rho_{S_2} R_{S_2} T_g + \frac{\rho_{S_2} R_{S_2} \theta_v}{e^{\frac{\theta_v}{T_g}} - 1} - \frac{7}{4}\rho R_S T_f \tag{2.76}$$

and

$$\rho e_g = \rho h_g - \rho_{S_2} R_{S_2} T_g - (\rho_S + \rho_{S+}) R_S T_g \tag{2.77}$$

are the heavy species enthalpy per unit volume and energy per unit volume, respectively. As can be seen Equations 2.76 and 2.77 are indeed Equations 2.68 and 2.69 minus the terms associated with kinetic energy and dissociation energy. The energy per unit mass of the species is

$$e_{S_2} = \frac{5}{2} R_{S_2} T_g - \frac{7}{2} R_{S_2} T_f + \frac{R_{S_2}\theta_v}{e^{\frac{\theta_v}{T_g}} - 1} \tag{2.78}$$

for molecules, and

$$e_S = e_{S+} = \frac{3}{2} R_S T_g - \frac{7}{4} R_S T_f \tag{2.79}$$

for atoms and ions. The species enthalpies are given by

$$h_s = e_s + \frac{p_s}{\rho_s} = e_s + R_s T_g . \tag{2.80}$$

Electrons

Equation 2.20 written for the electrons becomes:

$$\frac{\partial}{\partial t}\left(\rho_e E_e\right) + \nabla \cdot \left(\rho_e E_e \vec{u}_e\right) + \nabla \cdot \left(\overline{\overline{p}}_e \cdot \vec{u}_e\right) - \nabla \cdot \left(\kappa_e \nabla T_e\right) = \vec{j}_e \cdot \vec{E} + M_e. \tag{2.81}$$

Expanding the energy terms and including the ionization energy per particle, the electron energy conservation equation becomes

$$\frac{\partial}{\partial t}\left(\frac{3}{2}p_e + \frac{1}{2}\rho_e u_e^2 + \rho_e \frac{e_i}{m_e}\right) + \nabla \cdot \left(\frac{5}{2}p_e \vec{u}_e + \frac{1}{2}\rho_e u_e^2 \vec{u}_e + \rho_e \frac{e_i}{m_e}\vec{u}_e\right) - \nabla \cdot \left(\kappa_e \nabla T_e\right)$$

$$= \frac{j^2}{\sigma} - E_l - e_d\, k_d^e\, n_e n_{S_2} - \dot{R}, \tag{2.82}$$

where viscous shear stress terms have been neglected. As in the heavy species energy equation, E_l represents the collisional energy transfer to the heavy species from the electrons. The energy lost per unit volume due to electron impact dissociation is denoted by $e_d\, k_d^e\, n_e n_{S_2}$, and $\dot{R}$ represents energy lost per unit volume due to radiation. As with the heavy species energy conservation equation, it is advantageous to relegate the ionization energy term to the right hand side as a source term. Using the species mass conservation equation applied to the electrons and the definitions of total species energy and enthalpy, Equation 2.82 becomes

$$\frac{\partial}{\partial t}\left(\rho_e E_e\right) + \frac{\partial}{\partial r}\left(\rho_e H_e u_{er} + q_{er}\right) + \frac{1}{r}\left(\rho_e u_{er} H_e + q_{er}\right) + \frac{\partial}{\partial z}\left(\rho_e H_e u_{ez} + q_{ez}\right)$$

$$= \frac{j^2}{\sigma} - E_l - e_d\, k_d^e\, n_e n_{S_2} - e_i \dot{n}_e - \dot{R}, \tag{2.83}$$

where

$$E_e = \frac{3}{2}R_e T_e + \frac{1}{2}u_e^2, \tag{2.84}$$

$$H_e = E_e + R_e T_e, \tag{2.85}$$

$$q_{er} = -\kappa_e \frac{\partial T_e}{\partial r} \quad \text{and} \quad q_{ez} = -\kappa_e \frac{\partial T_e}{\partial z}. \tag{2.86}$$

2.2.7 Additional Equations

In addition to the equations already derived, the specific heat ratio, γ, is required in the calculation of the Mach number and in obtaining the stability criteria used in calculating the time step for integrating the fluid equations. For monatomic species, $\gamma_S = \frac{5}{3}$, while for diatomic species at low temperatures $\gamma_{S_2} = \frac{7}{5}$. At higher temperatures, the vibrational excitation decreases the specific heat ratio of the molecule according to

$$\gamma_{S_2} = 1 + \frac{1}{\frac{5}{2} + \delta}, \tag{2.87}$$

where

$$\delta = \frac{\theta_v/T_g}{e^{\theta_v/T_g} - 1}. \tag{2.88}$$

The factor δ goes to zero as T_g approaches zero and goes to one as T_g becomes much larger than θ_v. This implies that at very high temperatures, $\gamma_{S_2} = \frac{9}{7}$. In general, the specific heat ratio of a mixture is approximated by

$$\gamma_{mix} = \frac{\overline{c}_p}{\overline{c}_v} = \frac{\overline{c}_v + \hat{R}}{\overline{c}_v}, \tag{2.89}$$

where $\overline{c}_v$ is the mole-averaged constant volume specific heat of the mixture, given by

$$\overline{c}_v = \sum_s x_s \hat{c}_{v,s} \quad [\mathrm{J/mol \cdot K}], \tag{2.90}$$

and $\hat{R}$ is the universal gas constant. For a monatomic species, the constant volume specific heat is

$$\hat{c}_{v,atomic} = \frac{3}{2}\hat{R}, \tag{2.91}$$

while for a diatomic species, the constant volume specific heat is

$$\hat{c}_{v,diatomic} = \hat{R}\left\{\frac{5}{2} + \left[\frac{\theta_v/2T}{\sinh(\theta_v/2T)}\right]^2\right\}. \tag{2.92}$$

For a heavy species mixture composed of diatomic molecules, atoms, monatomic ions and electrons, the specific heat ratio becomes

$$\gamma_{mix} = \frac{\frac{5}{2} + x_{S_2}\left\{1 + \left[\frac{\theta_v/2T_g}{\sinh(\theta_v/2T_g)}\right]^2\right\}}{\frac{3}{2} + x_{S_2}\left\{1 + \left[\frac{\theta_v/2T_g}{\sinh(\theta_v/2T_g)}\right]^2\right\}}. \tag{2.93}$$

Also of use are equations defining the mole and mass fractions of the different species. Assuming quasi-neutrality ($n_{S+} \approx n_e$), the mole fractions follow the relation

$$x_{S_2} + x_S + 2x_{S+} = 1. \tag{2.94}$$

Assuming that the mass of electrons is negligible, the mass fractions are found according to

$$\omega_{S_2} + \omega_S + \omega_{S+} = 1. \tag{2.95}$$

2.3 Dissociation and Ionization Processes

2.3.1 Overview

The chemical equation for the general reaction i with N_s species has the form

$$\sum_{j=1}^{N_s} \nu_{ij} s_j \rightleftharpoons \sum_{j=1}^{N_s} \nu'_{ij} s_j, \tag{2.96}$$

where s_j is the j^{th} species of the reaction, and ν_{ij} and ν'_{ij} are the stoichiometric coefficients of species s_j of reaction i. The arrows ($\rightleftharpoons$) denote the ability of a reaction to proceed in the forward ($\rightharpoonup$) or backward ($\leftharpoondown$) direction. In general, the forward and backward reactions need not occur at the same rate, resulting in a net production or depletion of a species.

Simple kinetic theory suggests, and experimental studies of chemical reactions corroborate, a certain form for the production and depletion rates of the various species involved in the reactions [53]. In this form, the rate of production of a species C is proportional to the product of the concentrations of the species from which C is produced. In other words, if a reaction is given by $aA + bB \rightarrow C$, then the production of C is governed by

$$\frac{d[C]}{dt} = k[A]^a [B]^b . \tag{2.97}$$

This form will be assumed in the discussion that follows. In terms of molar concentrations,

the net rate of production of species s_j for the *forward* reaction i is

$$\left(\frac{d\hat{n}_j}{dt}\right)_{f,i} = k_{f,i}\left(\nu'_{ij} - \nu_{ij}\right)\prod_{j=1}^{N_s}\left(\hat{n}_j\right)^{\nu_{ij}}, \tag{2.98}$$

while the net rate of production of species s_j for the *backward* reaction i is found to be

$$\left(\frac{d\hat{n}_j}{dt}\right)_{b,i} = k_{b,i}\left(\nu_{ij} - \nu'_{ij}\right)\prod_{j=1}^{N_s}\left(\hat{n}_j\right)^{\nu'_{ij}}. \tag{2.99}$$

Adding Equations 2.98 and 2.99 and summing over all reactions N_r results in the total net rate of production of species s_j:

$$\frac{d\hat{n}_j}{dt} = \sum_{i=1}^{N_r}\left(\nu'_{ij} - \nu_{ij}\right)\left[k_{f,i}\prod_{j=1}^{N_s}\left(\hat{n}_j\right)^{\nu_{ij}} - k_{b,i}\prod_{j=1}^{N_s}\left(\hat{n}_j\right)^{\nu'_{ij}}\right]. \tag{2.100}$$

This equation can also be applied to partial pressures, p_j, and number densities, n_j, with corresponding changes in the units of $k_{f,i}$ and $k_{b,i}$. In some situations, it is advantageous to use a forward rate constant of the form

$$k_{f,i} = A_i T^{n_{f,i}} \exp\left(-\frac{B_i}{\hat{R}T}\right), \tag{2.101}$$

where A_i, B_i and $n_{f,i}$ are constants obtained from curve fitting experimental data. This equation is known as the Arrhenius formula. The rate constant for the corresponding backward reaction usually has a simpler form,

$$k_{b,i} = C_i T^{n_{b,i}}. \tag{2.102}$$

In equilibrium, the net rate of production of all species over all reactions is zero. If we also assume micro-reversibility, then each individual reaction has a zero net production rate, and Equation 2.100 yields

$$k_{f,i}\prod_{j=1}^{N_s}\left(\hat{n}_j^*\right)^{\nu_{ij}} - k_{b,i}\prod_{j=1}^{N_s}\left(\hat{n}_j^*\right)^{\nu'_{ij}} = 0, \tag{2.103}$$

or

$$K_{c,i} \equiv \frac{k_{f,i}}{k_{b,i}} = \frac{\prod_{j=1}^{N_s} \left(\hat{n}_j^*\right)^{\nu'_{ij}}}{\prod_{j=1}^{N_s} \left(\hat{n}_j^*\right)^{\nu_{ij}}}, \tag{2.104}$$

where $K_{c,i}$ is defined as the equilibrium constant of reaction i, and the asterisks (*) denote equilibrium quantities. From Equations 2.101 and 2.102 it can be seen that the equilibrium constant is a function of temperature only. Substituting Equation 2.104 into Equation 2.100 yields another form of the net production rate:

$$\frac{d\hat{n}_j}{dt} = \sum_{i=1}^{N_r} \left(\nu'_{ij} - \nu_{ij}\right) k_{f,i} \left[\prod_{j=1}^{N_s} \left(\hat{n}_j\right)^{\nu_{ij}} - \frac{1}{K_{c,i}} \prod_{j=1}^{N_s} \left(\hat{n}_j\right)^{\nu'_{ij}}\right]. \tag{2.105}$$

By using different versions of the ideal gas law, the equilibrium constant may be obtained in terms of partial pressures or number densities. With $p_j^* = \hat{n}_j^* \hat{R} T$ the equilibrium constant can be written as

$$K_{p,i} = \frac{\prod_{j=1}^{N_s} \left(p_j^*\right)^{\nu'_{ij}}}{\prod_{j=1}^{N_s} \left(p_j^*\right)^{\nu_{ij}}}, \tag{2.106}$$

with

$$K_{p,i} = K_{c,i} \left(\hat{R}T\right)^{\sum_{j=1}^{N_s} \left(\nu'_{ij} - \nu_{ij}\right)}. \tag{2.107}$$

Alternatively, with $\hat{n}_j^* = n_j^*/N_A$, the equilibrium constant becomes

$$K_{n,i} = \frac{\prod_{j=1}^{N_s} \left(n_j^*\right)^{\nu'_{ij}}}{\prod_{j=1}^{N_s} \left(n_j^*\right)^{\nu_{ij}}}, \tag{2.108}$$

with

$$K_{n,i} = K_{c,i} \left(N_A\right)^{\sum_{j=1}^{N_s} \left(\nu'_{ij} - \nu_{ij}\right)} = K_{p,i} \left(kT\right)^{\sum_{j=1}^{N_s} \left(\nu_{ij} - \nu'_{ij}\right)}, \tag{2.109}$$

where N_A is Avogadro's number and $\hat{R}$ is the universal gas constant.

The equilibrium constant may be found from more theoretical arguments through the methods of statistical mechanics. Specifically, the equilibrium constant can be written in terms of partition functions, which indicate how the total energy of a population of particles may be partitioned over the various possible energy levels in which a particle can exist. For

example, the number of particles of species a existing in an energy level l is

$$\bar{N}_a^l = g_l \exp\left(-\frac{\epsilon_l + \mu_a}{kT}\right), \tag{2.110}$$

where μ_a is the chemical potential os species a and g_l is the degeneracy of level l, or the number of particles of type a populating level l at one time. The total number of particles of species a is simply

$$\bar{N}_a = \sum_l g_l \exp\left(-\frac{\epsilon_l + \mu_a}{kT}\right). \tag{2.111}$$

The sum on the right hand side of Equation 2.111 is known as the partition function of species a, denoted by Q_a.

It can be easily shown that this total partition function is expressible as the product of the individual partition functions for each independent energy type. For example, the partition function of a species a with translational, rotational, vibrational, and electronic excitation energies can be written as

$$Q_a = Q_{a,tr} Q_{a,rot} Q_{a,vib} Q_{a,el}. \tag{2.112}$$

For diatomic molecules, these partitions functions are given as

$$Q_{a,tr} = V\left(\frac{2\pi m_a kT}{h^2}\right)^{\frac{3}{2}} \tag{2.113}$$

$$Q_{a,rot} = \frac{1}{\sigma}\left(\frac{T}{\theta_r}\right) \tag{2.114}$$

$$Q_{a,vib} = \frac{1}{1 - e^{\theta_v/T}} \tag{2.115}$$

$$Q_{a,el} = \sum_m g_m e^{-\epsilon_m/kT} \tag{2.116}$$

for translation, rotation, vibration, end electronic excitation, respectively; where V is the volume, $h = 6.6261 \times 10^{-34}\ J \cdot s$ is Planck's constant, σ is a molecular symmetry factor (1 for heteronuclear diatomic molecules, 2 for homonuclear diatomic molecules), θ_r and θ_v are characteristic rotational and vibrational temperatures, and m denotes only the electron energy levels.

It is often easier to deal with partition functions per unit volume. Since only the translational partition function is proportional to volume, the total partition function per unit volume is given simply as

$$q_a = \frac{Q_a}{V} = \frac{Q_{a,tr}Q_{a,rot}Q_{a,vib}Q_{a,el}}{V} = q_{a,tr}q_{a,rot}q_{a,vib}q_{a,el} \tag{2.117}$$

Since $n_a = \frac{\tilde{N}_a}{V} = \frac{Q_a}{V} = q_a$, an explicit form of the equilibrium constant can be obtained by inserting Equation 2.117 into Equation 2.108:

$$K_{n,i} = \frac{\prod_{j=1}^{N_s}\left(n_j^*\right)^{\nu'_{ij}}}{\prod_{j=1}^{N_s}\left(n_j^*\right)^{\nu_{ij}}} = \frac{\prod_{j=1}^{N_s}\left(q_j\right)^{\nu'_{ij}}}{\prod_{j=1}^{N_s}\left(q_j\right)^{\nu_{ij}}}. \tag{2.118}$$

Typically, the energy levels of the various species are measured relative to a reference energy level. In hydrogen, for example, the reference state is the ground state of the hydrogen molecule, and the exponential of Equation 2.110 must be modified to take into account the difference between the ground state of the hydrogen molecule and the ground state of, say, the hydrogen atom. After this modification, the equilibrium constant becomes

$$K_{n,i} = \frac{\prod_{j=1}^{N_s}\left(q_j\right)^{\nu'_{ij}}}{\prod_{j=1}^{N_s}\left(q_j\right)^{\nu_{ij}}}\exp\left[\frac{1}{kT}\sum_{j=1}^{N_s}\left(\nu_{ij}-\nu'_{ij}\right)\epsilon_j^0\right], \tag{2.119}$$

where ϵ_j^0 is the energy of the ground state of species j relative to the ground state of the reference species. The equilibrium pressure and concentration constants can easily be found by appropriate substitution of Equation 2.119 into Equation 2.109.

2.3.2 Dissociation Processes

The chemical equation for dissociation of a diatomic gas is given by

$$M + S_2 \rightleftharpoons 2S + M. \tag{2.120}$$

The third body, M, is necessary to provide the energy necessary to dissociate the molecule and to carry away energy liberated by the atomic recombination. Over the range of temperatures where dissociation occurs (typically 1000 - 12000 K), data is readily available, and the equilibrium constants and forward rate constants of the Arrhenius form are easily found.

The dissociation energy of the hydrogen molecule is 4.516 eV (7.236×10^{-19} J), while the dissociation energy of the nitrogen molecule is 9.800 eV (1.570×10^{-18} J).

Equilibrium Dissociation

For a diatomic gas, the equilibrium constant in terms of partial pressures is

$$\frac{p_S^2}{p_{S_2}} = K_{p,dis}, \tag{2.121}$$

while in terms of number densities the constant becomes

$$K_{n,dis} = \frac{K_p}{kT} = \frac{n_S^2}{n_{S_2}} = \frac{q_S^2}{q_{S_2}} e^{-\theta_d/T}. \tag{2.122}$$

Using hydrogen as an example, the equilibrium constant can be written in terms of partition functions (neglecting electron excitation) as

$$K_{n,dis} = \frac{2\theta_r}{T} \left(\frac{\pi m_H kT}{h^2} \right)^{\frac{3}{2}} \left(1 - e^{-\theta_v/T} \right) e^{-\theta_d/T}, \tag{2.123}$$

or

$$K_{p,dis} = 2k\theta_r \left(\frac{\pi m_H kT}{h^2} \right)^{\frac{3}{2}} \left(1 - e^{-\theta_v/T} \right) e^{-\theta_d/T}, \tag{2.124}$$

where m_H is the mass of the hydrogen atom and the characteristic temperatures are appropriate to the hydrogen dissociation reaction.

As can be seen, the equilibrium constant is a function of temperature only for a given reaction. The equilibrium constant K_p can easily be found or calculated from the literature. It is often easier to use these tabulated values, as it becomes more difficult to evaluate the constant for more complex compounds and reactions. Figure 2-2 shows $\log_{10} K_{p,dis}$ versus temperature for both the hydrogen and nitrogen dissociation reactions, from the JANAF Thermochemical Tables [8]. These values are listed in tabular form in Appendix B for temperatures up to 6000 K. As listed, these values are for the dissociation of one half mole of H_2 into one mole of H. Therefore, these values must be multiplied by a factor of 2 to be used in Equation 2.121.

The effect of the higher dissociation energy of the nitrogen molecule is to lower the curve, as shown. The partial pressures of the diatomic and monatomic species can then

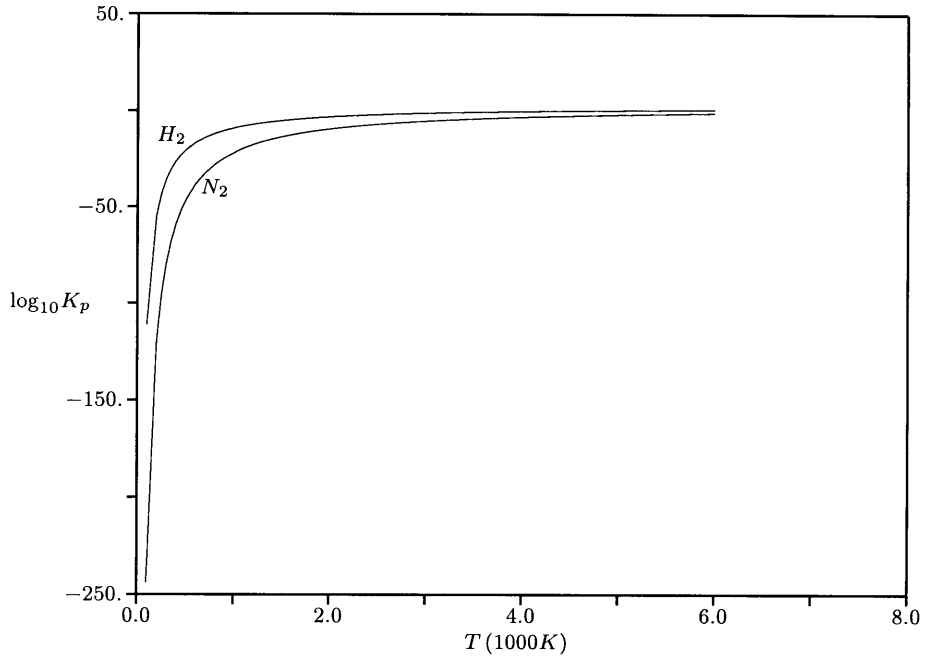

Figure 2-2: *Equilibrium Constant Versus Temperature for the Hydrogen and Nitrogen Dissociation Reactions*

be easily calculated using Equation 2.121. In practice, however, the partial pressures are usually obtained through simultaneous integration of the fluid equations. In this research, the equilibrium constant $K_{p,dis}$ is used solely to determine the nonequilibrium production of atomic species, to be discussed in the next section.

When only diatomic and monatomic neutrals are of concern, the equilibrium quantities can be calculated through the solution of a simple quadratic equation. Figures 2-3 and 2-4 show the equilibrium mole fraction of atomic hydrogen and nitrogen, respectively, for a range of temperatures and pressures. When ionization becomes a factor, simultaneous solution of this quadratic equation and another quadratic equation derived from the Saha equation is necessary.

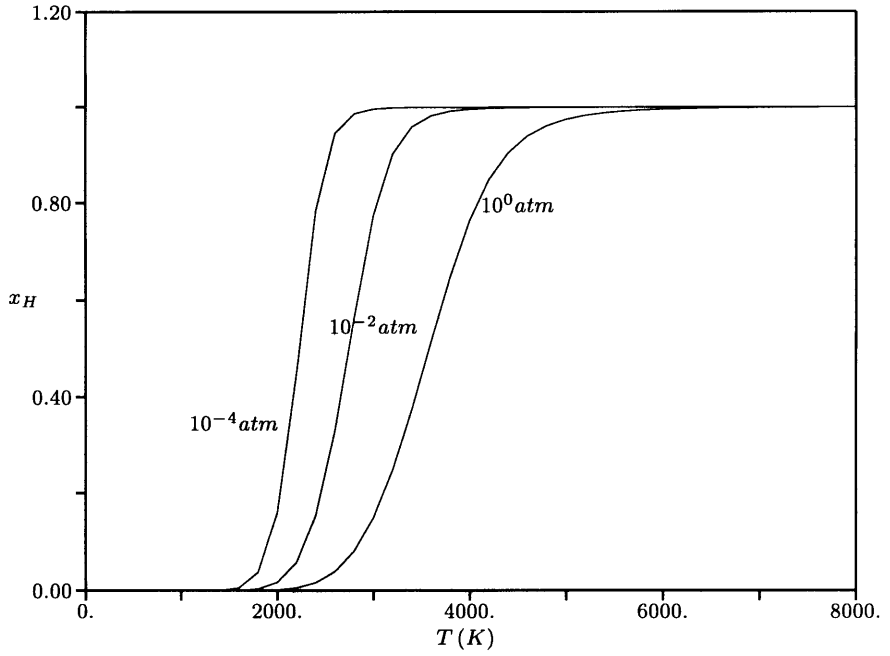

Figure 2-3: *Equilibrium Dissociation of Hydrogen versus Temperature and Pressure*

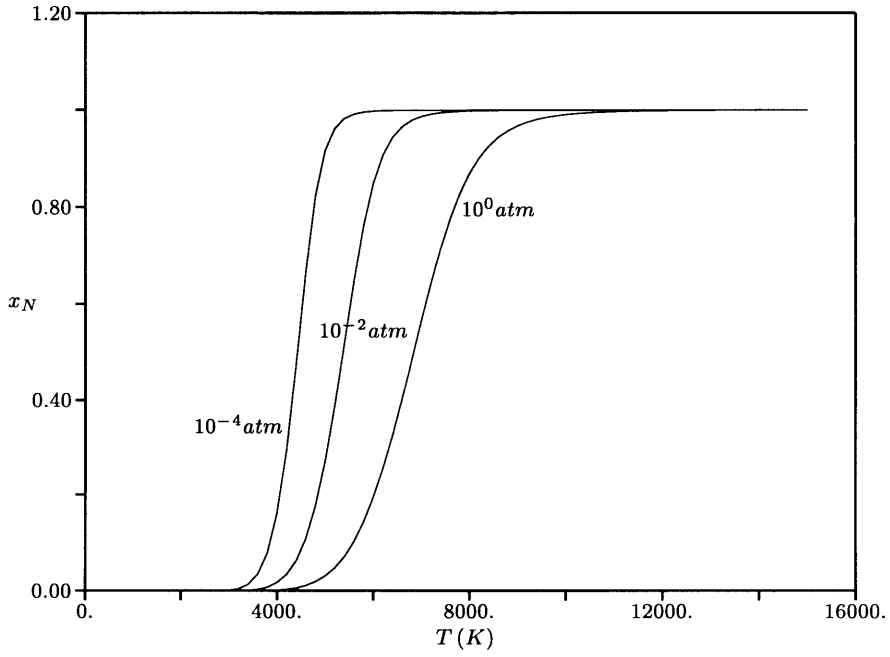

Figure 2-4: *Equilibrium Dissociation of Nitrogen versus Temperature and Pressure*

	Hydrogen	Nitrogen
$A\ (m^3/mol-s)$	5.5×10^{12}	2.1×10^{15}
$B\ (J/mol)$	435,600	943,800
n_f	-1.0	-1.5
$\hat{m}_S$	5.0	3.0
$\hat{m}_{S_2}$	2.0	5.0

Table 2.1: *Arrhenius Constants for the Hydrogen and Nitrogen Dissociation Rate Equations*

Nonequilibrium Dissociation

Nonequilibrium dissociation of diatomic species is considered so that a finite atomic production rate can exist. Equation 2.105, when applied to the dissociation-recombination process, becomes

$$\frac{d\hat{n}_S}{dt} = k_f \hat{n}_M \left(\hat{n}_{S_2} - \frac{1}{K_{c,dis}} \hat{n}_S^2 \right) \tag{2.125}$$

The third body molar concentration for reaction i is given as

$$\hat{n}_{M,i} = \sum_{j=1}^{N_s} \hat{m}_{ij} \hat{n}_j. \tag{2.126}$$

where the $\hat{m}_{ij}$ are known as the third body efficiencies. With the forward rate constant, k_f, given by Equation 2.101, and using Equation 2.125, the net production rate of atomic species can be written as

$$\dot{n}_S = A N_A T^{n_f} \exp\left(-\frac{B}{\hat{R}T} \right) \left(\hat{m}_S \hat{n}_S + \hat{m}_{S_2} \hat{n}_{S_2} \right) \left(\hat{n}_{S_2} - \frac{\hat{R}T}{K_{p,dis}} \hat{n}_S^2 \right). \tag{2.127}$$

The constants required by Equation 2.127 for hydrogen and nitrogen are listed in Table 2.1, and were taken from Rogers and Schexnayder [46] for hydrogen and Langan et al. [26] for nitrogen.

As it stands, Equation 2.127 does not take dissociation due to direct electron impact into account. To do so, a term of the form

$$\dot{n}_{S,e} = k_d^e n_e n_{S_2} \tag{2.128}$$

is added, where k_d^e is just the reaction rate coefficient of the $S_2 + e \rightarrow 2S + e$ reaction. For

the dissociation of diatomic hydrogen, the reaction rate coefficient[1] is taken from Janev et al. [23], and is shown id Figure 2-5. In the case of nitrogen, Capitelli and DiLonardo [6] calculate the value $k_d^e n_e$ for dissociation of diatomic nitrogen from the ground state. This modified form of the reaction rate coefficient is shown in Figure 2-6.

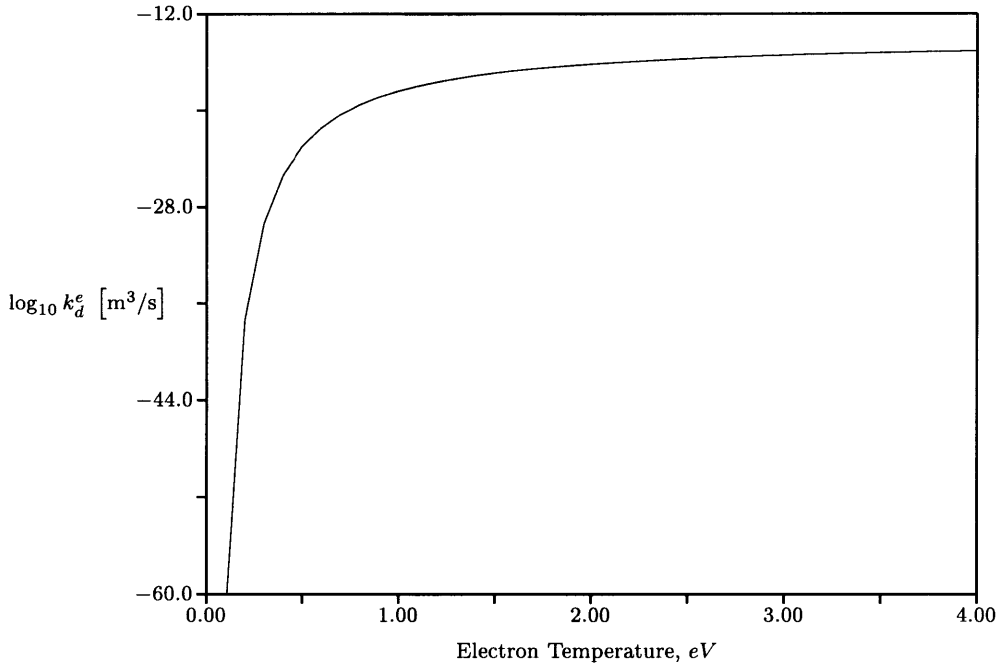

Figure 2-5: *Reaction Rate Coefficient k_d^e for the Electron Impact Dissociation of Hydrogen*

In the regions of flow within the arcjet where electron impact dissociation and the reverse reaction ($S + S + e \rightarrow S_2 + e$) may be important, it may be shown that the forward dissociation reaction dominates over the recombination reaction [23]. The total net rate of production of atomic species is then given by

$$\dot{n}'_S = \dot{n}_S + \dot{n}_{S,e}$$

$$= AN_A T^{n_f} \exp\left(-\frac{B}{\hat{R}T}\right)(\hat{m}_S \hat{n}_S + \hat{m}_{S_2}\hat{n}_{S_2})\left(\hat{n}_{S_2} - \frac{\hat{R}T}{K_{p,dis}}\hat{n}_S^2\right) + k_d^e n_e n_{S_2}. \qquad (2.129)$$

[1]Note: For hydrogen, the reaction rate coefficient k_d^e is identical to the reaction rate coefficient $< \sigma v >$ of Janev et al. [23] and Miller [34].

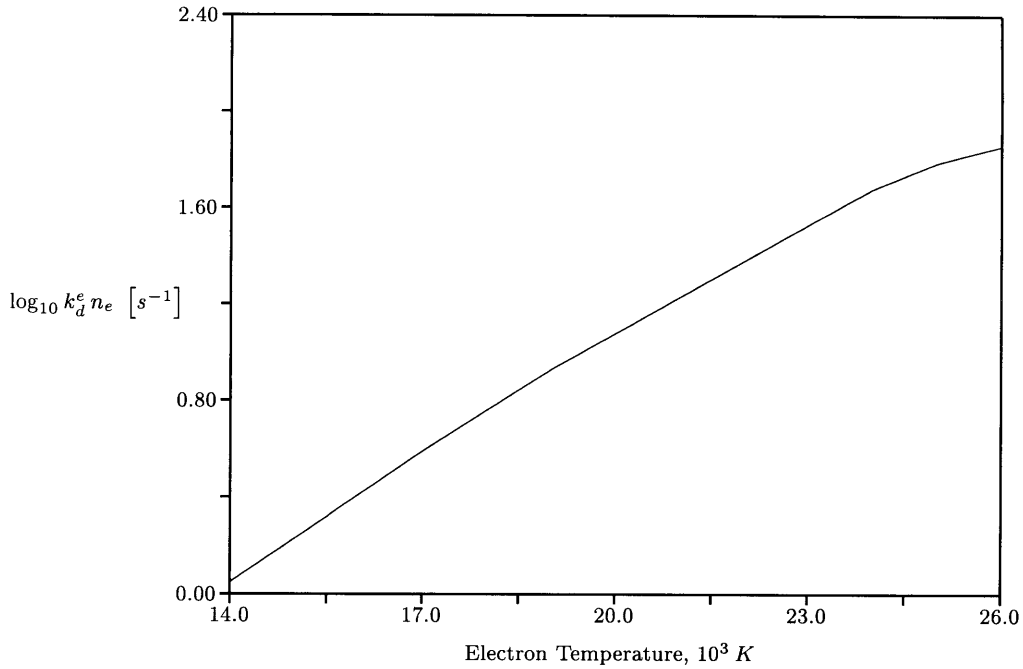

Figure 2-6: *Modified Reaction Rate Coefficient $k_d^e n_e$ for the Electron Impact Dissociation of Nitrogen*

2.3.3 Ionization Processes

The chemical equation for ionization of a monatomic gas is given by

$$e + S \rightleftharpoons e + e + S^+. \tag{2.130}$$

In the equation above, the electron is already assumed to be the third body. The reasoning for this is as follows. In the regions of the flow where significant amounts of molecules exist, a collision between an atom and a molecule would more likely dissociate the molecule, because of the lower molecular bond energy in comparison with the ionization energy. Also, in atom-atom collisions, it is highly improbable that the collision would ionize one of the atoms, since collisional coupling prevents the atoms from attaining the necessary translational energy. Therefore, it is the electron and its translational energy which directly accounts for ionization. The ionization energy of the hydrogen atom is 13.598 eV ($2.179 \times 10^{-18} J$), while the nitrogen atom has an ionization energy of 14.534 eV ($2.329 \times 10^{-18} J$).

Equilibrium Ionization

The equilibrium level of ionization can be calculated easily from the Saha equation, which is simply Equation 2.119 applied to the ionization reaction. Since quasi-neutrality is assumed ($n_e = n_{S+}$), the Saha equation may be written as

$$K_{n,ion} = \frac{n_e^2}{n_S} = \frac{2g_{S+}}{g_S}\left(\frac{2\pi m_e \kappa T_e}{h^2}\right)^{\frac{3}{2}} e^{-\epsilon_i/kT_e}, \tag{2.131}$$

where the g_s are the corresponding degeneracy functions ($g_e = 2$) and ϵ_i is the ionization energy of the atom considered. The electron temperature is used explicitly, since it is this temperature which is relevant to the ionization reaction, as suggested by the above discussion.

For the range of temperatures encountered within an arcjet, the degeneracies of the ground states of neutral and singly ionized atomic hydrogen can be approximated as $g_H \approx 2$ and $g_{H+} \approx 1$ [14]. The degeneracies of nitrogen vary appreciably, but can be approximated by linear curve fits [14],

$$g_N = 2.25 + 2.5 \times 10^{-4} T_g \quad \text{and} \quad g_{N+} = 7.95 + 1.5 \times 10^{-4} T_g. \tag{2.132}$$

Therefore, the Saha equation can be written as

$$\frac{n_e^2}{n_H} = 2.415 \times 10^{21} T_e^{\frac{3}{2}} \exp\left(\frac{-157,800}{T_e}\right) \tag{2.133}$$

for hydrogen, and

$$\frac{n_e^2}{n_N} = 4.83 \times 10^{21} \left(\frac{7.95 + 1.5 \times 10^{-4} T_g}{2.25 + 2.5 \times 10^{-4} T_g}\right) T_e^{\frac{3}{2}} \exp\left(\frac{-168,700}{T_e}\right) \tag{2.134}$$

for nitrogen.

Nonequilibrium Ionization

The net rate of production of electrons and, hence, ions is given by Equation 2.105 applied to the ionization reaction, and is given as

$$\dot{n}_e = k_f n_e \left(n_S - \frac{1}{K_{n,ion}} n_e^2\right). \tag{2.135}$$

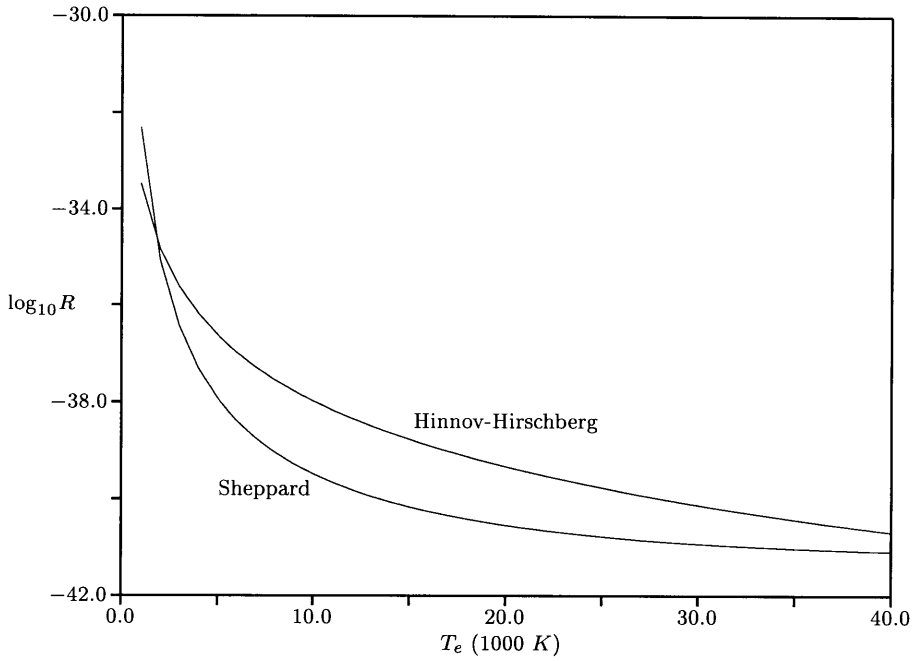

Figure 2-7: *Comparison of Hinnov-Hirschberg and Sheppard Reaction Rate Coefficients for the Recombination of Ionized Hydrogen*

This equation can be written in a generalized form after Mitchner and Kruger [35] as

$$\dot{n}_e = R\left(Sn_S - n_e^2\right), \tag{2.136}$$

where R is the recombination rate coefficient and $S = K_{n,ion}$. A typical recombination rate coefficient cited is that of Hinnov and Hirschberg [19]:

$$R_{HH} = 1.09 \times 10^{-20}\, T_e^{-\frac{9}{2}} n_e \quad \left[\mathrm{m}^3/\mathrm{s}\right]. \tag{2.137}$$

Hinnov and Hirschberg derived their recombination coefficient based on the structure of the hydrogen atom, and upon assumptions which break down above $3000K$. This coefficient does, indeed, give good results below this temperature, but can overestimate recombination dramatically at higher temperatures [35] [47]. Sheppard [47] found a hydrogen recombination rate coefficient based upon a three level collisional-radiative model valid for electron temperatures up to $60000K$:

$$R_{Sh} = 6.985 \times 10^{-42} \exp\left[\frac{\left(\ln\frac{T_e}{1000.0} - 4.0833\right)^2}{0.8179}\right] \quad \left[\mathrm{m}^3/\mathrm{s}\right]. \tag{2.138}$$

The Sheppard recombination rate coefficient is used in this research for hydrogen. Figure 2-7 shows a comparison of the Hinnov-Hirschberg and Sheppard recombination rate coefficients over a range of electron temperatures.

2.3.4 Dissociation and Ionization with Thermal Nonequilibrium

As mentioned in Section 2.2.1, an electron temperature different from the heavy species temperature is necessary in the non-equilibrium production of ions and electrons which are required for a self-consistent arc attachment at the anode. In the regions of arc attachment on the anode, Miller has shown that the electron temperature can be on the order of 20,000 K, while the heavy species temperature sits at a modest 1000 K. To demonstrate, the composition of hydrogen and nitrogen was calculated over a range of temperatures for two situations, the first assuming the electrons in thermal equilibrium with the heavy species and the second assuming an electron temperature at twice that of the heavy species temperature over the complete range of temperatures. Figures 2-8 and 2-10 show the composition of hydrogen and nitrogen, respectively, with the electron temperature in equilibrium with the heavy species temperature, at a pressure of one atmosphere. As can be seen, there are well defined regions of dominance for molecular, atomic, and ionic species. In comparison, Figures 2-9 and 2-11 show the composition of hydrogen and nitrogen, respectively, with the electron temperature fixed at $T_e = 2\,T_g$. The domain of dominance of the atomic species is greatly diminished, with the electrons pushing the composition towards ionization. In fact, for nitrogen, the domain of dominance is nearly nonexistent, due to the higher dissociation energy of the nitrogen molecule.

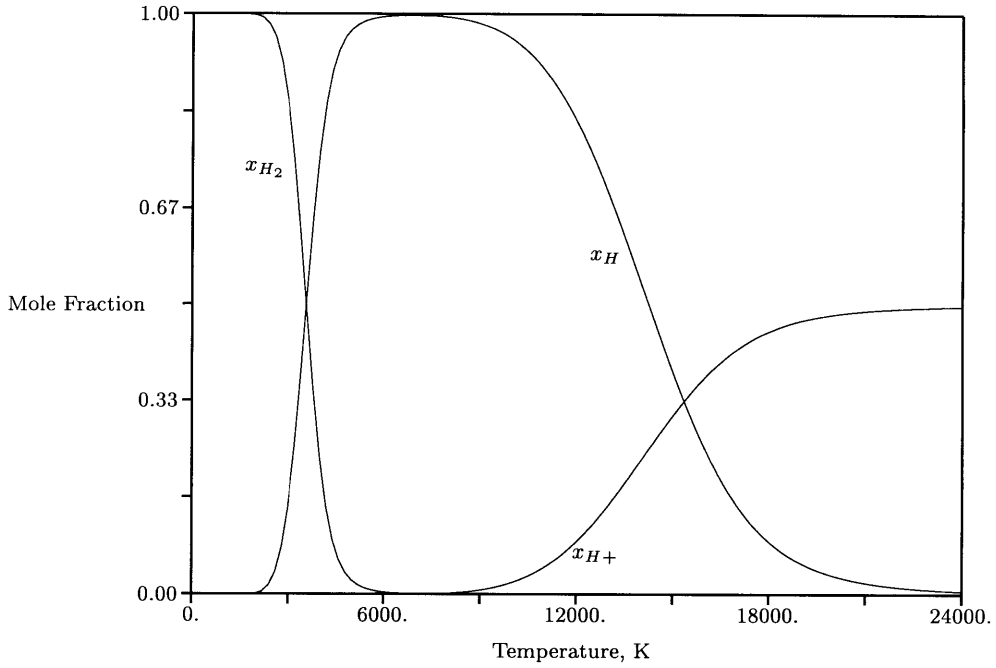

Figure 2-8: *Composition of Hydrogen in Chemical and Thermal Equilibrium, $p = 1\,atm$*

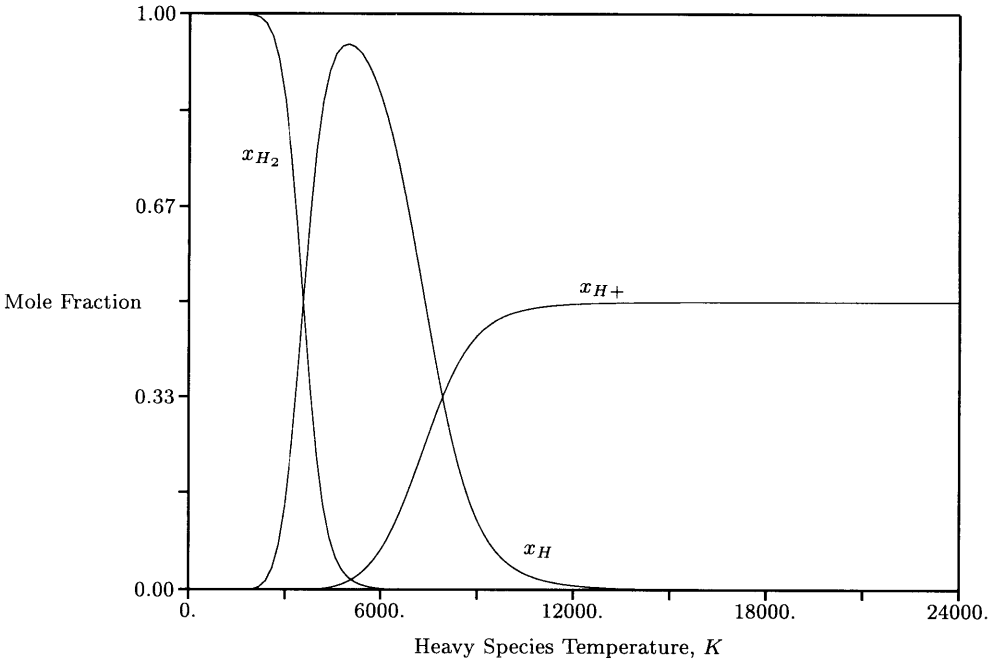

Figure 2-9: *Composition of Hydrogen, $p = 1\,atm$, $T_e = 2T_g$*

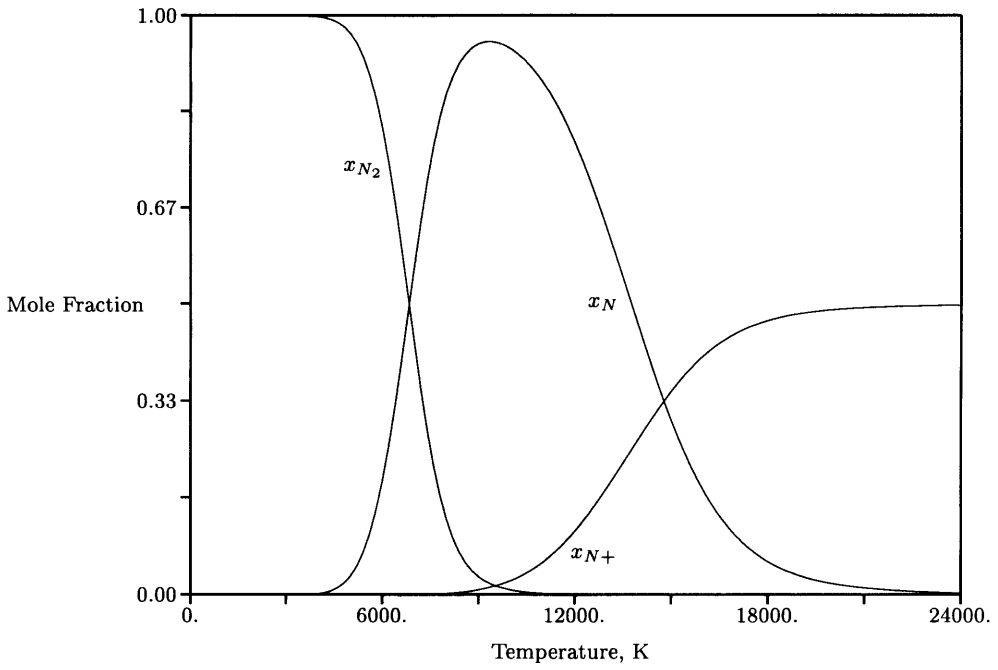

Figure 2-10: *Composition of Nitrogen in Chemical and Thermal Equilibrium, $p = 1\,atm$*

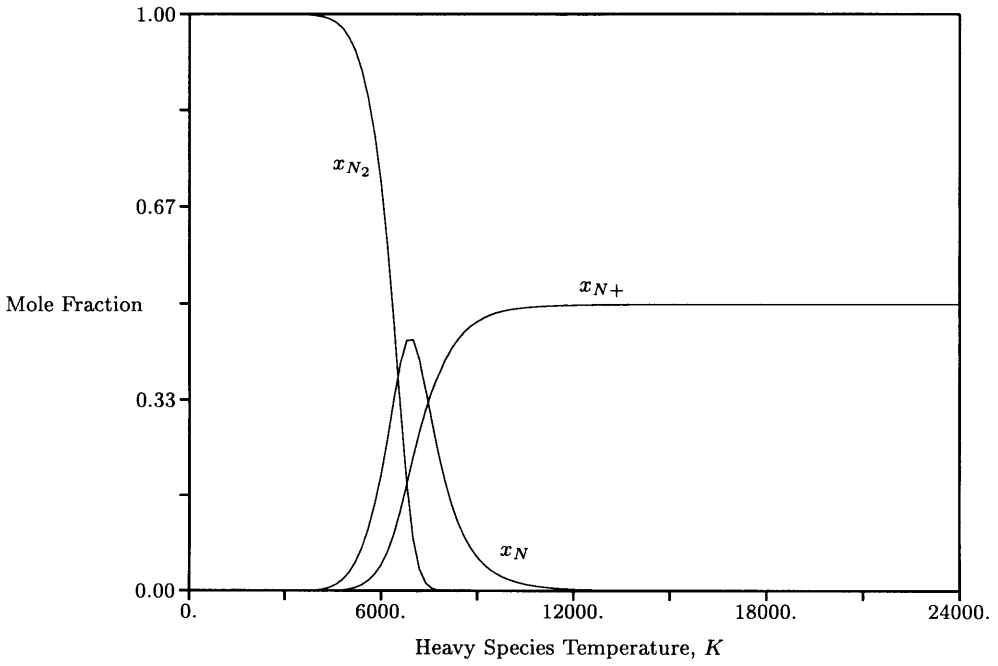

Figure 2-11: *Composition of Nitrogen, $p = 1\,atm$, $T_e = 2T_g$*

2.4 Transport Properties

Gradients in concentration, velocity, and temperature, cause a net transport of mass, momentum, and thermal energy, respectively. The general form of a flux of a property in terms of a gradient can be approximated by

$$\vec{J} = -c\nabla\varphi, \tag{2.139}$$

where $\vec{J}$ is the flux appropriate to quantity φ, and c is a proportionality constant known as the transport coefficient. The negative sign applies because the quantity is transported from regions of high concentration to regions of low concentration. The transport coefficient for mass transport is the diffusion coefficient, D ($m^2\,s^{-1}$), with the flux vector being represented as $\rho\vec{V}$, where $\vec{V}$ is the diffusion velocity. The diffusion velocity is only needed in cases where there are more than one species present. For momentum transport, the transport coefficient is the viscosity, μ ($kg\,m^{-1}\,s^{-1}$). This momentum flux has nine components, since both velocity and the gradient vector have three components each, and is typically called the viscous stress tensor, $\overline{\overline{\tau}}$. Finally, the transport coefficient applicable to the transport of thermal energy is the thermal conductivity, κ ($J\,m^{-1}\,s^{-1}\,K^{-1}$), with the flux vector being that of heat flux, $\vec{q}$. These flux vectors and their associated quantities and proportionality constants are summarized in Table 2.2.

Quantity	φ	c	$\vec{J}$
Mass	ρ	D	$\rho\vec{V}$
Momentum	$\vec{u}$	μ	$\overline{\overline{\tau}}$
Temperature	T	κ	$\vec{q}$

Table 2.2: *Flux Vectors and Associated Quantities Due to Gradients*

From mean free path arguments, the transport coefficients can only be found to an accuracy of the order of two or three [35]. Therefore, a more accurate method of determining the transport coefficients was deemed necessary. The Chapman-Enskog solution to the Boltzmann equation provides the required accuracy. The Chapman-Enskog solution is, technically, only valid in regions of thermal equilibrium and for distribution functions that are only slightly perturbed from Maxwellian (equilibrium). However, due to the highly

collisional flow within an electrothermal arcjet, it still gives a better approximation to the transport coefficients than do mean free path arguments.

2.4.1 Overview: Chapman-Enskog Solution to the Boltzmann Equation

The Chapman-Enskog solution is derived mathematically in texts by Chapman and Cowling [7] and Hirschfelder, Curtiss, and Bird [21]. In this section, the methods of Hirschfelder et al. will be utilized. To get the Chapman-Enskog solution, it is first assumed that the distribution function of species s is slightly perturbed from equilibrium:

$$f_s^1\left(\vec{r},\vec{v},t\right) = f_s^0\left(\vec{r},\vec{v},t\right)\left[1+\zeta_s\left(\vec{r},\vec{v},t\right)\right], \tag{2.140}$$

where

$$f_s^0 = n_s\left(\frac{m_s}{2\pi kT}\right)^{\frac{3}{2}}\exp\left(\frac{-m_s\left|\vec{v}_s\left(\vec{r},t\right)-\vec{u}\left(\vec{r},t\right)\right|^2}{2kT}\right) \tag{2.141}$$

is the Maxwellian distribution function in three dimensions and the perturbation function can be found to be

$$\zeta_s = -\left(\vec{A}_s\cdot\nabla\ln T\right) - \left(\overline{\overline{B}}_s{:}\nabla\vec{u}\right) + n\sum_r\left(\vec{C}_s^{(r)}\cdot\vec{d}_r\right), \tag{2.142}$$

where $\vec{A}_s$, $\overline{\overline{B}}_s$, and $\vec{C}_s^{(r)}$ are functions of velocity, concentration, and temperature; and $\vec{d}_r$ is the generalized driving force:

$$\vec{d}_r = \nabla x_r + \left(x_r-\omega_r\right)\frac{\nabla p}{p} - \left(\frac{n_r m_r}{p\rho}\right)\left[\frac{\rho}{m_r}\vec{F}_r - \sum_t n_t\vec{F}_t\right], \tag{2.143}$$

where x_r and ω_r are the mole and mass fractions of species r, respectively; and $\vec{F}_r$ and $\vec{F}_t$ are the body forces affecting species r and t, respectively.

By substituting Equation 2.140 into the Boltzmann equation (Equation 2.5) and taking the moments as in Section 2.1.2, a set of integral equations results. These equations are solved by the methods of variational calculus, using Sonine polynomials as test functions. The transport coefficients can then be represented as finite expansions of these polynomials. Chapman and Cowling assumed an infinite series of polynomials, while Hirschfelder et al. use a finite series of polynomials. The reason for this is that a very good approximation can be obtained with only a few terms of the Sonine polynomial expansion.

Chapman and Cowling have shown that these Sonine polynomial expansions can be written as a linear combination of *collision integrals*[2] :

$$\Omega_{ij}^{(l,s)}(T) = \sqrt{\frac{kT}{2\pi m_{ij}}} \int_0^\infty e^{-\gamma^2} \gamma^{2s+3} Q_{ij}^l(g)\, d\gamma, \tag{2.144}$$

where $\gamma^2 = \frac{1}{2} m_{ij} g^2/kT$, m_{ij} is the reduced mass of the colliding particles, g is the relative velocity of the colliding particles, and $Q_{ij}^l(g)$ is the integral cross section:

$$Q_{ij}^l(g) = 2\pi \int_0^\infty \left(1 - \cos^l \chi\right) b\, db\,. \tag{2.145}$$

The deflection angle, χ, is given by the equation

$$\chi(g,b) = \pi - 2b \int_{r_m}^\infty \frac{dr/r^2}{\left(1 - b^2/r^2 - V(r)/\frac{1}{2} m_{ij}\, g^2\right)^{\frac{1}{2}}}\,, \tag{2.146}$$

where b is the impact parameter and $V(r)$ is the interaction potential of the two colliding particles. The lower bound on the integral, r_m, occurs at the point where the denominator in Equation 2.146 vanishes. The interaction potential can have a variety of forms. Although the significance of l in Equation 2.144 is obvious, the significance of s is much more obscure. The factor s is the only remnant of the Sonine polynomial expansions left after construction of the collision integrals. They are directly related to the coefficients in the expansion and help take advantage of the unique orthogonality properties of the Sonine polynomials in defining macroscopic flow properties.

A common potential used in the calculation of collision integrals is the shielded Coulomb potential for charged particle interactions,

$$V(r) = Z_1 Z_2 \frac{e^2 \exp(-r/\lambda)}{r}, \tag{2.147}$$

where λ is a screening length, typically the Debye length:

$$\lambda_D = \sqrt{\frac{\epsilon_0 kT}{e^2 \sum_j Z_j^2 n_j}}. \tag{2.148}$$

[2]The notation of the collision integrals here is actually that of Hirschfelder et al. The $\Omega_{ij}^{(l,s)}$ integrals of Hirschfelder are identical to the $\Omega_{ij}^{(l)}(s)$ integrals of Chapman and Cowling.

This potential has an advantage in that the collision cross section of two colliding charged particles is not infinite, as is the case with the unscreened Coulomb potential. For neutral particle collisions, a potential which fits data very accurately is the Lennard-Jones potential

$$V(r) = 4\epsilon \left[\left(\frac{\sigma}{r}\right)^{12} - \left(\frac{\sigma}{r}\right)^{6} \right], \tag{2.149}$$

where ϵ and σ are parameters specific to the collision. For the simplest interaction potential, rigid hard spheres, the integral cross section and the collision integral have simple closed-form analytical solutions:

$$Q^l_{RS} = \left[1 - \frac{1}{2} \frac{1 + (-1)^l}{1 + l} \right] \pi \sigma_{ij}^2, \tag{2.150}$$

where σ_{ij} in this case is the effective radius of the colliding particles, and

$$\Omega^{(l,s)}_{RS} = \sqrt{\frac{kT}{2\pi m_{ij}}} \frac{(s+1)!}{2} Q^l_{RS}. \tag{2.151}$$

Rather than represent the transport coefficients in terms of pure collision integrals, the collision integrals are typically non-dimensionalized according to their rigid sphere values. These non-dimensional values can then be thought of as coefficients which correct for deviations from the rigid sphere model:

$$\Omega^{(l,s)*}_{ij} = \frac{\sqrt{\frac{2\pi m_{ij}}{kT}}\, \Omega^{(l,s)}_{ij}}{\frac{(s+1)!}{2} \left[1 - \frac{1}{2} \frac{1+(-1)^l}{1+l} \right] \pi \sigma_{ij}^2}. \tag{2.152}$$

The transport coefficients can be calculated using these non-dimensional values. In the equations representing the various transport coefficients, the effective collision radius (σ_{ij}) appears explicitly. Knowing this, the more frequent form of the collision integrals is that of an energy averaged cross section:

$$\langle \Omega^{(l,s)}_{ij} \rangle = \sigma_{ij}^2 \Omega^{(l,s)*}_{ij} = \left[\frac{\pi}{2} (s+1)! \left(1 - \frac{1}{2} \frac{1 + (-1)^l}{1 + l} \right) \right]^{-1} \int_0^\infty e^{-\gamma^2} \gamma^{2s+3} Q^l_{ij}(g)\, d\gamma. \tag{2.153}$$

It is this form of the collision integrals which is typically found in the literature.

2.4.2 Diffusion Coefficient

The first approximation to the diffusion coefficient of a pure substance (coefficient of *self diffusion*) is

$$D = 2.628 \times 10^{-7} \sqrt{\frac{T^3}{M}} \frac{1}{p \langle \Omega^{(1,1)} \rangle} \quad \left[\mathrm{m^2\,s^{-1}}\right], \tag{2.154}$$

where M is the molecular weight of the species, p is the pressure in atmospheres, T is in Kelvins, and $\langle \Omega^{(1,1)} \rangle$ is in units of $\mathring{A}^2$. The first approximation for the coefficient of *binary* diffusion (i.e. two species) is

$$D_{12} = 2.628 \times 10^{-7} \sqrt{\frac{T^3 \left(M_1 + M_2\right)}{2 M_1 M_2}} \frac{1}{p \langle \Omega_{12}^{(1,1)} \rangle}. \tag{2.155}$$

For flows where there are more than two species, the *multicomponent* diffusion coefficients $\overline{D}_{ij}$ are given in terms of binary diffusion coefficients by Hirschfelder as:

$$\overline{D}_{ij} = \frac{1}{M_j} \left(\sum_k x_k M_k \right) \frac{K^{ji} - K^{ii}}{|K|}, \tag{2.156}$$

where the summation is taken to be over all species, x_k is the mole fraction of species k,

$$K_{ij} = \frac{x_i}{D_{ij}} + \frac{M_j}{M_i} \sum_{k \neq i} \frac{x_k}{D_{ik}}, \quad i \neq j \tag{2.157}$$

$K_{ii} = 0$, $|K|$ is the determinant of the K_{ij} and the K^{ji} are the minor determinants

$$K^{ji} = (-1)^{i+j} \begin{vmatrix} 0 & \cdots & K_{1,i-1} & K_{1,i+1} & \cdots & K_{1,\nu} \\ \vdots & & \vdots & \vdots & & \vdots \\ K_{j-1,1} & \cdots & K_{j-1,i-1} & K_{j-1,i+1} & \cdots & K_{j-1,\nu} \\ K_{j+1,1} & \cdots & K_{j+1,i-1} & K_{j+1,i+1} & \cdots & K_{j+1,\nu} \\ \vdots & & \vdots & \vdots & & \vdots \\ K_{\nu,1} & \cdots & K_{\nu,i-1} & K_{\nu,i+1} & \cdots & K_{\nu,\nu} \end{vmatrix}, \tag{2.158}$$

and ν is the total number of species present.

As can be seen, the multicomponent diffusion coefficients are given as ratios of determinants. For a ternary mixture, the mathematics is relatively straight forward. However, as the number of species increases, Equations 2.156 - 2.158 become increasingly cumbersome

and computationally intensive. Therefore an alternative formulation according to Krier et al. [24] is used. In this formulation, the multicomponent diffusion coefficients are replaced by *effective* diffusion coefficients D_i. For species i,

$$D_i = \frac{1 - x_i}{\sum_{j \neq i} \frac{x_j}{D_{ij}}}, \tag{2.159}$$

where the D_{ij} are the binary diffusion coefficients defined above. As will be shown in Section 4.1.3, this approximation of the diffusion coefficients is crude, and doesn't always yield desirable results. However, it does take into account a flow's multicomponent nature, and is easy to calculate.

Throughout this thesis, ambipolar diffusion for the charge particles is assumed. Ambipolar diffusion may be described in the following way. Gradients in pressure and concentration cause a diffusion of electrons and ions. Since the electrons have a much smaller mass than the ions, they tend to diffuse at a much higher speed than do the ions. This causes a local charge separation, which in turn creates a local electric field. This local field tends to retard the electrons and speed up the ions, so that both ions and electrons tend to diffuse at the same common speed. Since the only charged particles modeled in this thesis are electrons and monatomic ions, the ambipolar diffusion coefficient can be written as

$$D_a = \frac{D_e \psi_{S+} + D_{S+} \psi_e}{\psi_{S+} + \psi_e}, \tag{2.160}$$

where ψ_{S+} and ψ_e are the monatomic ion and electron mobilities, respectively. The mobilities are given by the Einstein relation

$$\psi_i = \frac{eD_i}{kT_i}. \tag{2.161}$$

In a flow in which the ions are collisionally coupled to the other heavy species, the electron mobility is much greater than the ion mobility, so that

$$D_a \approx D_{S+} + \frac{\psi_{S+}}{\psi_e} D_e \,. \tag{2.162}$$

Substituting Equation 2.159 and the Einstein relation (Equation 2.161) for both ions and

electrons into Equation 2.162 yields the ambipolar diffusion coefficient used in this research

$$D_a = \left(1 + \frac{T_e}{T_g}\right) D_{S+} = \left(1 + \frac{T_e}{T_g}\right) \frac{1 - x_{S+}}{\frac{x_{S+}}{D_{S+,e}} + \frac{x_S}{D_{S+,S}} + \frac{x_{S_2}}{D_{S+,S_2}}}. \tag{2.163}$$

The formulation of this ambipolar diffusion coefficient is different than the formulation used by Miller. These differences are discussed in Section 4.1.2, along with differences in the other transport coefficients.

In this research, four species are modeled, diatomic molecules, atoms, monatomic ions and electrons. Consequently, Equations 2.28 and 2.34 become

$$\rho_{S_2}\vec{V}_{S_2} + \rho_S\vec{V}_S + \rho_{S+}\vec{V}_{S+} + \rho_e\vec{V}_e = 0 \tag{2.164}$$

and

$$\vec{j} = en_e\left(\vec{V}_{S+} - \vec{V}_e\right), \tag{2.165}$$

respectively. Substituting Equation 2.165 into Equation 2.164 and neglecting terms of order $\frac{m_e}{m_S}$ yields

$$\rho_{S_2}\vec{V}_{S_2} + \rho_S\vec{V}_S + \rho_{S+}\vec{V}_{S+} = \frac{m_e}{e}\vec{j}. \tag{2.166}$$

With the current density $\vec{j}$ determined from the electric potential equation and armed with Equation 2.166, two gradients and two effective diffusion coefficients are necessary to determine the diffusion velocities uniquely. Due to the crudeness of the effective diffusion coefficient approximation, care must be taken in choosing which species are calculated explicitly. In this research, it was found that the best results were achieved by calculating the ambipolar and molecular diffusion explicitly, with the atomic species "taking up the slack" in Equation 2.166. When this is the case, the ion, atomic, and molecular diffusive mass fluxes are, respectively,

$$\rho_{S+}\vec{V}_{S+} = -D_a\frac{m_S}{m_e}\nabla\rho_e\,, \tag{2.167}$$

$$\rho_S\vec{V}_S = \frac{m_e}{e}\vec{j} + D_a\frac{m_S}{m_e}\nabla\rho_e + D_{S_2}\nabla\rho_{S_2}\,, \tag{2.168}$$

and

$$\rho_{S_2}\vec{V}_{S_2} = -D_{S_2}\nabla\rho_{S_2}. \tag{2.169}$$

2.4.3 Viscosity

The first approximation to the viscosity coefficient is (from [21])

$$\mu = 2.6693 \times 10^{-6} \frac{\sqrt{MT}}{\langle \Omega^{(2,2)} \rangle} \qquad \left[\mathrm{kg\,m^{-1}\,s^{-1}}\right], \tag{2.170}$$

while the first approximation of a binary mixture is given as

$$\mu_{12} = 2.6693 \times 10^{-6} \sqrt{\frac{2M_1M_2T}{M_1+M_2}} \frac{1}{\langle \Omega_{12}^{(2,2)} \rangle}, \tag{2.171}$$

with $\langle \Omega_{12}^{(2,2)} \rangle$ in $\mathring{A}^2$. As with the diffusion coefficient, the first approximation for the viscosity of a multicomponent mixture can be represented as a ratio of determinants:

$$\mu_{mix} = -\frac{\begin{vmatrix} H_{11} & H_{12} & H_{13} & \cdots & H_{1\nu} & x_1 \\ H_{12} & H_{22} & H_{23} & \cdots & H_{2\nu} & x_2 \\ H_{13} & H_{23} & H_{33} & \cdots & H_{3\nu} & x_3 \\ \vdots & \vdots & \vdots & & \vdots & \vdots \\ H_{1\nu} & H_{2\nu} & H_{3\nu} & \cdots & H_{\nu\nu} & x_\nu \\ x_1 & x_2 & x_3 & \cdots & x_\nu & 0 \end{vmatrix}}{\begin{vmatrix} H_{11} & H_{12} & H_{13} & \cdots & H_{1\nu} \\ H_{12} & H_{22} & H_{23} & \cdots & H_{2\nu} \\ H_{13} & H_{23} & H_{33} & \cdots & H_{3\nu} \\ \vdots & \vdots & \vdots & & \vdots \\ H_{1\nu} & H_{2\nu} & H_{3\nu} & \cdots & H_{\nu\nu} \end{vmatrix}}, \tag{2.172}$$

where

$$H_{ii} = \frac{x_i^2}{\mu_i} + \sum_{k \neq i} \frac{2x_ix_k}{M_i+M_k} \frac{\hat{R}T}{pD_{ik}} \left(1 + \frac{3}{5}\frac{M_k}{M_i}\frac{\langle \Omega_{ik}^{(2,2)} \rangle}{\langle \Omega_{ik}^{(1,1)} \rangle}\right) \tag{2.173}$$

for the diagonal terms and

$$H_{ij} = -\frac{2x_ix_j}{M_i+M_j} \frac{\hat{R}T}{pD_{ij}} \left(1 - \frac{3}{5}\frac{\langle \Omega_{ij}^{(2,2)} \rangle}{\langle \Omega_{ij}^{(1,1)} \rangle}\right) \tag{2.174}$$

for the off diagonal terms, and where $\hat{R}$ is the universal gas constant.

As before for the diffusion coefficient, the matrix form for the multicomponent viscosity coefficient is much too cumbersome to use in a fluid dynamic code. Instead, the pure viscosity coefficients for each species are calculated according to Equation 2.170. The mixture rule of Mitchner and Kruger is then used to obtain the mixture viscosity. This mixture rule is given as [35]

$$\mu_{mix} \approx \sum_{i=1}^{\nu} \frac{n_i \mu_i}{\sum_{j=1}^{\nu} n_j \chi_{ij}}, \tag{2.175}$$

where

$$\chi_{ij} = \sqrt{\frac{2m_{ij}}{m_i}} \frac{\langle \Omega_{ij}^{(2,2)} \rangle}{\langle \Omega_{ii}^{(2,2)} \rangle}. \tag{2.176}$$

Using this equation, the heavy species viscosity coefficient is approximated as

$$\mu_g \approx \frac{n_{S_2}\mu_{S_2}}{n_{S_2} + n_S\sqrt{\frac{2}{3}}\frac{\langle \Omega_{S_2S}^{(2,2)} \rangle}{\langle \Omega_{S_2S_2}^{(2,2)} \rangle} + n_{S+}\sqrt{\frac{2}{3}}\frac{\langle \Omega_{S_2S+}^{(2,2)} \rangle}{\langle \Omega_{S_2S_2}^{(2,2)} \rangle}} + \frac{n_S\mu_S}{n_{S_2}\sqrt{\frac{4}{3}}\frac{\langle \Omega_{S_2S}^{(2,2)} \rangle}{\langle \Omega_{SS}^{(2,2)} \rangle} + n_S + n_{S+}\frac{\langle \Omega_{SS+}^{(2,2)} \rangle}{\langle \Omega_{SS}^{(2,2)} \rangle}}$$

$$+ \frac{n_{S+}\mu_{S+}}{n_{S_2}\sqrt{\frac{4}{3}}\frac{\langle \Omega_{S_2S+}^{(2,2)} \rangle}{\langle \Omega_{S+S+}^{(2,2)} \rangle} + n_S\frac{\langle \Omega_{SS+}^{(2,2)} \rangle}{\langle \Omega_{S+S+}^{(2,2)} \rangle} + n_{S+}}. \tag{2.177}$$

This version differs from that of Miller, who neglects the ion-molecule interaction, and compensates by adding a multiplicative factor of 2 to certain terms in the denominators.

In fluid mechanical calculations considered within this research, the mass fractions are never allowed to vanish, for numerical reasons. In Miller's research, he took the minimum mass fractions of molecules, atoms, and ions to be 3×10^{-3}, 1×10^{-4}, and 1×10^{-6}, respectively. It was found that if Miller's formulation was applied as is, and if these limiters were used, the viscosity heavily favors the molecular viscosity in the ionization regions, due to the lack of a n_{S+} term in the denominator of the molecular viscosity term. When one adds a term proportional to n_{S+} in the denominators of the first term and third terms, or if the mass fractions are allowed to vanish, the viscosity exhibits the behavior as stated in Miller's thesis. Therefore, great care must be taken when considering the limiting mass fractions. For this reason, the terms due to the ion-molecule interaction were retained, utilizing the appropriate collision integrals. In addition, it was found that the multiplicative factor of 2 did not affect the viscosity appreciably. As no justification was given or found for this factor, it was omitted in this research.

Finally, to reduce roundoff error in the actual computation, a variation of Equation 2.177, utilizing the mole fractions of the various species, is used instead:

$$\mu_g \approx \frac{x_{S_2}\mu_{S_2}}{x_{S_2} + x_S\sqrt{\frac{2}{3}}\frac{\langle\Omega^{(2,2)}_{S_2S}\rangle}{\langle\Omega^{(2,2)}_{S_2S_2}\rangle} + x_{S+}\sqrt{\frac{2}{3}}\frac{\langle\Omega^{(2,2)}_{S_2S+}\rangle}{\langle\Omega^{(2,2)}_{S_2S_2}\rangle}} + \frac{x_S\mu_S}{x_{S_2}\sqrt{\frac{4}{3}}\frac{\langle\Omega^{(2,2)}_{S_2S}\rangle}{\langle\Omega^{(2,2)}_{SS}\rangle} + x_S + x_{S+}\frac{\langle\Omega^{(2,2)}_{SS+}\rangle}{\langle\Omega^{(2,2)}_{SS}\rangle}}$$

$$+ \frac{x_{S+}\mu_{S+}}{x_{S_2}\sqrt{\frac{4}{3}}\frac{\langle\Omega^{(2,2)}_{S_2S+}\rangle}{\langle\Omega^{(2,2)}_{S+S+}\rangle} + x_S\frac{\langle\Omega^{(2,2)}_{SS+}\rangle}{\langle\Omega^{(2,2)}_{S+S+}\rangle} + x_{S+}}. \tag{2.178}$$

This form of the viscosity coefficient is compared to Miller's form in Section 4.1.2.

2.4.4 Thermal Conductivity

The first approximation of the coefficient of thermal conductivity is

$$\kappa = 8.3227 \times 10^{-5}\frac{\sqrt{T/M}}{\langle\Omega^{(2,2)}\rangle} = \frac{15}{4}\frac{\hat{R}}{M}\mu \qquad \left[\mathrm{J\,m^{-1}\,s^{-1}\,K^{-1}}\right]. \tag{2.179}$$

However, this equation only applies to particles without internal degrees of freedom. To account for internal degrees of freedom, the Eucken correction is applied to Equation 2.179 to make the conductivity

$$\kappa_{polyatomic} = \frac{15}{4}\frac{\hat{R}}{M}\mu\left(\frac{4}{15}\frac{\hat{c}_v}{\hat{R}} + \frac{3}{5}\right), \tag{2.180}$$

where $\hat{c}_v$ is the constant volume specific heat of the molecule. For monatomic species, the thermal conductivity simplifies to Equation 2.179. For diatomic molecules, $\hat{c}_v = \frac{5}{2}\hat{R}$, and the thermal conductivity becomes

$$\kappa_{diatomic} = \frac{19}{4}\frac{\hat{R}}{M}\mu. \tag{2.181}$$

As with the previous transport coefficients, the multicomponent thermal conductivity can be represented as a ratio of matrices. The mixture rule of Mitchner and Kruger is employed in this case, as well, resulting in the heavy species thermal conductivity:

$$\kappa_g \approx \frac{x_{S_2}\kappa_{S_2}}{x_{S_2} + x_S\sqrt{\frac{2}{3}}\frac{\langle\Omega^{(2,2)}_{S_2S}\rangle}{\langle\Omega^{(2,2)}_{S_2S_2}\rangle} + x_{S+}\sqrt{\frac{2}{3}}\frac{\langle\Omega^{(2,2)}_{S_2S+}\rangle}{\langle\Omega^{(2,2)}_{S_2S_2}\rangle}} + \frac{x_S\kappa_S}{x_{S_2}\sqrt{\frac{4}{3}}\frac{\langle\Omega^{(2,2)}_{S_2S}\rangle}{\langle\Omega^{(2,2)}_{SS}\rangle} + x_S + x_{S+}\frac{\langle\Omega^{(2,2)}_{SS+}\rangle}{\langle\Omega^{(2,2)}_{SS}\rangle}}$$

$$+ \frac{x_{S+}\kappa_{S+}}{x_{S_2}\sqrt{\frac{4}{3}}\frac{\langle\Omega^{(2,2)}_{S_2S+}\rangle}{\langle\Omega^{(2,2)}_{S+S+}\rangle} + x_S\frac{\langle\Omega^{(2,2)}_{SS+}\rangle}{\langle\Omega^{(2,2)}_{S+S+}\rangle} + x_{S+}}. \tag{2.182}$$

In Miller's formulation, a factor of $\frac{3}{2}$ multiplied the terms as the factor of 2 did in the viscosity equations. Again, as with the viscosity, the choice of mass fractions was critical in the final values obtained for the heavy species thermal conductivity. Consequently, the ion-molecule interaction terms were retained in the formulation.

Since the electrons are treated as a separate fluid, the electron thermal conductivity is needed in the electron energy equation. Applying Mitchner and Kruger's mixing rule (Equation 2.175) to the electrons only results in

$$\kappa_e \approx \frac{x_{S+}\kappa_e}{x_{S+} + x_{S+}\sqrt{2}\frac{\langle\Omega^{(2,2)}_{eS+}\rangle}{\langle\Omega^{(2,2)}_{ee}\rangle} + x_S\sqrt{2}\frac{\langle\Omega^{(2,2)}_{eS}\rangle}{\langle\Omega^{(2,2)}_{ee}\rangle} + x_{S_2}\sqrt{2}\frac{\langle\Omega^{(2,2)}_{eS_2}\rangle}{\langle\Omega^{(2,2)}_{ee}\rangle}}. \tag{2.183}$$

From this equation it becomes obvious that, unlike the formulation of Miller, $\langle\Omega^{(2,2)}_{eS+}\rangle \neq \langle\Omega^{(2,2)}_{ee}\rangle$, because of the difference in the attractive and repulsive shielded Coulomb potentials. As with the previous transport coefficients, the solution as obtained by these formulations is compared with the solution as found by Miller in Section 4.1.2.

2.4.5 Electrical Conductivity

For an ionized gas in the presence of electrical and magnetic fields, all of the transport coefficients are functions of the direction of these fields as well as pressure and concentration gradients. For example, if we take the magnetic field to be in the $\hat{z}$ direction, and ion currents and pressure gradients are neglected, Ohm's Law can be represented in matrix notation as

$$\begin{bmatrix} j_{ex} \\ j_{ey} \\ j_{ez} \end{bmatrix} = \begin{bmatrix} \sigma_\perp & -\sigma_H & 0 \\ \sigma_H & \sigma_\perp & 0 \\ 0 & 0 & \sigma_\parallel \end{bmatrix} \begin{bmatrix} E'_x \\ E'_y \\ E'_z \end{bmatrix}, \tag{2.184}$$

where

$$\sigma_\parallel = \frac{e^2 n_e}{m_e \sum_r \overline{\nu}_{er}} \qquad \sigma_\perp = \frac{\sigma_\parallel}{1+\beta^2} \qquad \sigma_H = \frac{\beta\sigma_\parallel}{1+\beta^2}, \tag{2.185}$$

where β is the Hall parameter. The subscripts denote the conductivity in the directions parallel to $\vec{B}$, perpendicular to $\vec{B}$ and parallel to $\vec{E} \times \vec{B}$, respectively. In the absence of magnetic fields, $\sigma_\perp = \sigma_\parallel$ and $\sigma_H = 0$, and Ohm's Law reduces to $\vec{j} = \sigma \vec{E}$.

The electrical conductivity of an ionized gas is given approximately as

$$\sigma = \sigma_e + \sigma_i, \tag{2.186}$$

where

$$\sigma_e = \frac{e^2 n_e}{m_e \sum_g \overline{\nu}_{eg}} \quad \text{and} \quad \sigma_i = \frac{e^2 n_i}{m_i \sum_g \overline{\nu}_{eg}} \left[1 + \frac{\rho_n}{\rho_i} \frac{\overline{\nu}_{en}}{\overline{\nu}_{in}} \right], \tag{2.187}$$

where $\overline{\nu}_{eg}$ is the average collision frequency of electrons with all heavy species, $\overline{\nu}_{en}$ is the average electron-neutral collision frequency, and $\overline{\nu}_{in}$ is the ion-neutral collision frequency. With the quasi-neutrality assumption ($n_e \approx n_i$) and noting that $\frac{m_e}{m_i} \ll 1$ implies that the conductivity is due almost totally to the electrons:

$$\sigma \approx \sigma_e = \frac{e^2 n_e}{m_e \sum_g \overline{\nu}_{eg}}. \tag{2.188}$$

Analytic values of the electrical conductivity are only known in the limits of weak and full ionization. In the weak ionization limit, the conductivity is given by the Lorentzian conductivity

$$\sigma = \frac{4\pi}{3} \frac{e^2 n_e}{kT_e} \int_0^\infty \frac{v^4 f_e^M(v)}{\sum_n \overline{\nu}_{en}(v)} dv, \tag{2.189}$$

where $f_e^M(v)$ is the electron Maxwellian velocity distribution function. At the fully ionized limit, the Spitzer-Härm conductivity applies, and is given as

$$\sigma = 1.975 \frac{e^2 n_e}{m_e \overline{\nu}_{ei}}. \tag{2.190}$$

For ionization between the limits of weak and full ionization, a number of different methods can be used. Devoto [12] proposed a formula based on the multicomponent diffusion coefficients

$$\sigma \approx \frac{e^2 n}{\rho k T} \sum_j n_j m_j Z_j \overline{D}_{ej}, \tag{2.191}$$

where the summation is taken over all charged species and thermal equilibrium is assumed. The major drawback of this method is the need to calculate the multicomponent diffusion

coefficients $\overline{D}_{ej}$ by the matrix methods as discussed in Section 2.4.2. An alternative method which yields accurate results for all degrees of ionization is the Frost conductivity [35]:

$$\sigma_F = \frac{4\pi n_e e^2}{3kT_e} \int_0^\infty \frac{C^4 f_e^M}{\nu_F} dC, \tag{2.192}$$

where, in this case, f_e^M is the electron Maxwellian *speed* distribution function, and

$$\nu_F = \sum_n \nu_{en}^{(1)} + 0.476 \frac{8\pi n_i}{C^2} \left(\frac{m_e}{2kT_e}\right)^{\frac{1}{2}} \left(\frac{e^2}{4\pi\epsilon_0 m_e}\right)^2 \ln\Lambda, \tag{2.193}$$

where the superscript (1) indicates that the collision frequency calculation is performed using the total momentum cross section, and

$$\Lambda = \frac{\lambda_D}{\bar{b}_0} = \frac{12\pi \left(\epsilon_0 k T_e\right)^{\frac{3}{2}}}{e^3\sqrt{n_e}} = 1.238 \times 10^7 \sqrt{\frac{T_e^3}{n_e}}, \tag{2.194}$$

where λ_D is the Debye length given in Equation 2.148 and

$$\bar{b}_0 = \frac{Ze^2}{12\pi\epsilon_0 kT_e} \tag{2.195}$$

is the impact parameter for 90^o scattering. The calculation of all of the collision frequencies and the subsequent evaluation of the integral rules out the use of this formulation in the context of a fluid dynamic code.

The method adopted by Miller in his research was the method developed by Grier [16] for hydrogen. In Grier's formulation, the first approximation is modified by a correction factor according to a method as first stipulated by Pipkin [42]. Grier performed calculations on ionizing monatomic hydrogen, and did not consider diatomic hydrogen in the calculations. The resulting electrical conductivity can be expressed as

$$\sigma_0 = \frac{3}{16}\sqrt{\frac{2e^4}{\pi m_e k T_e}} \frac{x_{H+}}{x_{H+}\langle\Omega_{eH+}^{(1,1)}\rangle + (1 - x_{H+})\langle\Omega_{eH}^{(1,1)}\rangle} \tag{2.196}$$

and

$$\sigma = \frac{\sigma_0}{1 - \Delta_c}, \tag{2.197}$$

where Δ_c is the correction factor. Miller further modified this calculation by including a collision integral for the $e - H_2$ interaction. In the fluid dynamic code, the calculation of the

correction factor requires a good deal of computational effort, as Grier's calculations were made discretely between 10^{-5} and 10^{2} atmospheres. To avoid this computation, a simpler, more general calculation based on the ideas of Krier et al. [24] was used to calculate the electrical conductivity. This form of the conductivity is

$$\sigma = \frac{3}{16}\sqrt{\frac{2e^4}{\pi m_e k T_e}}\frac{x_{S+}}{\sum_{s\neq e} x_s \langle \Omega_{es}^{(1,1)} \rangle}. \tag{2.198}$$

2.4.6 Collision Frequencies

Collision frequencies are needed to calculate the energy transfer between the heavy species and electrons. In general, the average collision frequency of a particle of species s with all particles of species r is

$$\overline{\nu}_{sr} = n_r \overline{g}_{sr} \overline{Q}_{sr}, \tag{2.199}$$

where $\overline{Q}_{sr}$ is the average collision cross section of the colliding particles and $\overline{g}_{sr}$ is the average relative speed of the colliding particles. For electron collisions with the heavy species, the relative speed can be approximated as the thermal speed of the electrons, since the mass of the electron is so much smaller than that of the other species. In other words,

$$\overline{g}_{er} \approx \overline{c}_e = \sqrt{\frac{8kT_e}{\pi m_e}}, \tag{2.200}$$

which makes the collision frequencies of the electrons with the heavy species

$$\overline{\nu}_{eS_2} = n_{S_2} \overline{c}_e \overline{Q}_{eS_2} \tag{2.201}$$

$$\overline{\nu}_{eS} = n_S \overline{c}_e \overline{Q}_{eS} \tag{2.202}$$

$$\overline{\nu}_{eS+} = n_{S+} \overline{c}_e \overline{Q}_{eS+}. \tag{2.203}$$

The hydrogen atom collision cross-section, $\overline{Q}_H$, is taken from Devoto [13], while $\overline{Q}_N$ is taken from Burke et al.[5]. Both of the molecular cross-sections, $\overline{Q}_{H_2}$ and $\overline{Q}_{N_2}$, are taken from Itikawa [22]. These cross-sections are listed in tabular form in Table C of Appendix C. For electron-ion collisions, the collision cross section is the approximate Coulomb cross section:

$$\overline{Q}_{ei} = 6\pi \overline{b}_0^2 \ln\Lambda, \tag{2.204}$$

where Λ is given by Equation 2.194. In this equation, it has been assumed that $\ln\Lambda \gg 1$. This assumption is valid in a majority of physical situations, but breaks down at lower temperature and higher electron densities. If this situation were to occur, the collision cross section becomes negative. In the rare occasions where this would occur, a more accurate form of the Coulomb cross section for electron-ion collisions is [35]

$$\overline{Q}_{ei} = 4\pi b_0^2 \ln\left[1 + \left(\frac{\lambda_D}{b_0}\right)^2\right]^{1/2}, \tag{2.205}$$

where (note the lack of the overbar)

$$b_0 = \frac{Ze^2}{32\epsilon_0 kT_e}. \tag{2.206}$$

2.4.7 Collision Integrals

The necessary collision integrals for the calculation of the various transport coefficients are primarily the $\langle\Omega_{ij}^{(1,1)}\rangle$ and $\langle\Omega_{ij}^{(2,2)}\rangle$ collision integrals. For the various interactions, collision integrals have been calculated by a number of authors, for temperatures in the range 1,000-35,000 K. The $\langle\Omega_{ij}^{(1,1)}\rangle$ integrals are listed in Table D.1 for hydrogen and Table D.2 for nitrogen, while the $\langle\Omega_{ij}^{(2,2)}\rangle$ integrals are listed in Table D.3 for hydrogen and Table D.4 for nitrogen, all of which are in Appendix D. These non-Coulombic integrals are independent of pressure, so therefore, apply to all pressures. For the hydrogen interactions, the data were taken from Vanderslice et al. [52] for the $\langle\Omega_{H_2H_2}^{(2,2)}\rangle$, $\langle\Omega_{H_2H}^{(2,2)}\rangle$, $\langle\Omega_{HH}^{(2,2)}\rangle$, $\langle\Omega_{H_2H_2}^{(1,1)}\rangle$, and $\langle\Omega_{HH}^{(1,1)}\rangle$ for temperatures up to 15,000 K; from Belov [3] for $\langle\Omega_{HH}^{(2,2)}\rangle$ and from Grier [16] for $\langle\Omega_{HH+}^{(2,2)}\rangle$, $\langle\Omega_{eH}^{(2,2)}\rangle$, $\langle\Omega_{eH}^{(1,1)}\rangle$ for the temperature range 5,000-35,000 K. In Miller's work, the $\langle\Omega_{H_2e}^{(1,1)}\rangle$ integral was estimated as $\frac{1}{4}\overline{Q}_{eH_2}$. In this research, the $\langle\Omega_{H_2e}^{(1,1)}\rangle$ and $\langle\Omega_{H_2e}^{(2,2)}\rangle$ integrals were calculated using Equation 2.153 and the total elastic cross-section of Itikawa (see above). These calculated values are also in Tables D.1 and D.3.

Cubley and Mason [10] have calculated the $\langle\Omega_{N_2N_2}^{(1,1)}\rangle$ and $\langle\Omega_{N_2N_2}^{(2,2)}\rangle$ collision integrals using the exponential repulsive potential, and have curve-fitted their results to the form

$$\langle\Omega_{ij}^{(l,s)}\rangle = AT^{-n}, \tag{2.207}$$

A and n being constants. For the $N_2 - N_2$ interaction, these curve fits are

$$\langle \Omega^{(1,1)}_{N_2N_2} \rangle = 60.6\, T^{-0.274}, \tag{2.208}$$

and

$$\langle \Omega^{(2,2)}_{N_2N_2} \rangle = 51.3\, T^{-0.231}, \tag{2.209}$$

which are valid for a temperature range of 300 - 15,000 K. The $\langle \Omega^{(1,1)}_{N_2N} \rangle$ and $\langle \Omega^{(2,2)}_{N_2N} \rangle$ integrals are taken from Yun and Mason [56] for 1,000 - 15,000 K, the $\langle \Omega^{(1,1)}_{NN} \rangle$ and $\langle \Omega^{(2,2)}_{NN} \rangle$ integrals are taken from Rainwater et al. [44] for 1,000 - 20,000 K, and the $\langle \Omega^{(1,1)}_{NN+} \rangle$ and $\langle \Omega^{(2,2)}_{NN+} \rangle$ integrals are from Stallcop, Partridge, and Levin [48] for 1,000 - 35,000 K.

The Coulombic collision integrals are functions of both pressure and temperature, as evidenced by Equations 2.194 and 2.204. To account for this, Miller originally took the Coulombic integrals to be the collision cross section multiplied by some factor, with satisfactory results. Instead of this method, the methods of Paquette et al. [37] for the repulsive static screened Coulomb potential (SSCP) (see Equation 2.147) were used for the S+-S+ and e-e interactions, while Paquette's methods as modified by MacDonald [30] for the attractive SSCP were used for the e-S+ interaction. In both methods, the collision integrals are non-dimensionalized and expressed as a function of a dimensionless variable ψ_{ij}, defined as

$$\psi_{ij} = \ln\left[\ln\left(1 + \gamma_{ij}^2\right)\right], \tag{2.210}$$

where γ_{ij} is another dimensionless variable defined as

$$\gamma_{ij} = \frac{16\pi\epsilon_0 kT\lambda}{Z_i Z_j e^2}, \tag{2.211}$$

where the length scale λ is in meters. In terms of the $\langle \Omega^{(i,j)} \rangle$ collision integrals defined previously, the collision integrals for the repulsive SSCP are

$$\langle \Omega^{(1,1)} \rangle_{rep} = \frac{1}{4}\left(\frac{Z_i Z_j e^2}{4\pi\epsilon_0 kT}\right)^2 F^{(1,1)}_{Paq} \tag{2.212}$$

and

$$\langle \Omega^{(2,2)} \rangle_{rep} = \frac{1}{8}\left(\frac{Z_i Z_j e^2}{4\pi\epsilon_0 kT}\right)^2 F^{(2,2)}_{Paq}, \tag{2.213}$$

while the integrals for the attractive SSCP are

$$\langle \Omega^{(1,1)} \rangle_{att} = \frac{1}{8} \left(\frac{Z_i Z_j e^2}{4\pi\epsilon_0 kT} \right)^2 F_{Mac}^{(1,1)}, \tag{2.214}$$

and

$$\langle \Omega^{(2,2)} \rangle_{att} = \frac{1}{16} \left(\frac{Z_i Z_j e^2}{4\pi\epsilon_0 kT} \right)^2 F_{Mac}^{(2,2)}, \tag{2.215}$$

where the $F_{Paq}^{(i,j)}$ and $F_{Mac}^{(i,j)}$ are the dimensionless collision integrals as defined by Paquette et al. and MacDonald, respectively. The factor of $\frac{1}{2}$ difference occurs because of a difference in the way the quantities are defined between the two methods. The resulting expressions for the Coulomb collision integrals are very close in form to Equation 2.205. In fact, the methods of Paquette and MacDonald can be thought of as a refinement to the methods which yield the expression for the Coulomb cross section. The advantage of these methods is that both temperature and pressure (concentration) are accounted for implicitly in the γ_{ij}. Table D.5 of Appendix D lists the $F^{(i,j)}$ for both Paquette and MacDonald. At or above $\psi_{ij} = 3.0$, both methods provide simple expressions for the dimensionless collision integrals:

$$F_{Paq}^{(1,1)} = 1.00141\, e^{\psi_{i,j}} - 3.18209 \tag{2.216}$$

$$F_{Paq}^{(2,2)} = 1.99016\, e^{\psi_{i,j}} - 4.56958 \tag{2.217}$$

$$\ln F_{Mac}^{(1,1)} = \psi_{i,j} - 3.30447\, e^{-\psi_{i,j}} - 6.00170\, e^{-2\psi_{i,j}} \tag{2.218}$$

$$\ln F_{Mac}^{(2,2)} = \psi_{i,j} - 2.30571\, e^{-\psi_{i,j}} - 2.92018\, e^{-2\psi_{i,j}} + 0.69315\,. \tag{2.219}$$

For the range of values within an arcjet, however, $\psi_{st} < 3$.

2.5 Summary of Equations

The equations comprising the axisymmetric flow model are summarized below in conservative form:

Conservation of Mass

$$\frac{\partial \rho_s r}{\partial t} + \frac{\partial \rho_s u_{sr} r}{\partial r} + \frac{\partial \rho_s u_{sz} r}{\partial z} = m_s \dot{n}_s r \quad \text{(species)} \tag{2.220}$$

$$\frac{\partial \rho r}{\partial t} + \frac{\partial \rho u_r r}{\partial r} + \frac{\partial \rho u_z r}{\partial z} = 0 \quad \text{(global)} \tag{2.221}$$

$$\dot{n}_e = R\left(S n_S - n_e^2\right) \tag{2.222}$$

$$\dot{n}_S = A N_A T_g^{n_f} \exp\left(-\frac{B}{\hat{R} T_g}\right)\left(\hat{m}_S \hat{n}_S + \hat{m}_{S_2} \hat{n}_{S_2}\right)\left(\hat{n}_{S_2} - \frac{\hat{R} T_g}{K_{p,dis}} \hat{n}_S^2\right) + k_d^e n_e n_{S_2} \tag{2.223}$$

Conservation of Momentum

$$\frac{\partial}{\partial t}\left(\rho u_r r\right) + \frac{\partial}{\partial r}\left(\rho u_r^2 r + p r - \tau_{rr} r\right) + \frac{\partial}{\partial z}\left(\rho u_r u_z r - \tau_{rz} r\right) = \rho u_\theta^2 - \tau_{\theta\theta} + p \tag{2.224}$$

$$\frac{\partial}{\partial t}\left(\rho u_\theta r\right) + \frac{\partial}{\partial r}\left(\rho u_r u_\theta r - \tau_{r\theta} r\right) + \frac{\partial}{\partial z}\left(\rho u_\theta u_z r - \tau_{\theta z} r\right) = \tau_{r\theta} - \rho u_r u_\theta \tag{2.225}$$

$$\frac{\partial}{\partial t}\left(\rho u_z r\right) + \frac{\partial}{\partial r}\left(\rho u_r u_z r - \tau_{rz} r\right) + \frac{\partial}{\partial z}\left(\rho u_z^2 r + p r - \tau_{zz} r\right) = 0 \tag{2.226}$$

$$\tau_{rr} = \frac{2}{3}\mu_g\left(2\frac{\partial u_r}{\partial r} - \frac{\partial u_z}{\partial z} - \frac{u_r}{r}\right) \tag{2.227}$$

$$\tau_{\theta\theta} = \frac{2}{3}\mu_g\left(2\frac{u_r}{r} - \frac{\partial u_r}{\partial r} - \frac{\partial u_z}{\partial z}\right) \tag{2.228}$$

$$\tau_{zz} = \frac{2}{3}\mu_g\left(2\frac{\partial u_z}{\partial z} - \frac{\partial u_r}{\partial r} - \frac{u_r}{r}\right) \tag{2.229}$$

$$\tau_{r\theta} = \mu_g\left(\frac{\partial u_\theta}{\partial r} - \frac{u_\theta}{r}\right) \tag{2.230}$$

$$\tau_{rz} = \mu_g\left(\frac{\partial u_r}{\partial z} + \frac{\partial u_z}{\partial r}\right) \tag{2.231}$$

$$\tau_{\theta z} = \mu_g \frac{\partial u_\theta}{\partial z} \tag{2.232}$$

Conservation of Energy

Heavy Species Energy Equation:

$$\frac{\partial}{\partial t}\left(\rho e_g r\right) + \frac{\partial}{\partial r}\left(\rho h_g u_r r + \rho_{S_2} h_{S_2} V_{S_2 r} r + \rho_S h_S V_{Sr} r + \rho_{S+} h_{S+} V_{S+r} r + q_{gr} r\right)$$

$$+\frac{\partial}{\partial z}\left(\rho h_g u_z r + \rho_{S_2} h_{S_2} V_{S_2 z} r + \rho_S h_S V_{Sz} r + \rho_{S+} h_{S+} V_{S+z} r + q_{gz} r\right)$$

$$= \left[V_{S_2 r}\frac{\partial p_{S_2}}{\partial r} + V_{Sr}\frac{\partial p_S}{\partial r} + V_{S+r}\frac{\partial p_{S+}}{\partial r} + V_{S_2 z}\frac{\partial p_{S_2}}{\partial z} + V_{Sz}\frac{\partial p_S}{\partial z} + V_{S+z}\frac{\partial p_{S+}}{\partial z}\right.$$

$$\left. + u_r\frac{\partial p_g}{\partial r} + u_z\frac{\partial p_g}{\partial z} + \Phi + E_l - \frac{1}{2}e_d\left(\dot{n}_S + k_d^e n_e n_{S_2}\right)\right] r \tag{2.233}$$

$$\rho h_g = \frac{5}{2}\left(\rho_S + \rho_{S+}\right) R_S T_g + \frac{7}{2}\rho_{S_2} R_{S_2} T_g + \frac{\rho_{S_2} R_{S_2}\theta_v}{e^{\theta_v/T_g} - 1} - \frac{7}{4}\rho R_S T_f \tag{2.234}$$

$$\rho e_g = \rho h_g - \rho_{S_2} R_{S_2} T_g - \left(\rho_S + \rho_{S+}\right) R_S T_g \tag{2.235}$$

$$E_l = 3\frac{\rho_e}{m_S}\left(\overline{\nu}_{eS+} + \overline{\nu}_{eS} + \delta_{S_2}\overline{\nu}_{eS_2}\right) k\left(T_e - T_g\right) \tag{2.236}$$

$$\Phi = \mu_g\left[2\left(\frac{\partial u_r}{\partial r}\right)^2 + 2\left(\frac{\partial u_z}{\partial z}\right)^2 + 2\left(\frac{u_r}{r}\right)^2 + \left(\frac{\partial u_r}{\partial z} + \frac{\partial u_z}{\partial r}\right)^2\right.$$

$$\left. + \left(\frac{\partial u_\theta}{\partial r} - \frac{u_\theta}{r}\right)^2 + \left(\frac{\partial u_\theta}{\partial z}\right)^2 - \frac{2}{3}\left(\frac{\partial u_r}{\partial r} + \frac{\partial u_z}{\partial z} + \frac{u_r}{r}\right)^2\right] \tag{2.237}$$

Electron Energy Equation:

$$\frac{\partial}{\partial t}\left(\rho_e E_e r\right) + \frac{\partial}{\partial r}\left(\rho_e H_e u_{er} r + q_{er} r\right) + \frac{\partial}{\partial z}\left(\rho_e H_e u_{ez} r + q_{ez} r\right)$$

$$= \left(\frac{j^2}{\sigma} - E_l - e_d k_d^e n_e n_{S_2} - e_i \dot{n}_e - \dot{R}\right) r \tag{2.238}$$

$$E_e = \frac{3}{2}R_e T_e + \frac{1}{2}u_e^2 \tag{2.239}$$

$$H_e = E_e + R_e T_e \tag{2.240}$$

Electrical Potential

$$\frac{\partial}{\partial r}\left(r\sigma\frac{\partial\phi}{\partial r}\right) + \frac{\partial}{\partial z}\left(r\sigma\frac{\partial\phi}{\partial z}\right) = \frac{\partial}{\partial r}\left(r\psi\frac{\partial p_e}{\partial r}\right) + \frac{\partial}{\partial z}\left(r\psi\frac{\partial p_e}{\partial z}\right). \tag{2.241}$$

Equation of State

$$p_g = \rho_{S_2} R_{S_2} T_g + \rho_S R_S T_g + \rho_{S+} R_{S+} T_g \tag{2.242}$$

$$p_e = \rho_e R_e T_e \tag{2.243}$$

Auxiliary Equations

Current Density:

$$j_z = \psi \frac{\partial p_e}{\partial z} - \sigma \frac{\partial \phi}{\partial z} \qquad j_r = \psi \frac{\partial p_e}{\partial r} - \sigma \frac{\partial \phi}{\partial r} \tag{2.244}$$

Heat Flux:

$$q_{gz} = -\kappa_g \frac{\partial T_g}{\partial z} \qquad q_{gr} = -\kappa_g \frac{\partial T_g}{\partial r} \tag{2.245}$$

$$q_{ez} = -\kappa_e \frac{\partial T_e}{\partial z} \qquad q_{er} = -\kappa_e \frac{\partial T_e}{\partial r} \tag{2.246}$$

Diffusion Velocity:

$$u_{sz} = u_z + V_{sz} \qquad u_{sr} = u_r + V_{sr} \tag{2.247}$$

$$V_{S+z} = -\frac{D_a}{\rho_e} \frac{\partial \rho_e}{\partial z} \qquad V_{S+r} = -\frac{D_a}{\rho_e} \frac{\partial \rho_e}{\partial r} \tag{2.248}$$

$$V_{Sz} = -\frac{D_S}{\rho_S} \frac{\partial \rho_S}{\partial z} \qquad V_{Sr} = -\frac{D_S}{\rho_S} \frac{\partial \rho_S}{\partial r} \tag{2.249}$$

$$V_{S_2 z} = \frac{1}{\rho_{S_2}} \left(\frac{m_e}{e} j_z - \rho_S V_{Sz} - \rho_{S+} V_{S+z} \right) \qquad V_{S_2 r} = \frac{1}{\rho_{S_2}} \left(\frac{m_e}{e} j_r - \rho_S V_{Sr} - \rho_{S+} V_{S+r} \right) \tag{2.250}$$

$$u_{ez} = u_z + V_{S+z} - \frac{j_z}{e n_e} \qquad u_{er} = u_r + V_{S+r} - \frac{j_r}{e n_e} \tag{2.251}$$

Chapter 3

Numerical Method

Once the equations governing the physics have been derived, it is then necessary to put the equations in a form suitable for numerical calculations. The reason for using numerical methods to find the solution to a problem to begin with is that no closed form analytical solutions to the problem exist, nor are there any hopes for finding any. This is especially true for the system of highly nonlinear partial differential equations which make up the governing equations described in the previous chapter. Typically, the equations are put in strong conservative form, in anticipation of shocks or other discontinuities within the flow. The reason for this is that the fluxes as defined in the conservative formulation are conserved across discontinuities such as shocks. Although no shocks are anticipated within the flow to be modeled, the strong conservative form convention will be followed throughout the following discussion.

The governing equations are, basically, a modified form of the compressible Navier-Stokes equations, with terms added due to diffusive fluxes of the different species and due to net production of the different species. In axisymmetric coordinates, the governing equations can be represented as

$$\frac{\partial \mathbf{U}}{\partial t} + \frac{\partial \mathbf{F}}{\partial z} + \frac{\partial \mathbf{G}}{\partial r} = \mathbf{S}, \tag{3.1}$$

where $\mathbf{U}$ is the state vector, $\mathbf{F}$ and $\mathbf{G}$ are flux vectors in the z and r directions, respectively, and $\mathbf{S}$ is a vector of source terms. Putting the previously derived equations in vector form, these vector quantities are:

$$\mathbf{U} = \begin{bmatrix} \rho r \\ \rho_S r \\ \rho_e r \\ \rho u_r r \\ \rho u_\theta r \\ \rho u_z r \\ \rho e_g r \\ \rho_e E_e r \end{bmatrix},$$

$$\mathbf{F} = \begin{bmatrix} \rho u_z r \\ \rho_S \left(u_z + V_{Sz}\right) r \\ \rho_e \left(u_z + V_{ez}\right) r \\ \left(\rho u_r u_z - \tau_{rz}\right) r \\ \left(\rho u_\theta u_z - \tau_{\theta z}\right) r \\ \left(\rho u_z^2 + p - \tau_{zz}\right) r \\ \left[\rho h_g u_z + q_{gz} + F\left(V_s\right)\right] r \\ \left(\rho_e H_e u_{ez} + q_{ez}\right) r \end{bmatrix},$$

$$\mathbf{G} = \begin{bmatrix} \rho u_r r \\ \rho_S \left(u_r + V_{Sr}\right) r \\ \rho_e \left(u_r + V_{er}\right) r \\ \left(\rho u_r^2 + p - \tau_{rr}\right) r \\ \left(\rho u_r u_\theta - \tau_{r\theta}\right) r \\ \left(\rho u_r u_z - \tau_{rz}\right) r \\ \left[\rho h_g u_r + q_{gr} + G\left(V_s\right)\right] r \\ \left(\rho_e H_e u_{er} + q_{er}\right) r \end{bmatrix},$$

$$\mathbf{S} = \begin{bmatrix} 0 \\ m_S\left(\dot{n}_{S+} < \sigma v > n_e n_{S_2} - \dot{n}_e\right) r \\ m_e \dot{n}_e r \\ \rho u_\theta^2 - \tau_{\theta\theta} + p \\ \tau_{r\theta} - \rho u_r u_\theta \\ 0 \\ \left[u_r \frac{\partial p_g}{\partial r} + u_z \frac{\partial p_g}{\partial z} + S\left(V_s\right) + \Phi + E_l - \frac{1}{2} E_d \left(\dot{n}_{S+} < \sigma v > n_e n_{S_2}\right)\right] r \\ \left(\frac{j^2}{\sigma} - E_l - E_d < \sigma v > n_e n_{S_2} - E_i \dot{n}_e - \dot{R}\right) r \end{bmatrix}, \tag{3.2}$$

where

$$F\left(V_s\right) = \rho_{S_2} h_{S_2} V_{S_2 z} + \rho_S h_S V_{Sz} + \rho_{S+} h_{S+} V_{S+z} \tag{3.3}$$

$$G\left(V_s\right) = \rho_{S_2} h_{S_2} V_{S_2 r} + \rho_S h_S V_{Sr} + \rho_{S+} h_{S+} V_{S+r} \tag{3.4}$$

and

$$S\left(V_s\right) = V_{S_2 r} \frac{\partial p_{S_2}}{\partial r} + V_{Sr} \frac{\partial p_S}{\partial r} + V_{S+r} \frac{\partial p_{S+}}{\partial r} + V_{S_2 z} \frac{\partial p_{S_2}}{\partial z} + V_{Sz} \frac{\partial p_S}{\partial z} + V_{S+z} \frac{\partial p_{S+}}{\partial z} \tag{3.5}$$

Because of the complexity of the equations and the boundary conditions, an explicit numerical scheme was chosen to integrate the fluid equations. In addition, since transient phenomena may be of interest in arcjet research, the numerical scheme should also be accurate in time. MacCormack's Method was chosen as the scheme, because in its explicit form, it is simpler to code than an implicit scheme, and also because this scheme is second order accurate in both space and time. Due to its elliptic nature, the potential equation (Equation 2.43) is solved using Successive Over-Relaxation (SOR).

3.1 Coordinate Transformation

Both MacCormack's Method and Successive Over-Relaxation use finite differences to approximate the derivatives. Since the computational grid used may be complex, and not necessarily Cartesian, the governing equations must be transformed into the coordinate system of the grid, also known as the natural or $\xi - \eta$ coordinate system, to be modeled accurately.

Using the chain rule of calculus, the derivatives in r and z may be represented as:

$$\frac{\partial}{\partial r} = \frac{\partial \xi}{\partial r}\frac{\partial}{\partial \xi} + \frac{\partial \eta}{\partial r}\frac{\partial}{\partial \eta} = \xi_r \frac{\partial}{\partial \xi} + \eta_r \frac{\partial}{\partial \eta}, \tag{3.6}$$

$$\frac{\partial}{\partial z} = \frac{\partial \xi}{\partial z}\frac{\partial}{\partial \xi} + \frac{\partial \eta}{\partial z}\frac{\partial}{\partial \eta} = \xi_z \frac{\partial}{\partial \xi} + \eta_z \frac{\partial}{\partial \eta}, \tag{3.7}$$

where ξ_r, ξ_z, η_r, and η_z are the metrics of the transformation. From the definition of a total derivative, it can be shown that ([1], [39])

$$\begin{bmatrix} \xi_z & \xi_r \\ \eta_z & \eta_r \end{bmatrix} = \begin{bmatrix} z_\xi & z_\eta \\ r_\xi & r_\eta \end{bmatrix}^{-1} = \frac{1}{J}\begin{bmatrix} r_\eta & -z_\eta \\ -r_\xi & z_\xi \end{bmatrix}, \tag{3.8}$$

where $J = z_\xi r_\eta - z_\eta r_\xi$ is the Jacobian of the transformation. Similarly, the second derivatives in r and z may be written as

$$\frac{\partial^2}{\partial r^2} = \left(\xi_r \frac{\partial}{\partial \xi} + \eta_r \frac{\partial}{\partial \eta}\right)\left(\xi_r \frac{\partial}{\partial \xi} + \eta_r \frac{\partial}{\partial \eta}\right)$$

$$= {\xi_r}^2 \frac{\partial^2}{\partial \xi^2} + 2\xi_r \eta_r \frac{\partial^2}{\partial \xi \partial \eta} + {\eta_r}^2 \frac{\partial^2}{\partial \eta^2} + \xi_{rr}\frac{\partial}{\partial \xi} + \eta_{rr}\frac{\partial}{\partial \eta} \tag{3.9}$$

$$\frac{\partial^2}{\partial z^2} = \left(\xi_z \frac{\partial}{\partial \xi} + \eta_z \frac{\partial}{\partial \eta}\right)\left(\xi_z \frac{\partial}{\partial \xi} + \eta_z \frac{\partial}{\partial \eta}\right)$$

$$= {\xi_z}^2 \frac{\partial^2}{\partial \xi^2} + 2\xi_z \eta_z \frac{\partial^2}{\partial \xi \partial \eta} + {\eta_z}^2 \frac{\partial^2}{\partial \eta^2} + \xi_{zz}\frac{\partial}{\partial \xi} + \eta_{zz}\frac{\partial}{\partial \eta}, \tag{3.10}$$

where

$$\xi_{rr} = \xi_r (\xi_r)_\xi + \eta_r (\xi_r)_\eta = \left[z_\eta (z_{\xi\eta} J - z_\eta J_\xi) - z_\xi (z_{\eta\eta} J - z_\eta J_\eta)\right]/J^3 \tag{3.11}$$

$$\xi_{zz} = \xi_z (\xi_z)_\xi + \eta_z (\xi_z)_\eta = \left[r_\eta (r_{\xi\eta} J - r_\eta J_\xi) - r_\xi (r_{\eta\eta} J - r_\eta J_\eta)\right]/J^3 \tag{3.12}$$

$$\eta_{rr} = \xi_r (\eta_r)_\xi + \eta_r (\eta_r)_\eta = \left[z_\xi (z_{\xi\eta} J - z_\xi J_\eta) - z_\eta (z_{\xi\xi} J - z_\xi J_\xi)\right]/J^3 \tag{3.13}$$

$$\eta_{zz} = \xi_z (\eta_z)_\xi + \eta_z (\eta_z)_\eta = \left[r_\xi (r_{\xi\eta} J - r_\xi J_\eta) - r_\eta (r_{\xi\xi} J - r_\xi J_\xi)\right]/J^3. \tag{3.14}$$

Using Equations 3.6,3.7 and 3.8, the vector form of the governing fluid equations becomes

$$\frac{\partial \mathbf{U}}{\partial t} + \frac{r_\eta}{J}\frac{\partial \mathbf{F}}{\partial \xi} - \frac{r_\xi}{J}\frac{\partial \mathbf{F}}{\partial \eta} - \frac{z_\eta}{J}\frac{\partial \mathbf{G}}{\partial \xi} + \frac{z_\xi}{J}\frac{\partial \mathbf{G}}{\partial \eta} = S. \tag{3.15}$$

Multiplying both sides by J and noting that

$$r_\eta \frac{\partial \mathbf{F}}{\partial \xi} = \frac{\partial}{\partial \xi}(\mathbf{F} r_\eta) - \mathbf{F} r_{\xi\eta} \tag{3.16}$$

$$r_\xi \frac{\partial \mathbf{F}}{\partial \eta} = \frac{\partial}{\partial \eta}(\mathbf{F} r_\xi) - \mathbf{F} r_{\xi\eta} \tag{3.17}$$

$$z_\eta \frac{\partial \mathbf{G}}{\partial \xi} = \frac{\partial}{\partial \xi}(\mathbf{G} z_\eta) - \mathbf{G} z_{\xi\eta} \tag{3.18}$$

$$z_\xi \frac{\partial \mathbf{G}}{\partial \eta} = \frac{\partial}{\partial \eta}(\mathbf{G} z_\xi) - \mathbf{G} z_{\xi\eta}, \tag{3.19}$$

the conservative form of the governing equations in natural coordinates can be written as

$$J\frac{\partial \mathbf{U}}{\partial t} + \frac{\partial \tilde{\mathbf{F}}}{\partial \xi} + \frac{\partial \tilde{\mathbf{G}}}{\partial \eta} = J\mathbf{S}, \tag{3.20}$$

where $\tilde{\mathbf{F}} = \mathbf{F} r_\eta - \mathbf{G} z_\eta$ and $\tilde{\mathbf{G}} = \mathbf{G} z_\xi - \mathbf{F} r_\xi$. Since the grid is not changing with time, the Jacobian of the transformation can be lumped with the state vector inside the $\frac{\partial}{\partial t}$ term or left outside with equal accuracy. Computationally, the latter formulation is performed, since the state vector can then be found directly from the integration.

As with all numerical methods, some sort of numerical smoothing is necessary so that the discretized set of equations does not diverge. Applying this numerical smoothing to the right hand side of Equation 3.20, the resulting form can be written as

$$J\frac{\partial \mathbf{U}}{\partial t} + \frac{\partial \tilde{\mathbf{F}}}{\partial \xi} + \frac{\partial \tilde{\mathbf{G}}}{\partial \eta} = J\mathbf{S} + \nu_2 \left(\frac{\partial^2 \mathbf{U}}{\partial \xi^2} + \frac{\partial^2 \mathbf{U}}{\partial \eta^2} \right) + \nu_4 \left(\frac{\partial^4 \mathbf{U}}{\partial \xi^4} + \frac{\partial^4 \mathbf{U}}{\partial \eta^4} \right), \tag{3.21}$$

where ν_2 and ν_4 are artificial viscosity coefficients, and are adjusted depending on the amount of smoothing necessary. It is this form of the governing equations which is integrated. The damping terms themselves can have different forms, but the end result is the same. The second order terms are needed in regions of steep gradients, while the fourth order terms are needed to damp out oscillations due to inadequate grid refinement (sawtooth modes). A more detailed discussion of these damping terms can be found in Section 3.2.3.

Transforming the electrical potential equation is more difficult, due to the second derivative terms and the elliptical nature of the potential equation. The electrical potential equa-

tion in axisymmetric coordinates is given by Equation 2.241 and restated here:

$$\frac{\partial}{\partial r}\left(r\sigma\frac{\partial\phi}{\partial r}\right)+\frac{\partial}{\partial z}\left(r\sigma\frac{\partial\phi}{\partial z}\right)=\frac{\partial}{\partial r}\left(r\psi\frac{\partial p_e}{\partial r}\right)+\frac{\partial}{\partial z}\left(r\psi\frac{\partial p_e}{\partial z}\right), \tag{3.22}$$

which becomes, after expanding the derivative terms,

$$\sigma\frac{\partial^2\phi}{\partial z^2}+\sigma\frac{\partial^2\phi}{\partial r^2}+\frac{\partial\sigma}{\partial z}\frac{\partial\phi}{\partial z}+\left(\frac{\partial\sigma}{\partial r}+\frac{\sigma}{r}\right)\frac{\partial\phi}{\partial r}=\psi\frac{\partial^2 p_e}{\partial z^2}+\psi\frac{\partial^2 p_e}{\partial r^2}+\frac{\partial\psi}{\partial z}\frac{\partial p_e}{\partial z}+\left(\frac{\partial\psi}{\partial r}+\frac{\psi}{r}\right)\frac{\partial p_e}{\partial r}. \tag{3.23}$$

Using Equations 3.6-3.14 the potential equation is transformed into

$$a\frac{\partial^2\phi}{\partial\xi^2}+b\frac{\partial^2\phi}{\partial\eta^2}+c\frac{\partial^2\phi}{\partial\xi\partial\eta}+d\frac{\partial\phi}{\partial\xi}+e\frac{\partial\phi}{\partial\eta}=f\left(p_e,\sigma,\psi,r\right), \tag{3.24}$$

where

$$a=\sigma\left(\xi_r^2+\xi_z^2\right) \tag{3.25}$$

$$b=\sigma\left(\eta_r^2+\eta_z^2\right) \tag{3.26}$$

$$c=2\sigma\left(\xi_r\eta_r+\xi_z\eta_z\right) \tag{3.27}$$

$$d=\sigma\left(\xi_{rr}+\xi_{zz}+\frac{\xi_r}{r}\right)+\frac{a}{\sigma}\frac{\partial\sigma}{\partial\xi}+\frac{c}{2\sigma}\frac{\partial\sigma}{\partial\eta} \tag{3.28}$$

$$e=\sigma\left(\eta_{rr}+\eta_{zz}+\frac{\eta_r}{r}\right)+\frac{c}{2\sigma}\frac{\partial\sigma}{\partial\xi}+\frac{b}{\sigma}\frac{\partial\sigma}{\partial\eta} \tag{3.29}$$

and

$$f\left(p_e,\sigma,\psi,r\right)=\frac{\psi}{\sigma}\left(a\frac{\partial^2 p_e}{\partial\xi^2}+b\frac{\partial^2 p_e}{\partial\eta^2}+c\frac{\partial^2 p_e}{\partial\xi\partial\eta}\right)+d'\frac{\partial p_e}{\partial\xi}+e'\frac{\partial p_e}{\partial\eta}, \tag{3.30}$$

where

$$d'=\psi\left(\xi_{rr}+\xi_{zz}+\frac{\xi_r}{r}\right)+\frac{a}{\sigma}\frac{\partial\sigma}{\partial\xi}+\frac{c}{2\sigma}\frac{\partial\sigma}{\partial\eta} \tag{3.31}$$

$$e'=\psi\left(\eta_{rr}+\eta_{zz}+\frac{\eta_r}{r}\right)+\frac{c}{2\sigma}\frac{\partial\sigma}{\partial\xi}+\frac{b}{\sigma}\frac{\partial\sigma}{\partial\eta}. \tag{3.32}$$

3.2 MacCormack's Method

3.2.1 Description

MacCormack's method [27], developed in 1969, is a two step predictor-corrector scheme based on the Lax-Wendroff method. The overall scheme is accurate to $O\left[(\Delta t)^2,(\Delta x)^2\right]$,

allowing accurate prediction of transient phenomena if necessary. In terms of the transformed fluid equations, MacCormack's method is written as

Predictor:

$$\mathbf{U}_{i,j}^{P} = \mathbf{U}_{i,j}^{n} - \frac{\Delta t}{\Delta \xi}\left(\tilde{\mathbf{F}}_{i,j}^{n} - \tilde{\mathbf{F}}_{i-1,j}^{n}\right) - \frac{\Delta t}{\Delta \eta}\left(\tilde{\mathbf{G}}_{i,j}^{n} - \tilde{\mathbf{G}}_{i,j-1}^{n}\right) + \Delta t \mathbf{S}_{i,j}^{n} \tag{3.33}$$

Corrector:

$$\mathbf{U}_{i,j}^{n+1} = \frac{1}{2}\left[\mathbf{U}_{i,j}^{P} + \mathbf{U}_{i,j}^{n} - \frac{\Delta t}{\Delta \xi}\left(\tilde{\mathbf{F}}_{i+1,j}^{P} - \tilde{\mathbf{F}}_{i,j}^{P}\right) - \frac{\Delta t}{\Delta \eta}\left(\tilde{\mathbf{G}}_{i,j+1}^{P} - \tilde{\mathbf{G}}_{i,j}^{P}\right) + \Delta t \mathbf{S}_{i,j}^{P}\right]. \tag{3.34}$$

The finite differences are taken in the direction opposite to that stipulated in the original paper by MacCormack. In other words, the fluxes are differenced in the backward direction in the predictor and forward in the corrector, opposite to the method as first described. The reason for this is that in regions of supersonic flow, a forward stepping predictor can produce instabilities. In general, it is better to vary the differences from forward to backward to reduce systematic errors [20]. In practice, this can be difficult to implement, and has not been done in this research. In addition, because of the coordinate transformation, $\Delta\xi = \Delta\eta = 1$, which lowers the number of necessary calculations.

In addition to the flux differencing, finite differences are needed for the viscous stress. It is important to difference the velocity gradients properly to ensure second order accuracy. The way this is accomplished is as follows, where fluxes in the $z - r$ coordinate system are used for simplicity. In the $\mathbf{F}$ flux vectors, the derivatives with respect to z are differenced opposite to the way $\mathbf{F}$ is differenced, while the r derivatives are differenced centrally. In the $\mathbf{G}$ flux vectors, the derivatives with respect to r are differenced opposite to the way $\mathbf{G}$ is differenced, while the z derivatives are differenced centrally. For example, take the z-momentum term in the radial momentum equation:

$$F_4 = \left(\rho u_r u_z - \mu \frac{\partial u_r}{\partial z} - \mu \frac{\partial u_z}{\partial r}\right) r. \tag{3.35}$$

When used in the predictor step above, the $\frac{\partial u_r}{\partial z}$ term is differenced in the forward direction, since the flux vector itself is differenced in the backward direction. The $\frac{\partial u_z}{\partial r}$ is differenced centrally. Therefore, a correctly differenced z-momentum term in the predictor step would

appear as

$$\frac{F^n_{4\,i,j} - F^n_{4\,i-1,j}}{\Delta z} = \frac{1}{\Delta z}\left[(\rho u_r u_z r)_{i,j} - \mu_{i,j}\frac{u_{r\,i+1,j} - u_{r\,i,j}}{\Delta z} r_{i,j} - \mu_{i,j}\frac{u_{z\,i,j+1} - u_{z\,i,j-1}}{2\Delta r} r_{i,j}\right.$$

$$\left. - (\rho u_r u_z r)_{i-1,j} + \mu_{i-1,j}\frac{u_{r\,i,j} - u_{r\,i-1,j}}{\Delta z} r_{i-1,j} + \mu_{i-1,j}\frac{u_{z\,i-1,j+1} - u_{z\,i-1,j-1}}{2\Delta r} r_{i-1,j}\right]. \quad (3.36)$$

3.2.2 Consistency, Stability and Convergence

Typically, any numerical scheme developed properly is consistent, due to the way in which it is developed [1]. In other words, the discrete equation being used in the calculation becomes the differential equation in the limit of vanishing length and time steps. But, more than that is necessary for the discrete equation to yield a correct solution. By the Lax Equivalence Theorem (see Richtmyer and Morton [45]), stability is the necessary and sufficient condition for a finite difference scheme to converge to the solution of the differential equation. Implicit numerical schemes, by their very nature, are unconditionally stable. Explicit methods such as MacCormack's method just described are only conditionally stable. The condition for convergence manifests itself as a limit on the time step used in the calculation. However, the same situation which necessitates numerical calculation, namely nonlinearity, also prevents one from getting better that a rough estimate of the limiting time step.

Anderson, Tannehill, and Pletcher [1] give an approximate time step criterion for MacCormack's method

$$\Delta t \leq \frac{\alpha\,(\Delta t)_{CFL}}{1 + \frac{2}{Re_\Delta}}, \quad (3.37)$$

where α is a safety factor and $(\Delta t)_{CFL}$ is the inviscid Courant-Friedrichs-Lewy criterion [28]

$$(\Delta t)_{CFL} \leq \left(\frac{|u|}{\Delta\xi} + \frac{|v|}{\Delta\eta} + c\sqrt{\frac{1}{(\Delta\xi)^2} + \frac{1}{(\Delta\eta)^2}}\right)^{-1}, \quad (3.38)$$

where

$$Re_\Delta = \min\left(Re_{\Delta\xi}, Re_{\Delta\eta}\right), \quad (3.39)$$

$$Re_{\Delta\xi} = \frac{\rho|u|\Delta\xi}{\mu}, \quad (3.40)$$

$$Re_{\Delta\eta} = \frac{\rho|v|\Delta\eta}{\mu}, \quad (3.41)$$

and where

$$c = \sqrt{\frac{\gamma p}{\rho}} \tag{3.42}$$

is the local speed of sound. The time step is calculated over the entire mesh by this method. When doing time accurate transient calculations, the smallest time step is used globally. When steady state solutions are desired, the equations could possibly be integrated according to the local time steps at each grid point, to decrease the number of iterations necessary for convergence. It was found, however, that due to the complexity of the equations, local time-stepping could not be used.

3.2.3 Numerical Smoothing

Due to numerical oscillations, computations involving the Navier-Stokes equations sometimes diverge. Numerical oscillations arise in areas where the computational grid is not refined adequately to resolve large gradients which occur. To overcome this problem, numerical smoothing terms, sometimes called artificial viscosity terms, are added to the equations to reduce the effect of these oscillations. Typically, the smoothing terms are made up of components which are proportional to the second derivative and fourth derivative of the state vector. The second order numerical smoothing is used in regions of shocks, so as to prevent Gibbs phenomena from appearing around the discontinuity. The fourth order smoothing is needed to dampen the "saw tooth" modes, which are actually solutions of the discrete equation, but not the partial differential equation.

For MacCormack's method, MacCormack and Baldwin [29] devised product type fourth order smoothing terms of the form

$$D_\xi = \nu_{4\xi} (\Delta\xi)^4 \frac{\partial}{\partial\xi} \left[\frac{|u| + c}{4p} \left| \frac{\partial^2 p}{\partial \xi^2} \right| \frac{\partial \mathbf{U}}{\partial \xi} \right] \tag{3.43}$$

$$D_\eta = \nu_{4\eta} (\Delta\eta)^4 \frac{\partial}{\partial\eta} \left[\frac{|u| + c}{4p} \left| \frac{\partial^2 p}{\partial \eta^2} \right| \frac{\partial \mathbf{U}}{\partial \eta} \right], \tag{3.44}$$

where $\nu_{4\xi}$ and $\nu_{4\eta}$ are fourth order artificial viscosity coefficients. For stability, $0 \leq \nu_4 \leq 0.5$. Miller [34] found that this form of the numerical smoothing terms was inadequate to dampen the oscillations, because of the ambiguity in the calculation of the pressure switch terms due to the fluid consisting of several different species. Instead, he used a simple one step

smoothing term based on the method of Kutler, Sakell, and Aiello [25]:

$$D^n_{i,j} = \nu_{2\xi}\left(\mathbf{U}^n_{i+1,j} - 2\mathbf{U}^n_{i,j} + \mathbf{U}^n_{i-1,j}\right) + \nu_{2\eta}\left(\mathbf{U}^n_{i,j+1} - 2\mathbf{U}^n_{i,j} + \mathbf{U}^n_{i,j-1}\right)$$

$$-\nu_{4\xi}\left(\mathbf{U}^n_{i+2,j} - 4\mathbf{U}^n_{i+1,j} + 6\mathbf{U}^n_{i,j} - 4\mathbf{U}^n_{i-1,j} + \mathbf{U}^n_{i-2,j}\right)$$

$$-\nu_{4\eta}\left(\mathbf{U}^n_{i,j+2} - 4\mathbf{U}^n_{i,j+1} + 6\mathbf{U}^n_{i,j} - 4\mathbf{U}^n_{i,j-1} + \mathbf{U}^n_{i,j-2}\right) \tag{3.45}$$

which was added to the corrector step only. This method was effective, but required much hands on adjustment of the artificial viscosity coefficients, with very little autonomy within the numerical smoothing subroutines. Given a discretized governing equation, several artificial viscosity coefficients were needed for different regions of the flow, and getting the right damping in the right areas of the flow while getting a good solution proved to be a very difficult and time consuming task.

To make the smoothing subroutine less hands on and more autonomous, an alternative smoothing scheme based on the suggestions of Peraire [39] was devised in which the damping terms were included within the flux vectors. This modified form of the fluid equations is

$$J\frac{\partial \mathbf{U}}{\partial t} + \frac{\partial}{\partial \xi}\left(\tilde{\mathbf{F}} - \nu_2 S_\xi \frac{J}{\Delta t}\frac{\partial \mathbf{U}}{\partial \xi} + \nu_4 \frac{J}{\Delta t}\frac{\partial^3 \mathbf{U}}{\partial \xi^3}\right)$$

$$+\frac{\partial}{\partial \eta}\left(\tilde{\mathbf{G}} - \nu_2 S_\eta \frac{J}{\Delta t}\frac{\partial \mathbf{U}}{\partial \eta} + \nu_4 \frac{J}{\Delta t}\frac{\partial^3 \mathbf{U}}{\partial \eta^3}\right) = J\mathbf{S}, \tag{3.46}$$

where the $\frac{J}{\Delta t}$ term is used for dimensional consistency, and S_ξ and S_η are switches analogous to the pressure switches in Equations 3.43 and 3.44. The switches in this case, however, are defined according to the quantity which they help modify. For example, in the global mass conservation equation, the switches are defined as

$$S_{\xi,i,j} = \frac{\left|\rho^n_{i+1,j} - 2\rho^n_{i,j} + \rho^n_{i-1,j}\right|}{\left|\rho^n_{i+1,j} - 2\rho^n_{i,j} + \rho^n_{i-1,j}\right|_{max}} \tag{3.47}$$

$$S_{\eta,i,j} = \frac{\left|\rho^n_{i,j+1} - 2\rho^n_{i,j} + \rho^n_{i,j-1}\right|}{\left|\rho^n_{i,j+1} - 2\rho^n_{i,j} + \rho^n_{i,j-1}\right|_{max}} \tag{3.48}$$

where the subscript max denotes the maximum over the entire grid. With this definition of the switches, the ambiguity due the multicomponent nature of the flow is removed. In

addition, there is a degree of autonomy introduced, in that the switches are scaled to the maximum value of the gradient, which allows artificial viscosity coefficients to be defined for the entire flow field instead of for just regions of the flow.

In discussing the formulation of the smoothing terms, it is useful to define difference and averaging operators. Taking cues from Anderson, Tannehill, and Pletcher; forward, backward and central difference operators are defined as

$$\Delta_\xi \varphi_{i,j} = \varphi_{i+1,j} - \varphi_{i,j} \ , \tag{3.49}$$

$$\nabla_\xi \varphi_{i,j} = \varphi_{i,j} - \varphi_{i-1,j} \ , \tag{3.50}$$

and

$$\delta_\xi \varphi_{i,j} = \varphi_{i+\frac{1}{2},j} - \varphi_{i-\frac{1}{2},j} \ , \tag{3.51}$$

respectively, while the averaging operator is defined as

$$\mu_\xi \varphi_{i,j} = \frac{1}{2}\left(\varphi_{i+\frac{1}{2},j} + \varphi_{i-\frac{1}{2},j}\right) \ , \tag{3.52}$$

where $\varphi_{i,j}$ is any quantity of interest at the grid point (i,j). Using Taylor series expansions, it can easily be shown that the order of accuracy of these operators is

$$\frac{\Delta_\xi \varphi_{i,j}}{\Delta\xi} = \frac{\partial\varphi}{\partial\xi}\Big)_{i,j} + O\left(\Delta\xi\right) \tag{3.53}$$

$$\frac{\nabla_\xi \varphi_{i,j}}{\Delta\xi} = \frac{\partial\varphi}{\partial\xi}\Big)_{i,j} + O\left(\Delta\xi\right) \tag{3.54}$$

$$\frac{\delta_\xi \varphi_{i,j}}{\Delta\xi} = \frac{\partial\varphi}{\partial\xi}\Big)_{i,j} + O\left[(\Delta\xi)^2\right] \tag{3.55}$$

$$\mu_\xi \varphi_{i,j} = \varphi_{i,j} + O\left[(\Delta\xi)^2\right] \ . \tag{3.56}$$

Also, from the above expressions it is easily seen that

$$\nabla_\xi \varphi_{i+\frac{1}{2},j} = \delta_\xi \varphi_{i,j} = \Delta_\xi \varphi_{i-\frac{1}{2},j} \tag{3.57}$$

and

$$\Delta_\xi \nabla_\xi \varphi_{i,j} = \nabla_\xi \Delta_\xi \varphi_{i,j} = \delta_\xi^2 \varphi_{i,j} \ , \tag{3.58}$$

where

$$\delta_\xi^2 \varphi_{i,j} = \varphi_{i+1,j} - 2\varphi_{i,j} + \varphi_{i-1,j} \tag{3.59}$$

is the central second difference operator.

With regards to the smoothing terms in the context of MacCormack's method, the first derivatives within are differenced in the same manner as the velocity gradients in the shear stress terms, that is, opposite to the way the fluxes are differenced. The third derivatives are differenced in a manner similar to the way the first derivatives are differenced, but done so with the overall goal being a second order accurate fourth difference to dampen saw tooth oscillations. Using the difference operators, the second order damping terms can be written as

$$\frac{\partial}{\partial \xi}\left(S_\xi J \frac{\partial u}{\partial \xi}\right)_P \approx \nabla_\xi \left(S_{\xi\, i,j}\, J_{i,j}\, \Delta_\xi\, u_{i,j}\right) \tag{3.60}$$

and

$$\frac{\partial}{\partial \eta}\left(S_\eta J \frac{\partial u}{\partial \eta}\right)_P \approx \nabla_\eta \left(S_{\eta\, i,j}\, J_{i,j}\, \Delta_\eta\, u_{i,j}\right) \tag{3.61}$$

for the predictor step and

$$\frac{\partial}{\partial \xi}\left(S_\xi J \frac{\partial u}{\partial \xi}\right)_C \approx \Delta_\xi \left(S_{\xi\, i,j}\, J_{i,j}\, \nabla_\xi\, u_{i,j}\right) \tag{3.62}$$

and

$$\frac{\partial}{\partial \eta}\left(S_\eta J \frac{\partial u}{\partial \eta}\right)_C \approx \Delta_\eta \left(S_{\eta\, i,j}\, J_{i,j}\, \nabla_\eta\, u_{i,j}\right) \tag{3.63}$$

for the corrector step, where u is an element of the vector $\mathbf{U}$. Using the differences in ξ as an example, using Equations 3.60 and 3.62 and the relation in Equation 3.57 and performing the summing and averaging procedure as in MacCormack's method yields

$$\frac{1}{2}\left[\frac{\partial}{\partial \xi}\left(S_\xi J \frac{\partial u}{\partial \xi}\right)_P + \frac{\partial}{\partial \xi}\left(S_\xi J \frac{\partial u}{\partial \xi}\right)_C\right] \approx \frac{1}{2}\left[\nabla_\xi \left(S_{\xi\, i,j}\, J_{i,j}\, \Delta_\xi\, u_{i,j}\right) + \Delta_\xi \left(S_{\xi\, i,j}\, J_{i,j}\, \nabla_\xi\, u_{i,j}\right)\right]$$

$$= \frac{1}{2}\delta_\xi \left(S_{\xi\, i-\frac{1}{2},j}\, J_{i-\frac{1}{2},j}\, \Delta_\xi\, u_{i-\frac{1}{2},j} \;+\; S_{\xi\, i+\frac{1}{2},j}\, J_{i+\frac{1}{2},j}\, \nabla_\xi\, u_{i+\frac{1}{2},j}\right)$$

$$= \delta_\xi \left[\frac{1}{2}\left(S_{\xi\, i-\frac{1}{2},j}\, J_{i-\frac{1}{2},j} + S_{\xi\, i+\frac{1}{2},j}\, J_{i+\frac{1}{2},j}\right)\delta_\xi\, u_{i,j}\right] = \delta_\xi \left[\mu_\xi (S_{\xi\, i,j}\, J_{i,j})\, \delta_\xi\, u_{i,j}\right], \tag{3.64}$$

which is exactly second order accurate. For second order accuracy in the fourth order

smoothing terms, the differences are as follows:

$$\frac{\partial}{\partial \xi}\left(J\frac{\partial^3 u}{\partial \xi^3}\right)_P \approx \nabla_\xi\left(J_{i,j}\,\Delta_\xi\,\delta_\xi^2\,u_{i,j}\right) = \delta_\xi\left(J_{i-\frac{1}{2},j}\,\delta_\xi^3\,u_{i,j}\right) \tag{3.65}$$

and

$$\frac{\partial}{\partial \eta}\left(J\frac{\partial^3 u}{\partial \eta^3}\right)_P \approx \nabla_\eta\left(J_{i,j}\,\Delta_\eta\,\delta_\eta^2\,u_{i,j}\right) = \delta_\eta\left(J_{i,j-\frac{1}{2}}\,\delta_\eta^3\,u_{i,j}\right) \tag{3.66}$$

for the predictor step and

$$\frac{\partial}{\partial \xi}\left(J\frac{\partial^3 u}{\partial \xi^3}\right)_C \approx \Delta_\xi\left(J_{i,j}\,\nabla_\xi\,\delta_\xi^2\,u_{i,j}\right) = \delta_\xi\left(J_{i+\frac{1}{2},j}\,\delta_\xi^3\,u_{i,j}\right) \tag{3.67}$$

and

$$\frac{\partial}{\partial \eta}\left(J\frac{\partial^3 u}{\partial \eta^3}\right)_C \approx \Delta_\eta\left(J_{i,j}\,\nabla_\eta\,\delta_\eta^2\,u_{i,j}\right) = \delta_\eta\left(J_{i,j+\frac{1}{2}}\,\delta_\eta^3\,u_{i,j}\right) \tag{3.68}$$

for the corrector step. As with the second order smoothing terms, the summing and averaging procedure in MacCormack's method yields smoothing terms which are second order accurate in space.

3.3 Successive Over-relaxation Method

Relaxation schemes start with an initial guess and iterate a system of equations. How the iteration is performed depends upon the relaxation scheme used. The general form of a system of equations is

$$\overline{\overline{A}} \cdot \vec{x} = \vec{b}, \tag{3.69}$$

where $\overline{\overline{A}}$ is a coefficient matrix, $\vec{x}$ is a vector of unknowns, and $\vec{b}$ is a vector of constants. The matrix $\overline{\overline{A}}$ can be decomposed into parts

$$\overline{\overline{A}} = \overline{\overline{L}} + \overline{\overline{D}} + \overline{\overline{U}}, \tag{3.70}$$

where $\overline{\overline{D}}$ is the diagonal part of $\overline{\overline{A}}$, $\overline{\overline{L}}$ is the lower triangular portion of $\overline{\overline{A}}$ with zeros along the diagonal, and $\overline{\overline{U}}$ is the upper triangular portion of $\overline{\overline{A}}$, also with zeros along the diagonal. Relaxation schemes require diagonal dominance to work correctly. In other words, the magnitude of the coefficients along the diagonal is larger than the other coefficients. For the sparse matrix generated by finite differencing, diagonal dominance is nearly guaranteed.

The starting point for understanding relaxation methods is Jacobi's method. In matrix notation, Jacobi's method appears as

$$\overline{\overline{D}} \cdot \vec{x}^{\,n} = \vec{b} - \left(\overline{\overline{L}} + \overline{\overline{U}}\right) \cdot \vec{x}^{\,n-1}, \tag{3.71}$$

where the superscripts indicate the iteration level. From this equation one can see that all of the values at time level $n-1$ are used to update the new values st time level n at each point. It terms of computer resources, this requires more memory, since there must be an array to hold the old values plus an array in which the new values are stored. In addition, Jacobi's method converges rather slowly. To reduce the overall error by a factor of 10^{-p} for an $m \times m$ grid, the approximate number of iterations needed for large m is [43]

$$n \approx \frac{1}{2} p m^2, \tag{3.72}$$

which is hopelessly large for many problems. For a 100×100 grid, an error of 10^{-4} requires about 20,000 iterations.

An improvement to Jacobi's method is the Gauss-Seidel method. In matrix notation, the Gauss-Seidel method is

$$\left(\overline{\overline{L}} + \overline{\overline{D}}\right) \cdot \vec{x}^{\,n} = \vec{b} - \overline{\overline{U}} \cdot \vec{x}^{\,n-1}. \tag{3.73}$$

If one were to write out Equation 3.73 in components, it would easily be seen that the updated values of $\vec{x}$ are used as they are acquired. This reduces the amount of necessary memory, as the old values of $\vec{x}$ are overwritten as the new values of $\vec{x}$ are found. The convergence characteristics are a bit better. For large m, the number of iterations needed to reduce the overall error by a factor of 10^{-p} is

$$n \approx \frac{1}{4} p m^2, \tag{3.74}$$

which is better, but still not very good.

The Successive Over-relaxation (SOR) method is yet another improvement. In the Successive Over-relaxation scheme, the answer from the Gauss-Seidel method is over-corrected through an overcorrection factor, ω. In matrix notation, Successive Over-relaxation is writ-

ten as

$$\overline{\overline{D}} \cdot \vec{x}^{\,n} = (1-\omega)\,\overline{\overline{D}} \cdot \vec{x}^{\,n-1} + \omega\left(\vec{b} - \overline{\overline{L}} \cdot \vec{x}^{\,n} - \overline{\overline{U}} \cdot \vec{x}^{\,n-1}\right). \tag{3.75}$$

The convergence characteristics of SOR are entirely determined by the overcorrection factor. The optimal value of ω is

$$\omega = \frac{2}{1+\sqrt{1-\rho_{Jacobi}^2}}, \tag{3.76}$$

where ρ_{Jacobi} is known as the spectral radius of Jacobi's method, which is given by Press et al. [43] as

$$\rho_{Jacobi} = \frac{\cos\frac{\pi}{m} + \left(\frac{\Delta\xi}{\Delta\eta}\right)^2 \cos\frac{\pi}{n}}{1+\left(\frac{\Delta\xi}{\Delta\eta}\right)^2}, \tag{3.77}$$

where m and n are the grid dimensions. For this optimal value of ω, the number of iterations to reduce the error by a factor of 10^{-p} on a square grid with large m is

$$n \approx \frac{1}{3}pm, \tag{3.78}$$

which is a dramatic improvement over both the Jacobi and Gauss-Seidel methods. For a 100×100 grid, the number of iterations needed to reduce the error by a factor of 10^{-4} is about 134 iterations, which is less than 1% of the iterations needed for Jacobi's method.

Using central differences for second order accuracy, the discretized electrical potential equation (Equation 3.24) becomes

$$\begin{aligned} &a_{i,j}\left(\phi_{i+1,j} - 2\phi_{i,j} + \phi_{i-1,j}\right) + b_{i,j}\left(\phi_{i,j+1} - 2\phi_{i,j} + \phi_{i,j-1}\right) \\ &\quad + \frac{c_{i,j}}{4}\left(\phi_{i+1,j+1} - \phi_{i+1,j-1} - \phi_{i-1,j+1} + \phi_{i-1,j-1}\right) \\ &\quad + \frac{d_{i,j}}{2}\left(\phi_{i+1,j} - \phi_{i-1,j}\right) + \frac{e_{i,j}}{2}\left(\phi_{i,j+1} - \phi_{i,j-1}\right) = f_{i,j}, \end{aligned} \tag{3.79}$$

where iteration levels have been left off to avoid confusion. When used with SOR just described, the solution to the electrical potential at each point of the grid is iterated according to

$$\phi_{i,j}^{n+1} = (1-\omega)\,\phi_{i,j}^{n} + \frac{\omega}{2\,(a_{i,j}+b_{i,j})}\left[\left(a_{i,j}+\frac{d_{i,j}}{2}\right)\phi_{i+1,j}^{n} + \left(a_{i.j}-\frac{d_{i,j}}{2}\right)\phi_{i-1,j}^{n+1}\right.$$

$$+\left(b_{i,j}+\frac{e_{i,j}}{2}\right)\phi_{i,j+1}^{n} + \left(b_{\imath,j}-\frac{e_{i,j}}{2}\right)\phi_{i,j-1}^{n+1}$$

$$\left.+\frac{c_{i,j}}{4}\left(\phi_{i+1,j+1}^{n} - \phi_{i+1,j-1}^{n} - \phi_{i-1,j+1}^{n} + \phi_{i-1,j-1}^{n+1}\right) - f_{i,j}\right], \tag{3.80}$$

where the $2\,(a_{i,j}+b_{i,j})$ factor in the denominator corresponds to the elements of $\overline{\overline{D}}$, while the other constants correspond to the off-diagonal elements in $\overline{\overline{L}}$ and $\overline{\overline{U}}$.

3.4 Grid Generation

Since the previously described numerical methods require a discretized domain, it would be of value to describe how the domain is discretized. In general, one wants to put a larger number of points in regions where one expects large gradients in the flow properties. When dealing with inviscid flow cases, extra points could be put in the areas where one would expect shocks. When dealing with the Navier-Stokes equations, it is also necessary to put extra points near the grid boundaries which are treated as walls to resolve the viscous boundary layer.

There are two major ways of discretizing a domain. One way is to use structured grids, the other is to use unstructured grids. In two dimensions, unstructured grids are typically made up of triangular cells and are determined using a Delaunay triangulation technique, and are used within the finite volume or finite element formulation. The "random" arrangement of cells, edges, and nodes in an unstructured grid makes the usage of finite difference methods unthinkable.

The error that a numerical scheme incurs is affected by the skewness of the grid. For unstructured grids, Delaunay triangulation is used to make the grid incur less error. Given a set of points, the Delaunay triangulation assures a unique, non-overlapping set of triangular cells such that the skewness of the grid is minimized. The criterion used in the Delaunay triangulation is the circumcircle criterion. The circumcircle criterion can be described as follows. A circle is uniquely defined by three points. If the circumcircle defined by the vertices of a triangular cell contains a vertex of another triangle, the cell fails the criterion,

and the triangular cell is not Delaunay, and the error in not minimized.

Unfortunately, the criterion which minimizes the truncation error for unstructured grids also makes an unstructured grid unsuited to numerical integration of the Navier-Stokes equations for problems involving a viscous boundary layer. In regions close to wall boundaries, the minimal skewness of an unstructured grid requires many more points along the wall than are needed, because of the large gradients in fluid properties perpendicular to the wall. In addition, there is no simple way of treating the viscous shear stress terms. Structured meshes are much better suited to resolving a boundary layer, since the structured cells can be stretched in the direction parallel to the wall. Aspect ratios of 100 to 1 are not uncommon in areas where a viscous boundary layer is present. In addition, the organized arrangement of cells in a structured grid makes the treatment of the viscous shear stress terms much simpler. One could conceivably create a structured grid to resolve the boundary layer, and then create an unstructured grid to mate to the structured mesh. For the purposes of this research, a structured grid was chosen, since viscous effects may be important and since a finite difference scheme was chosen to integrate the Navier-Stokes equations.

When using finite difference methods on structured meshes, the organization of the points in the final grid chosen to perform the calculations should be smooth, so that no major errors are created due to differencing on a discontinuous grid. To create a mesh of smoothed points, the elliptic partial differential equation method of Thompson et al. [51] is used. Once the initial guess grid is specified, the points are moved so as to satisfy the coupled Poisson equations

$$\xi_{zz} + \xi_{rr} = P(\xi, \eta), \tag{3.81}$$

and

$$\eta_{zz} + \eta_{rr} = Q(\xi, \eta), \tag{3.82}$$

where $P(\xi, \eta)$ and $Q(\xi, \eta)$ are source terms which control the grid spacing. In natural coordinates, these equations become

$$\alpha z_{\xi\xi} - 2\beta z_{\xi\eta} + \gamma z_{\eta\eta} = -J^2 (P z_\xi + Q z_\eta), \tag{3.83}$$

$$\alpha r_{\xi\xi} - 2\beta r_{\xi\eta} + \gamma r_{\eta\eta} = -J^2 (P r_\xi + Q r_\eta), \tag{3.84}$$

where

$$\alpha = z_\eta^2 + r_\eta^2, \tag{3.85}$$

$$\beta = z_\xi z_\eta + r_\xi r_\eta, \tag{3.86}$$

$$\gamma = z_\xi^2 + r_\xi^2, \tag{3.87}$$

and

$$J = z_\xi r_\eta - z_\eta r_\xi. \tag{3.88}$$

The form of the forcing functions can be many things. Thompson et al. proposed

$$P(\xi,\eta) = -\sum_{m=1}^{M} a_m \frac{\xi - \xi_m}{|\xi - \xi_m|} e^{-c_m|\xi-\xi_m|} - \sum_{i=1}^{I} b_i \frac{\xi - \xi_i}{|\xi - \xi_i|} e^{-d_i\left[(\xi-\xi_i)^2+(\eta-\eta_i)^2\right]^{\frac{1}{2}}}, \tag{3.89}$$

$$Q(\xi,\eta) = -\sum_{m=1}^{M} a_m \frac{\eta - \eta_m}{|\eta - \eta_m|} e^{-c_m|\eta-\eta_m|} - \sum_{i=1}^{I} b_i \frac{\eta - \eta_i}{|\eta - \eta_i|} e^{-d_i\left[(\xi-\xi_i)^2+(\eta-\eta_i)^2\right]^{\frac{1}{2}}}, \tag{3.90}$$

where a_m, b_i, c_m, and d_i are adjustable constants.

Instead of using Thompson's equations to solve the computational grid, an alternative method based on Thompson's equations can be used. Thompson's equations can be rewritten as

$$(K\xi_z)_z + (K\xi_r)_r = 0, \tag{3.91}$$

$$(K\eta_z)_z + (K\eta_r)_r = 0, \tag{3.92}$$

where K is called the variable conductivity [39]. In transformed natural coordinates, these equations can be rewritten as

$$\alpha z_{\xi\xi} - 2\beta z_{\xi\eta} + \gamma z_{\eta\eta} = J\left(\frac{K_\xi}{K} r_\eta - \frac{K_\eta}{K} r_\xi\right), \tag{3.93}$$

$$\alpha r_{\xi\xi} - 2\beta r_{\xi\eta} + \gamma r_{\eta\eta} = -J\left(\frac{K_\xi}{K} z_\eta - \frac{K_\eta}{K} z_\xi\right), \tag{3.94}$$

with α, β and γ defined as before. The variable conductivity can be a simple or complex function of ξ and η. In general, the grid spacing increases with increasing K. It is this version of Thompson's equations which was used to solve for the grids used in this research. In general the grid is calculated so that ξ increases from left to right and η increases from bottom to top.

Since this research is an extension of the work of Scott Miller, the way in which things are accomplished in this research is similar if not identical to the way things are accomplished in Miller's work. This applies to the electrical potential calculation as well. In the flow regions inside the constrictor and downstream to the exit, the potential calculation is performed on the fluid grid. In the region just downstream of the cathode tip, a separate grid was generated to take into account the regions of high gradients in electron density, current density, and electrical potential near the tip. The quantities which are calculated on this potential grid are then interpolated onto the fluid grid. Figure 3-1 shows an example of the overlapping potential and fluid grids as used in this research. The potential grid (the fine grid) can be seen superimposed on the fluid grid. The potential calculation transitions from the potential grid to the fluid grid at the grid point shown. The advantage of using this kind of potential grid is that the current is confined to a certain portion of the thruster, thus simplifying the calculation. This kind of arrangement also serves to prevent non-physical solutions such as the current flowing upstream. The disadvantage, of course, is that it introduces an extra calculation for interpolation between the two grids.

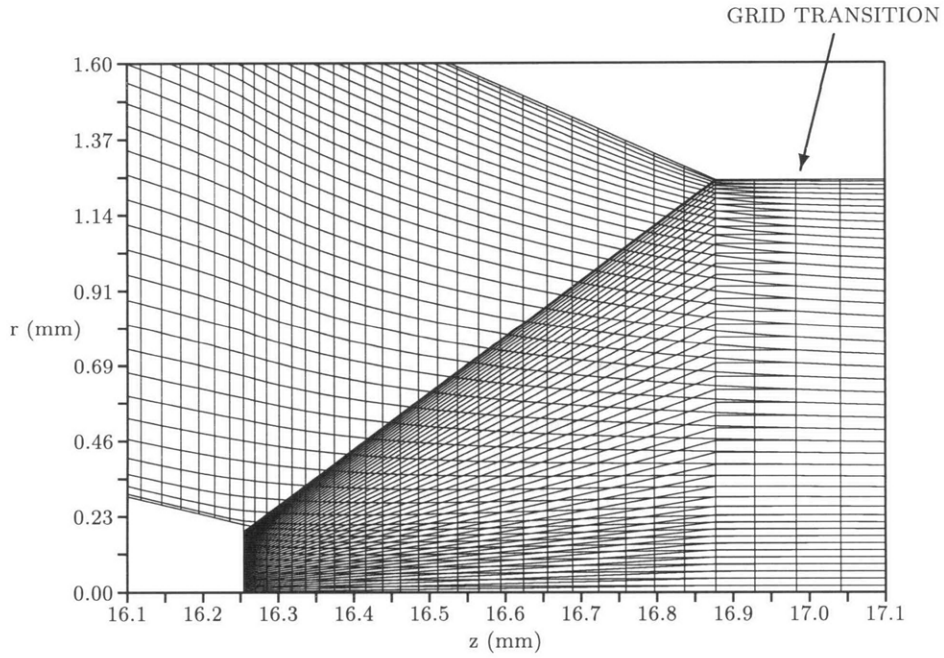

Figure 3-1: *Example of Overlapping Fluid and Potential Grids as Used in This Research*

3.5 Boundary Conditions

As with any numerical integration scheme, the correct boundary conditions are absolutely essential in getting a correct solution. Because of this, one typically spends more time getting the boundary conditions right than actually trying to get a solution. This research was no different. In fact, due to the multicomponent nature of the flow, the boundary conditions were found to be extremely volatile, and the slightest mistake in coding would send the solution over the edge, as it were. These details are left for discussion in the next chapter.

In calculating boundary conditions, the Dirichlet type of boundary conditions are easiest to implement, since the boundary values need only be specified once at the nodes on the boundary. Neumann conditions, on the other hand, require much more computational effort, since the gradient normal to the boundary is specified. For Neumann boundary conditions, the quantity φ at the boundary is specified according to

$$\left.\frac{\partial \varphi}{\partial \hat{n}}\right|_{bndy} = \Theta, \tag{3.95}$$

where $\hat{n}$ is the unit outward normal and Θ is often identically zero. This equation can be rewritten as

$$(\nabla\varphi \cdot \hat{n})_{bndy} = \left[\left(\frac{\partial \varphi}{\partial z}\,\hat{z} + \frac{\partial \varphi}{\partial r}\,\hat{r}\right) \cdot \hat{n}\right]_{bndy} = \Theta, \tag{3.96}$$

where $\nabla\varphi$ is the gradient in the $z-r$ coordinate system. The unit outward normal vector is defined as shown in Figure 3-2, where $\hat{z}$ and $\hat{r}$ are unit vectors in the z and r directions, respectively, and $\hat{n}$ and $\hat{s}$ are the outward unit surface normal and counterclockwise unit surface tangent vectors, respectively, and β is the angle between $\hat{z}$ and $\hat{n}$.

In terms of β, $\hat{z}$, and $\hat{r}$, the unit normal and tangent vectors can be written as

$$\hat{n} = \cos\beta\,\hat{z} + \sin\beta\,\hat{r} \tag{3.97}$$

and

$$\hat{s} = -\sin\beta\,\hat{z} + \cos\beta\,\hat{r}. \tag{3.98}$$

Since the z and r values are known at the boundary, the unit tangent vector can be written

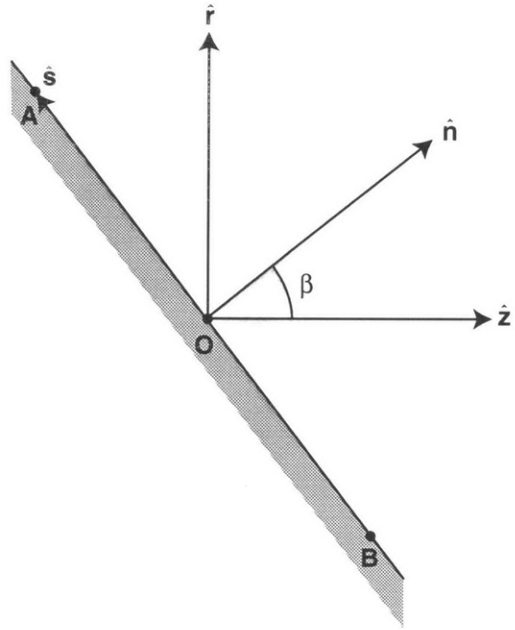

Figure 3-2: *Coordinate Axes Used for the Calculation of Boundary Conditions*

as

$$\hat{s} = \frac{z_A - z_B}{\Delta s}\,\hat{z} + \frac{r_A - r_B}{\Delta s}\,\hat{r}, \tag{3.99}$$

where

$$\Delta s = \sqrt{(z_A - z_B)^2 + (r_A - r_B)^2}\,, \tag{3.100}$$

and it has been assumed that $\overline{OB}$ and $\overline{OA}$ are collinear. From the above equations it is easily seen that

$$\cos\beta = \frac{r_A - r_B}{\Delta s} \tag{3.101}$$

and

$$\sin\beta = -\frac{z_A - z_B}{\Delta s}\,, \tag{3.102}$$

so that the unit normal vector can be written as

$$\hat{n} = \frac{r_A - r_B}{\Delta s}\,\hat{z} - \frac{z_A - z_B}{\Delta s}\,\hat{r}. \tag{3.103}$$

The differences $r_A - r_B$ and $z_A - z_B$ can be put in terms of the grid metrics at the boundaries. For example, at the exit boundary, if O is at the grid point (i, j), then A is located at $(i, j+1)$ and B is at $(i, j-1)$. The unit normal vector can then be calculated

as

$$\hat{n} = \frac{r_{i,j+1} - r_{i,j-1}}{\Delta s}\,\hat{z} - \frac{z_{i,j+1} - z_{i,j-1}}{\Delta s}\,\hat{r}, \tag{3.104}$$

with

$$\Delta s = \sqrt{(r_{i,j+1} - r_{i,j-1})^2 + (z_{i,j+1} - z_{i,j-1})^2}, \tag{3.105}$$

which can conveniently be written as

$$\hat{n} = \left.\frac{r_\eta}{\Delta s}\right|_{i,j}\hat{z} - \left.\frac{z_\eta}{\Delta s}\right|_{i,j}\hat{r}, \tag{3.106}$$

with

$$\Delta s = \sqrt{r_\eta^2 + z_\eta^2}, \tag{3.107}$$

where r_η and z_η are the same grid metrics which need to be calculated anyway in the transformation of the governing equations from real to natural coordinates. This form of the unit tangent vector makes boundary value calculations much easier, as the values of the grid metrics would already be stored in memory from the grid transformation calculations.

3.5.1 Fluid Boundary Conditions

Inlet Boundary

In the following discussion, a distinction must be made to avoid confusion. The *inlet flow* and the *inlet boundary* are distinct and separate. The term inlet flow denotes the flow upstream of the grid. This inlet flow is assumed to behave as a free stream flow, and cannot "see" the grid. The inlet boundary contains the first boundary nodes of the computational grid to be affected by the inlet flow. The inlet flow is assumed to be uniform and subsonic. The flow variables at an inlet boundary node are specified according to the assumed inlet flow and information about the first point inside the inlet boundary. In most experimental arcjets, either the total mass flow rate or the plenum pressure is specified. For this research, when doing computations, the pressure of the inlet flow is specified. The flow speed is found according to Riemann invariants (to be described shortly). By distributing the desired mass flow rate per unit area (mass flux) evenly amongst the inlet boundary nodes on the inlet boundary, the density, pressure, and temperature at the inlet boundary can then be found.

The inlet flow is assumed to be uniform and parallel to the thruster walls, so that $u_r = 0$. With information about the inlet velocity and the axial velocity at the first interior node, the axial velocity at the boundary can be calculated using Riemann invariants. In a nutshell, Riemann invariants are values which are constant along certain paths within an ideal fluid flow. These paths are called characteristic lines. Along these lines, the governing partial differential equations of motion can be reduced to ordinary differential equations [2]. For the present discussion, there are two characteristic lines of importance, the C_+ or "right-running" characteristic, and the C_- or "left-running" characteristic. The Riemann invariants are

$$J_+ = u + \frac{2c}{\gamma - 1} = \text{constant} \tag{3.108}$$

along the C_+ characteristic line and

$$J_- = u - \frac{2c}{\gamma - 1} = \text{constant} \tag{3.109}$$

along the C_- characteristic line, where u is the local flow speed, c is the local sound speed, and γ is the local specific heat ratio. For purposes of inlet boundary values, disturbances from the inlet propagate downstream into the grid domain along C_+, while disturbances propagate upstream from the grid domain along C_-. In other words, $J_{+,\,in} = J_{+,\,bndy}$ and $J_{-,\,grid} = J_{-,\,bndy}$, where the *in* and *grid* subscripts denote values taken from the inlet and grid, respectively. Usage of the Riemann invariants yields the axial boundary velocity

$$u_{z,bndy} = \frac{1}{2}\left(u_{z,in} + u_{z,grid}\right) + \frac{c_{in} - c_{grid}}{\gamma_b - 1}. \tag{3.110}$$

For the range of inlet conditions studied in this research, the inlet gas is very nearly diatomic. The ionization fraction is set to a limit of 10^{-6} and the atom mass fraction s set to a limit of 10^{-4} for numerical reasons. At the inlet, the effect of the electrons is negligible. Therefore, using $\gamma_b \approx 1.4$ is a very good approximation and the speeds of sound can be calculated using the heavy species gas temperature, T_g. In experimental arcjets, an azimuthal swirl velocity is added to stabilize the are during startup, and is typically 30-50% of the axial velocity. This azimuthal velocity at the boundary is set to be $u_{\theta,b} = 0.4\,u_{z,b}$.

Once the velocity at the boundary is obtained, the one-dimensional energy equation

$$\frac{\gamma}{\gamma-1}\left(\frac{p_1}{\rho_1}\right)+\frac{u_1^2}{2}=\frac{\gamma}{\gamma-1}\left(\frac{p_2}{\rho_2}\right)+\frac{u_2^2}{2} \tag{3.111}$$

and the isentropic relation

$$\frac{p_2}{p_1}=\left(\frac{\rho_2}{\rho_1}\right)^{\gamma}=\left(\frac{T_2}{T_1}\right)^{\frac{\gamma}{\gamma-1}} \tag{3.112}$$

are used to obtain the density, pressure, and temperature at the boundary nodes. In particular, the density is found through

$$\rho_{bndy}=\rho_{in}\left[1-\frac{\gamma_b-1}{2}\frac{\left(u_{z,in}^2-u_{z,b}^2\right)}{\gamma R_b T_{g,b}}\right]^{\frac{1}{\gamma-1}}. \tag{3.113}$$

and the pressure is found through the isentropic relation. Again, neglecting the effect of electrons, $R_b \approx R_{S_2}$. When the calculations are first begun, the temperature at the boundary can be approximated as $T_{g,b} \approx \frac{1}{2}\left(T_{g,in}+T_{g,grid}\right)$. After the first iteration, the temperature as calculated from the previous iteration can be used.

The electron temperature is a special case. Since the electrons are much more mobile than the heavy species, it is assumed that there is no electron temperature gradient at the inlet. The condition on the electron temperature from Equation 3.96 is then

$$\left(\frac{\partial T_e}{\partial z}\hat{z}+\frac{\partial T_e}{\partial r}\hat{r}\right)\cdot\hat{n}=0. \tag{3.114}$$

The unit normal for the inlet in terms of the grid metrics is

$$\hat{n}=-\frac{r_\eta}{\Delta s}\hat{z}+\frac{z_\eta}{\Delta s}\hat{r}. \tag{3.115}$$

Using Equations 3.6-3.8, 3.114 and 3.115 and rearranging, the electron temperature at the boundary can be calculated according to

$$\frac{\partial T_e}{\partial \xi}-\frac{z_\xi z_\eta+r_\xi r_\eta}{z_\eta^2+r_\eta^2}\frac{\partial T_e}{\partial \eta}=0. \tag{3.116}$$

For example, using forward differences in ξ and central differences in η, the electron tem-

perature at boundary point (i, j) is

$$T_{e\,i,j} = T_{e\,i+1,j} - \left.\frac{z_\xi z_\eta + r_\xi r_\eta}{z_\eta^2 + r_\eta^2}\right|_{i,j} \frac{T_{e\,i,j+1} - T_{e\,i,j-1}}{2}. \tag{3.117}$$

If the grid lines are perpendicular at the boundary, Equation 3.117 reduces to

$$T_{e\,i,j} = T_{e\,i+1,j}\,. \tag{3.118}$$

Outlet Boundary

The values at the outlet boundary typically vary according to whether the flow is subsonic or supersonic. In the supersonic regions of the exit plane, the flow variables can simply be extrapolated, since no information propagates upstream. Therefore, the variables at boundary node (i, j) are specified according to

$$\varphi_{i,j} = 2\varphi_{i-1,j} - \varphi_{i-2,j}. \tag{3.119}$$

The temperatures, densities, and mass fractions are all extrapolated at the exit plane. The heavy species and electron pressures are then calculated using these extrapolated temperatures and densities.

The subsonic regions at the outlet boundary are near the nozzle walls, in the viscous boundary layer. In the nonequilibrium boundary layer, the validity of using the Riemann invariants to find the flow variables is questionable at best. However, the subsonic region at the nozzle exit is typically very small. In addition, since the current is forced to attach upstream of the exit, the current effects are minimal. Therefore, the error incurred by using Riemann invariants is small. The static pressure in the subsonic regions is taken to be the average of the static pressure at the first upstream node and some exit static pressure. The exit static pressure is taken to be some small value near vacuum, but large enough to not cause numerical difficulties. The fluid density is then specified according to

$$\rho_{i,j} = \rho_{i-1,j} \left(\frac{p_{i,j}}{p_{i-1,j}}\right)^{\frac{1}{\gamma}}. \tag{3.120}$$

The heavy gas temperature is then extracted by using this density and the aforementioned

pressure. The axial velocity is specified using the J_+ invariant

$$u_{z\,i,j} = u_{z\,i-1,j} + \frac{2}{\gamma - 1}\left(c_{i-1,j} - c_{i,j}\right). \tag{3.121}$$

As with the inlet conditions, due to the mobility of the electrons, it is assumed that there is no electron temperature gradient at the exit. Using the grid metrics method described above, the electron temperature, this time using a backward difference in ξ, is

$$T_{e\,i,j} = T_{e\,i-1,j} + \left.\frac{z_\xi z_\eta + r_\xi r_\eta}{z_\eta^2 + r_\eta^2}\right|_{i,j} \frac{T_{e\,i,j+1} - T_{e\,i,j-1}}{2}. \tag{3.122}$$

However, it was found that this calculated electron temperature, when utilized with the coupled electrical potential calculation, was unstable. Due to this instability, the electron temperature was calculated according to

$$T_{e\,i,j} = T_{e\,i-1,j}. \tag{3.123}$$

This simpler calculation is accurate in regions of grid orthogonality, but it quickly degrades in regions where the grid lines are non-orthogonal. Nonetheless, the calculation seems to provide decent results.

Centerline Boundary

The centerline boundary of the arcjet is a symmetry boundary. As such, the Neumann or zero gradient condition is imposed on all of the flow variables. Since the centerline boundary is one of constant η, the variables at the centerline boundary are calculated using forward differences in η and central in ξ. In terms of the grid metrics, the flow variables at the centerline are calculated according to

$$\varphi_{i,j} = \varphi_{i,j+1} - \left.\frac{z_\xi z_\eta + r_\xi r_\eta}{z_\xi^2 + r_\xi^2}\right|_{i,j} \frac{\varphi_{i+1,j} - \varphi_{i-1,j}}{2}. \tag{3.124}$$

Wall Boundaries

Any solid surface immersed in a partially ionized gas develops a non-neutral sheath adjacent to it due to the higher mobility of the electrons. The thickness of this sheath depends on temperature and pressure and is of the order of the Debye length. For the range of

temperatures and pressures within arcjets, the Debye length is of the order of $10^{-8} - 10^{-6}$ meters. For this reason, the sheath region is neglected in the actual calculations, and the wall boundaries are treated as sheath boundaries.

Neumann boundary conditions are applied to the wall boundaries. In the case of the electron density, however, the gradient is not zero. The assumption is that the flux of ions arriving at the sheath boundary due to ambipolar diffusion is the same as the flux of ions reaching the wall at the Bohm velocity. This condition yields the following boundary condition on the electron density [55]:

$$D_a \frac{\partial \rho_e}{\partial \hat{n}} = 0.37 \rho_e v_B, \tag{3.125}$$

where

$$v_B = \sqrt{\frac{k\,(T_g + T_e)}{m_{S+}}} \tag{3.126}$$

is the Bohm velocity. Therefore, the electron density at the η = constant wall boundaries is calculated from

$$\rho_{e\,i,j} = \left(1 + \left. \frac{0.37 v_B J}{\sqrt{z_\xi^2 + r_\xi^2}} \right|_{i,j} \right)^{-1} \left(\rho_{e\,i,j\mp 1} \pm \left. \frac{z_\xi z_\eta + r_\xi r_\eta}{z_\xi^2 + r_\xi^2} \right|_{i,j} \frac{\rho_{e\,i+1,j} - \rho_{e\,i-1,j}}{2} \right), \tag{3.127}$$

where the upper sign is for the upper wall boundary and the lower sign is for the lower wall boundary and J is the Jacobian of the grid transformation. On the cathode tip, ξ = constant and

$$\rho_{e\,i,j} = \left(1 + \left. \frac{0.37 v_B J}{\sqrt{z_\eta^2 + r_\eta^2}} \right|_{i,j} \right)^{-1} \left(\rho_{e\,i+1,j} - \left. \frac{z_\xi z_\eta + r_\xi r_\eta}{z_\eta^2 + r_\eta^2} \right|_{i,j} \frac{\rho_{e\,i,j+1} - \rho_{e\,i,j-1}}{2} \right). \tag{3.128}$$

The first term in parentheses in both equations appears because of the non-zero gradient.

The heavy species temperature is specified according what is found in experiment. Miller incorporated an anode heat balance model into his original code to gauge the effects of a more realistic temperature condition on the anode boundaries, and found that there was no significant improvement in the flow calculations. As a result, to simplify the calculations, the temperatures on the anode walls were specified. For the radiatively-cooled TT1 thruster, the temperature on the cathode is specified at 1000 K at the inlet, and increases linearly

to 2000 K on the cathode tip. On the anode, the temperature is specified at 1000 K from the inlet to the beginning of the constrictor. In the constrictor region, the temperature increases linearly to 1100 K at the constrictor exit, and remains at 1100 K to the nozzle exit. For the water-cooled TT1 thruster, the cathode temperature is set at 300 K at the inlet, increasing to 2000 K at the cathode tip. The temperature along the anode is set to be 300 K at the inlet, increasing to 1100 K at the constrictor exit, and then reduced to 300 K at the nozzle exit. For the NASA Lewis thruster, the cathode temperature is specified to be 300 K at the inlet, increasing to 2000 K at the cathode tip. The anode temperature is set to 300 K at the inlet, increasing to 2000 K at the constrictor exit, and remaining at 2000 K thereafter.

The zero gradient condition is applied to the electron temperature. This means that

$$T_{e\,i,j} = T_{e\,i,j\mp1} \pm \left.\frac{z_\xi z_\eta + r_\xi r_\eta}{z_\xi^2 + r_\xi^2}\right|_{i,j} \frac{T_{e\,i+1,j} - T_{e\,i-1,j}}{2}, \tag{3.129}$$

is used to calculate the temperature on the η = constant boundaries, and

$$T_{e\,i,j} = T_{e\,i+1,j} - \left.\frac{z_\xi z_\eta + r_\xi r_\eta}{z_\eta^2 + r_\eta^2}\right|_{i,j} \frac{T_{e\,i,j+1} - T_{e\,i,j-1}}{2}. \tag{3.130}$$

on the cathode tip. Once the electron temperature is determined, the electron pressure is calculated. The zero gradient condition is then applied to the total static pressure ($p_g + p_e$), using equations of the form of 3.129 and 3.130. The heavy species pressure is then found by subtracting the electron pressure from the total static pressure. Once the heavy species pressure is found, the global density is then determined.

At the wall boundaries, the no-slip velocity condition is enforced. Therefore, the mass-averaged velocities at the walls are set to zero. In other words, $u_z = u_r = u_\theta = 0$. This case does not apply for the diffusion velocities normal to the wall boundaries. In fact, it cannot apply to the normal diffusion velocities if Equation 3.125 is to be enforced. Therefore, the different species do have a nonzero normal velocity at the walls equal to the diffusion velocity. It is only on the aggregate, mass-averaged sense that the velocity is zero.

3.5.2 Electrical Potential Boundary Conditions

Cathode Tip

The boundary condition on the cathode tip is of the Dirichlet type, but only in a convoluted sense. Since prediction of the potential drop in the sheath region is sketchy, at best, the best way to assure the correct current flow throughout the core of the thruster during numerical simulation is to specify the current on the cathode tip. As mentioned previously, the cathode tip is made to be a flat surface for simplicity. Therefore, since this flat area of the cathode tip is known, specifying the current on the cathode tip amounts to specifying the current density at the boundary nodes themselves.

The cathode tip is the most difficult of the electrical potential boundary conditions to calculate. Many different methods were tried in solving for the potential on this boundary. In the end, the somewhat convoluted method of Miller was retained. In this method, the axial current density is integrated over the first node downstream of the cathode tip according to

$$I = 2\pi \int_0^{R_c} \left| \vec{j} \cdot \hat{n} \right| r dr \approx \frac{\pi}{2} \sum_{j=0}^{N} |j_{z\,i,j+1} + j_{z\,i,j}| \left(r_{i,j+1}^2 - r_{i,j}^2 \right), \tag{3.131}$$

where

$$j_{z\,i,j} = \left. \frac{r_\eta}{J} \right|_{i,j} \left(-\sigma \frac{\partial \phi}{\partial \xi} + \psi \frac{\partial p_e}{\partial \xi} \right)_{i,j} + \left. \frac{r_\xi}{J} \right|_{i,j} \left(\sigma \frac{\partial \phi}{\partial \eta} - \psi \frac{\partial p_e}{\partial \eta} \right)_{i,j}. \tag{3.132}$$

The potential on the wall is then iterated upon until the error between the calculated current and the specified current is less than some error ϵ.

Outlet Boundary

At the outlet, the current density is forced to be zero, so that

$$\vec{j} \cdot \hat{n} = (\sigma \nabla \phi - \psi \nabla p_e) \cdot \hat{n} = 0 \tag{3.133}$$

at all of the boundary nodes. Transforming to natural coordinates, using backward differences for the derivatives in ξ and central differences for derivatives in η yields the difference

equation used to calculate the potential at the outlet:

$$\phi_{i,j} = \phi_{i-1,j} + \frac{p_{ei,j} - p_{ei-1,j}}{en_{ei,j}} + \frac{1}{2}\frac{z_\xi z_\eta + r_\xi r_\eta}{z_\eta^2 + r_\eta^2}\bigg|_{i,j}\left(\phi_{i,j+1} - \phi_{i,j-1} - \frac{p_{ei.j+1} - p_{ei,j-1}}{en_{ei,j}}\right), \tag{3.134}$$

where the relation $\sigma = en_e\psi$ has been used in simplifying. As mentioned above, the electron temperature can interact in a negative way with the above equation. Because of this, the following simplified equation was used to calculate the potential at the outlet boundary:

$$\phi_{i,j} = \phi_{i-1,j} + \frac{p_{ei,j} - p_{ei-1,j}}{en_{ei,j}}. \tag{3.135}$$

Centerline Boundary

The centerline is a symmetry boundary, so therefore, $\vec{j}\cdot\hat{n} = 0$. In transformed natural coordinates and using the necessary grid metrics, the potential along the centerline is calculated according to

$$\phi_{i,j} = \phi_{i,j+1} - \frac{p_{ei,j+1} - p_{ei,j}}{en_{ei,j}} - \frac{1}{2}\frac{z_\xi z_\eta + r_\xi r_\eta}{z_\xi^2 + r_\xi^2}\bigg|_{i,j}\left(\phi_{i+1,j} - \phi_{i-1,j} - \frac{p_{ei+1,j} - p_{ei-1,j}}{en_{ei,j}}\right). \tag{3.136}$$

Upper Wall Boundary

As mentioned in Section 3.4, the grid used for potential calculations only coincides in the region downstream of the constrictor entrance. As Figure 3-1 shows, the "upper wall" of a portion of the potential grid does not coincide with a wall at all, but lies within a region of the flow field. Since the current is not allowed to creep upstream, the portion of the potential grid within the flow field is treated as an insulator. At all points of the fluid upstream of this grid, the current density is set to zero, and no electrical potential calculation is performed. Along the insulating portions of the upper wall, the potential is calculated from

$$\phi_{i,j} = \phi_{i,j-1} + \frac{p_{ei,j} - p_{ei,j-1}}{en_{ei,j}} + \frac{1}{2}\frac{z_\xi z_\eta + r_\xi r_\eta}{z_\xi^2 + r_\xi^2}\bigg|_{i,j}\left(\phi_{i+1,j} - \phi_{i-1,j} - \frac{p_{ei+1,j} - p_{ei-1,j}}{en_{ei,j}}\right). \tag{3.137}$$

This insulated portion extends to the constrictor exit for numerical reasons. In real arcjets, the entire nozzle section is conducting. Miller found that if this boundary condition was

relaxed in the constrictor region, the current flow would tend to creep upstream, yielding significantly erroneous results. This was also the case in this research. Along the anode wall from the constrictor exit to the nozzle exit, the wall is treated as a conductor, and the potential is set to be at a reference potential of 100 V.

3.6 Initial Conditions

The initial conditions should be chosen as to most closely approximate the steady state solution. Evidence can be gathered from experimental results or other numerical solutions. In general, Miller used a previous solution from which to iterate, thus reducing the computation time. In this work, the same basic method was used. The difference lies in the fact that, in some cases, different grids were used to calculate the flow. To overcome this, a routine was written which interpolated the results as found by Miller onto the new grids. It was also helpful to specify a radially increasing potential, as well, to ease the calculation. This will be discussed in greater detail in the next chapter.

Chapter 4

Achievements of This Research

As mentioned in the introduction, the original goal of this thesis was to extend the work of Scott Miller to other gases and to other cases. As work progressed, errors in both coding and physics were found, although more in the coding than in the physics. (Considering the breadth of knowledge required to solve the physical and numerical problems which inevitably surfaced, it is a small wonder that there weren't more errors.) In addition, the author was sometimes pulled down unnecessary roads, spending too much time on things which, in the end, proved trivial. As a result, the accomplishments of this research bear little resemblance to the goals originally sought. However, much was learned along the way, especially by this author. This purpose of this chapter is to document and compare the differences between the formulations of Miller and the present formulations.

4.1 Physics

4.1.1 Coulomb Collision Integrals

As mentioned in Section 2.4.7, Miller took the Coulomb collision integrals to be some factor (≈ 0.2) of the Coulomb cross-section, for both diffusion and viscosity calculations. Although simpler, there is no physical basis for doing so, other than the fact that the collision integrals can be thought of as, basically, energy averaged cross-sections. In addition, Miller gave no justification for the factor used. Because of this, an alternative method of calculating the Coulomb collision integrals was sought. Unlike other collision integrals, Coulomb collision integrals are sensitive to pressure variations as well as temperature variations. Within an

electrothermal arcjet, the pressure varies from a few atmospheres at the inlet to near vacuum at the exit. Therefore, using a Coulomb collision integral calculated at, say, one atmosphere would be a very crude approximation.

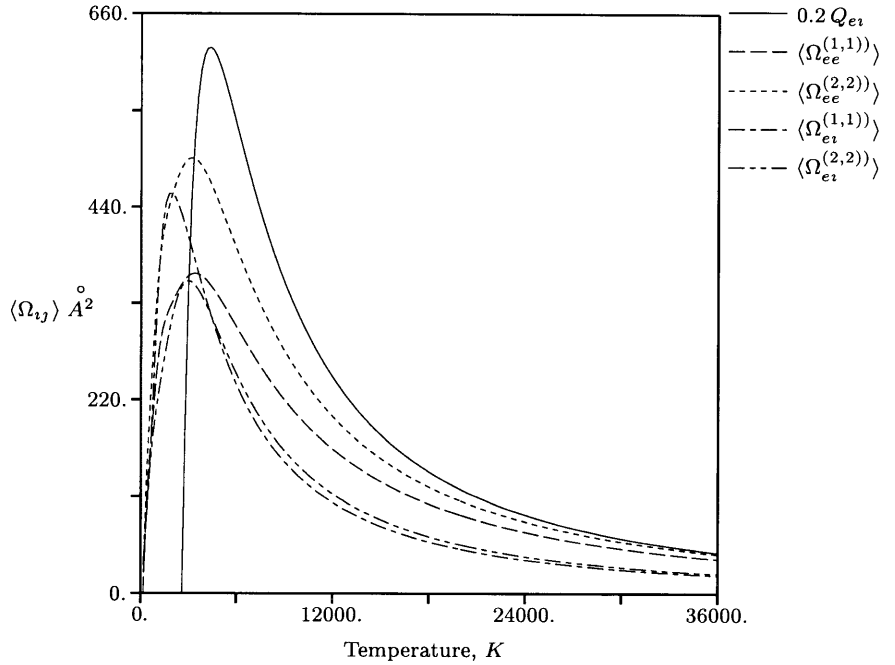

Figure 4-1: *Comparison of Charged Particle Collision Integrals, p_e = 1 atm*

In this work, the collision integrals as formulated by Paquette et al. and MacDonald were used in calculating the Coulomb collision integrals. Paquette et al. first formulated a method for calculating the Coulomb integrals for both the attractive and repulsive potentials. MacDonald modified and corrected the method, as it was found that the integral in the region of the singularity in Equation 2.146 behaves much differently for the attractive potential than the repulsive potential. Figure 4-1 compares the integral (cross-section) as used by Miller to the integrals as calculated in this research by the methods of Paquette and MacDonald, for temperatures in the range 0-40,000 K at one atmosphere.

As can be seen, the Coulomb collision integral as used by Miller is comparable to the repulsive collision integrals at high temperatures. However, for ion-electron collisions, it overestimates the collision integral of the interactions by about a factor of two in the high temperature regions. This difference can have a large affect on the calculated transport coefficients, as will be seen. At intermediate temperatures, there is a wide variance between the various collision integrals. At low temperatures, the Coulomb cross section becomes

negative, which is clearly non-physical. This is due to the approximation discussed in Section 2.4.6 concerning the $\ln \Lambda$ term in the equation for the Coulomb cross section. Since the number of electrons in a real situation is very small at lower temperatures, this is of little concern. In addition, at pressures lower than one atmosphere, the temperature range in which the cross section is negative shrinks quickly. The major advantage of the methods of Paquette and MacDonald is that the collision integrals are bounded, as the integral does not need to be calculated to an infinite upper bound, since a screened Coulomb cross section is not infinite. In addition, in calculating the collision integrals of a pure Coulomb interaction, many assumptions are usually made to give a closed form solution (see [37] for a more detailed discussion). These methods, therefore, give a more realistic approximation to the collision integrals. Another advantage of the methods of Paquette and MacDonald is the ability to calculate accurate Coulomb collision integrals using any dominant length scale, for any charged particle interaction. For example, in stellar plasmas, a dominant length scale is not the Debye length, but the inter-ionic distance,

$$\lambda_i = \left(\frac{3Z_i}{4\pi n_i} \right)^{\frac{1}{3}} . \tag{4.1}$$

Appropriate substitution of a new length scale enables a quick calculation of the Coulomb collision integrals without changing the $F^{(l,s)}$.

4.1.2 Transport Coefficients

The pure species thermal conductivity, viscosity and diffusion coefficients are all affected by the choice of the collision integrals. Specifically, the integrals discussed above affect μ_{H+} and k_{H+} through the $H+ - H+$ interaction terms and k_e through the $H+ - H+$ and $H+ - e$ interaction terms. Figures 4-2 and 4-3 show the equilibrium viscosity and thermal conductivity of pure ionized hydrogen, while Figure 4-4 compares the equilibrium thermal conductivity of electrons as calculated by Miller with the present methods, using the Coulomb collision integrals from the previous section and utilizing Equation 2.183. As can be seen, using the repulsive integrals of Paquette instead of the approximation of Miller does not change the viscosity and thermal conductivity of ionized hydrogen appreciably. This is expected, since Paquette's integral is very close in value to Miller's approximation at higher temperatures, as can be seen in Figure 4-1. However, the thermal conductivity

of the electrons is higher than that predicted by Miller, due to the fact that the attractive Coulomb integral of MacDonald is smaller than the approximation Miller uses by about a factor of two at higher temperatures.

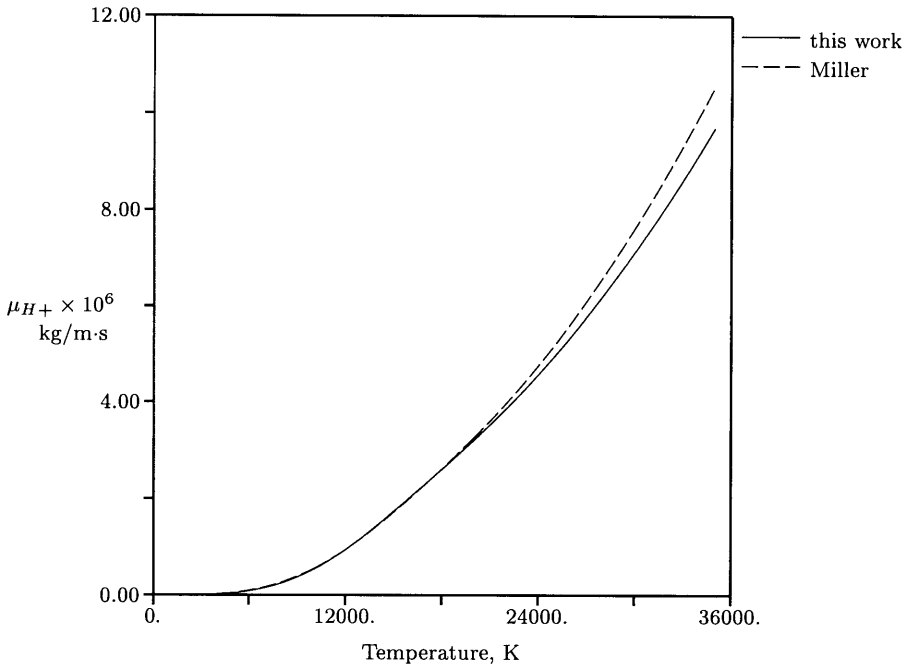

Figure 4-2: *Comparison of Calculated Viscosity of Ionized Hydrogen, p_e = 1 atm*

Since the choice of collision integrals has an effect on the pure species transport coefficients, the choice of collision integrals also has an effect on the mixture transport coefficients, albeit in a more dilute manner. Figure 4-5 compares the electrical conductivity as calculated in this work with the electrical conductivity as calculated by Miller at one atmosphere. The electrical conductivity of Miller is calculated using a variation of the methods of Grier [16], who uses a correction factor, Δ_c to better approximate the electrical conductivity. As can be seen, the electrical conductivity as calculated by the methods presented in this work over-predicts the electrical conductivity as calculated by Miller. Although the electrical conductivity as calculated by this thesis may be a bit high, the complex calculation of the correction factor is not needed.

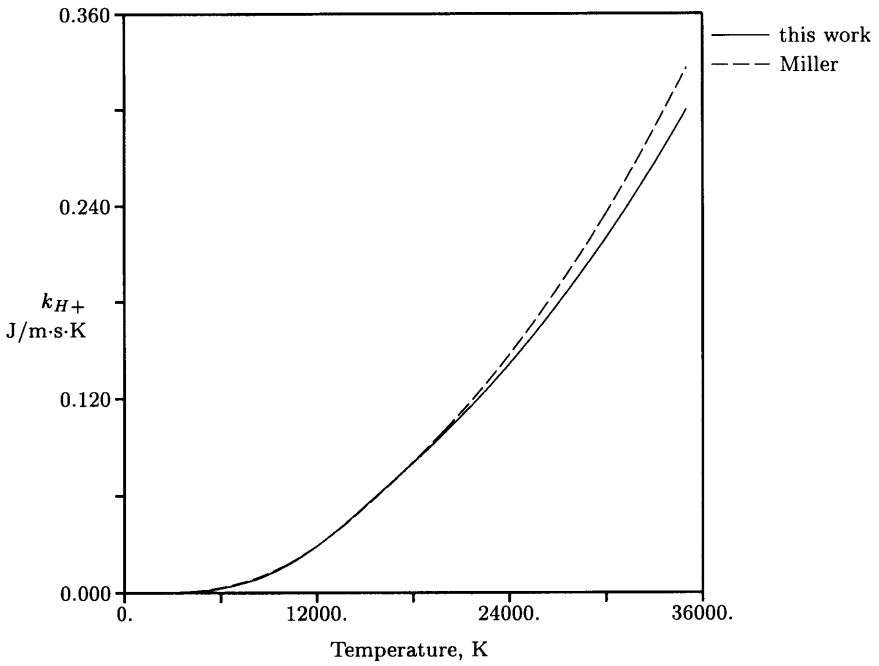

Figure 4-3: *Comparison of Calculated Thermal Conductivity of Ionized Hydrogen, p_e = 1 atm*

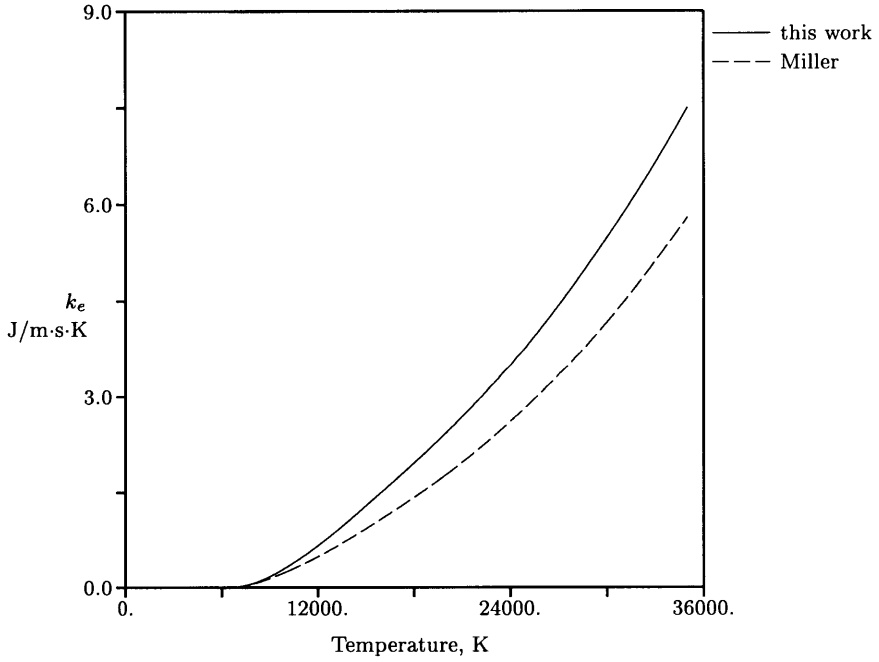

Figure 4-4: *Comparison of Calculated Thermal Conductivity of Electrons, p_e = 1 atm*

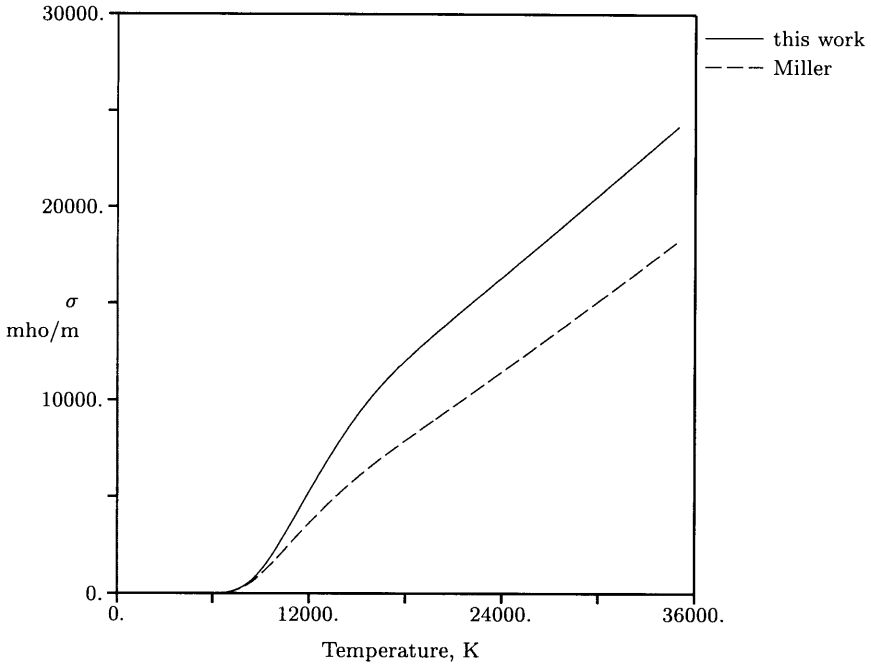

Figure 4-5: *Comparison of Calculated Electrical Conductivity of Hydrogen, p = 1 atm*

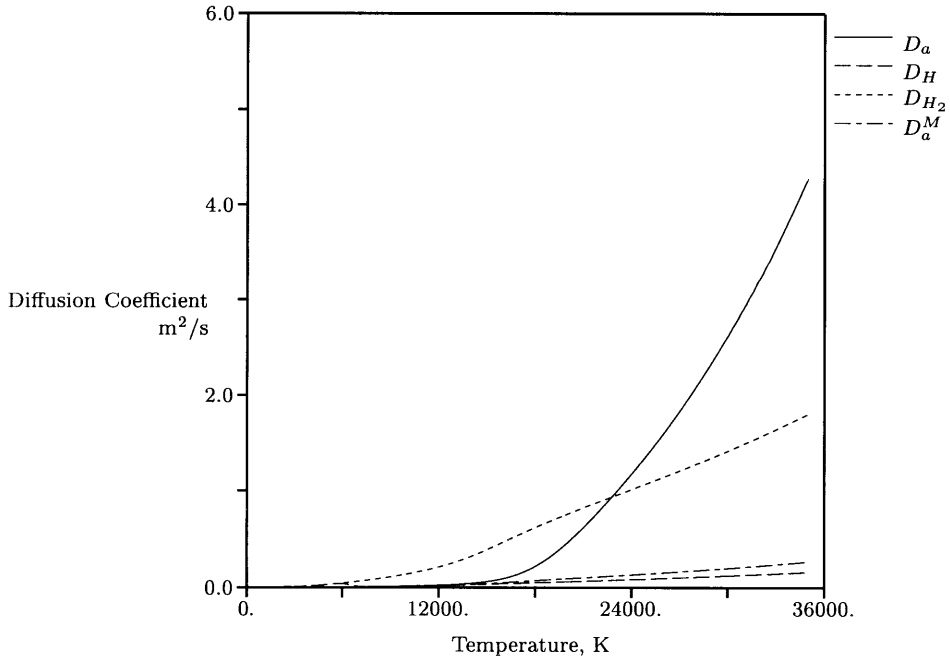

Figure 4-6: *Comparison of Calculated Diffusion Coefficients of Hydrogen, p = 1 atm*

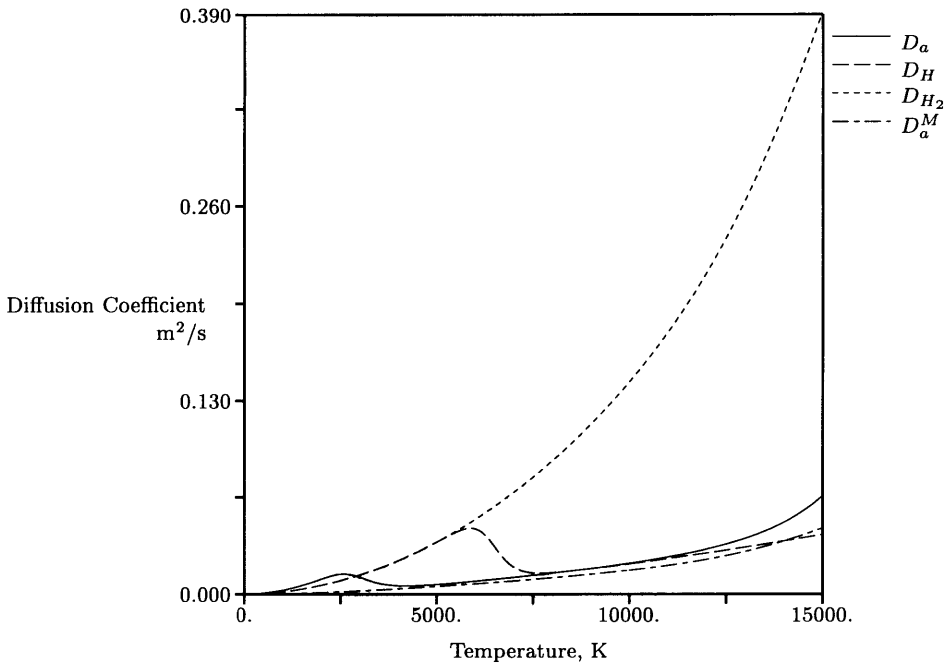

Figure 4-7: *Closeup: Comparison of Calculated Diffusion Coefficients*

The biggest change between the methodology of Miller and the methodology presented here, with respect to the calculation of transport coefficients, comes in the calculation of the ambipolar diffusion coefficient. Miller calculated the ambipolar diffusion coefficient according to

$$D_a = \sqrt{\frac{\pi k T_g}{4 m_S}} \frac{1 + T_e/T_g}{Q_{in}\,(n_e + n_n)}, \tag{4.2}$$

where Q_{in} is some effective collision cross section of ions with other neutral particles, and n_n is the number density of those neutral particles. This equation is fine when the flow is dominated by ambipolar diffusion only. However, as will be discussed in the following section, the diffusion of other species independently of ambipolar effects is necessary to correctly predict energy transport. As a consequence, a different form of the ambipolar diffusion coefficient is needed to more correctly take multi-species diffusion effects into account. As mentioned in Section 2.4.2, the methods of Krier are used to calculate both the diffusion coefficient of atomic hydrogen as well as the ambipolar diffusion coefficient. Figure 4-6 compares the ambipolar, atomic hydrogen, and molecular diffusion coefficients as calculated in this work with the ambipolar diffusion coefficient as calculated by Miller. The ambipolar diffusion coefficient found by this research is much higher in regions of high ionization, probably due to the use of MacDonald's attractive Coulomb collision integral in

combination with the use of the effective diffusion coefficient formulation. An interesting effect of the effective diffusion coefficient occurs in the areas of lower temperature, as shown in Figure 4-7 . As can be seen, there are distinctive "humps" in the values of the coefficients as calculated by Krier's method. This is due to the favoring of one binary diffusion coefficient over another in those regions.

Perhaps the most dramatic difference in the transport coefficients between Miller's results and the results discussed here has to do with the calculated values of the heavy species viscosity and thermal conductivity. In Sections 2.4.3 and 2.4.4, it was mentioned that Miller neglects the molecule-ion interaction when using the mixture rule of Mitchner and Kruger in the calculation of the mixture viscosity and mixture thermal conductivity. Miller's formulation is

$$\mu_{g,Miller} \approx \frac{x_{S_2}\mu_{S_2}}{x_{S_2} + x_S\sqrt{\frac{2}{3}}\frac{\langle\Omega^{(2,2)}_{S_2S}\rangle}{\langle\Omega^{(2,2)}_{S_2S_2}\rangle}} + \frac{x_S\mu_S}{x_{S_2}\sqrt{\frac{4}{3}}\frac{\langle\Omega^{(2,2)}_{S_2S}\rangle}{\langle\Omega^{(2,2)}_{SS}\rangle} + x_S + 2x_{S+}\frac{\langle\Omega^{(2,2)}_{SS+}\rangle}{\langle\Omega^{(2,2)}_{SS}\rangle}} + \frac{x_{S+}\mu_{S+}}{2x_S\frac{\langle\Omega^{(2,2)}_{SS+}\rangle}{\langle\Omega^{(2,2)}_{S+S+}\rangle} + x_{S+}} \tag{4.3}$$

for the heavy species viscosity and

$$\kappa_{g,Miller} \approx \frac{x_{S_2}\kappa_{S_2}}{x_{S_2} + x_S\sqrt{\frac{2}{3}}\frac{\langle\Omega^{(2,2)}_{S_2S}\rangle}{\langle\Omega^{(2,2)}_{S_2S_2}\rangle}} + \frac{x_S\kappa_S}{x_{S_2}\sqrt{\frac{4}{3}}\frac{\langle\Omega^{(2,2)}_{S_2S}\rangle}{\langle\Omega^{(2,2)}_{SS}\rangle} + x_S + \frac{3}{2}x_{S+}\frac{\langle\Omega^{(2,2)}_{SS+}\rangle}{\langle\Omega^{(2,2)}_{SS}\rangle}} + \frac{x_{S+}\kappa_{S+}}{\frac{3}{2}x_S\frac{\langle\Omega^{(2,2)}_{SS+}\rangle}{\langle\Omega^{(2,2)}_{S+S+}\rangle} + x_{S+}} \tag{4.4}$$

for the heavy species conductivity. As mentioned, the terms concerning the molecule-ion interaction are missing. This would not be a problem, except that in numerical calculations, the mole (mass) fractions of the different species are always made nonzero so as to alleviate numerical problems. If not done carefully, the nonzero mass fractions could have a dramatic effect on the calculated values of the transport coefficients.

As mentioned in Section 2.4.3, Miller uses mass fractions of $\omega_{H_2} = 3\times10^{-3}$, $\omega_H = 1 \times 10^{-4}$, and $\omega_{H+} = 1 \times 10^{-6}$ in his numerical fluid calculations. Figures 4-8 and 4-9 compare the calculated heavy species viscosity and thermal conductivity of hydrogen, respectively, as calculated by Miller with the values as calculated by this work. The effect of the limiting mass fractions is obvious. As no collision integrals could be found in the literature for the $H_2 - H+$ interaction, and time did not permit calculation of the collision integrals from existing potentials, the very crude approximation $\langle\Omega^{(l,s)}_{H_2H+}\rangle = 1.2\langle\Omega^{(l,s)}_{H_2H}\rangle$ was used, where the 1.2 factor was chosen to account for the effect of the ion charge. When using the above

limiting mass fractions, it was found that the values of the molecule-ion collision integrals weren't nearly as important as just having a term to account for the molecule-ion interaction included in the denominator. Since the viscosity and thermal conductivity of pure diatomic hydrogen are so much higher than the pure viscosity and thermal conductivity of ionized hydrogen at higher temperatures, the heavy species viscosity and thermal conductivity are dominated by the diatomic values. In the regions of intermediate temperature, the deviation between the two methods is caused by the multiplicative factors of 2 and $\frac{3}{2}$ in the denominators of the viscosity and thermal conductivity formulations, respectively, as used by Miller. If more care is taken in defining the limiting values of the mass fractions, this effect of the limiting mass fraction disappears, and the values found by both methods become nearly identical.

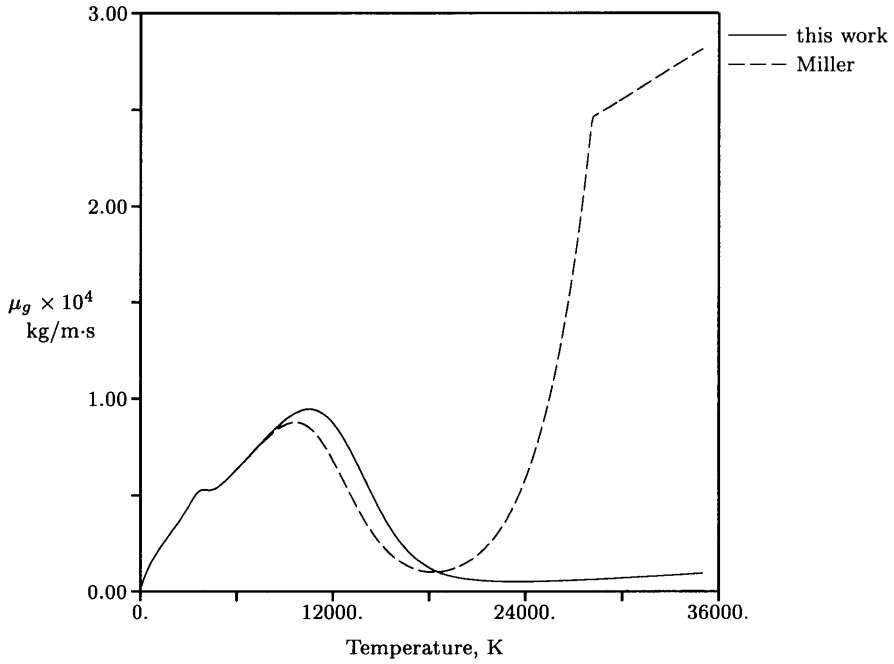

Figure 4-8: *Comparison of Calculated Viscosity of Hydrogen, p = 1 atm*

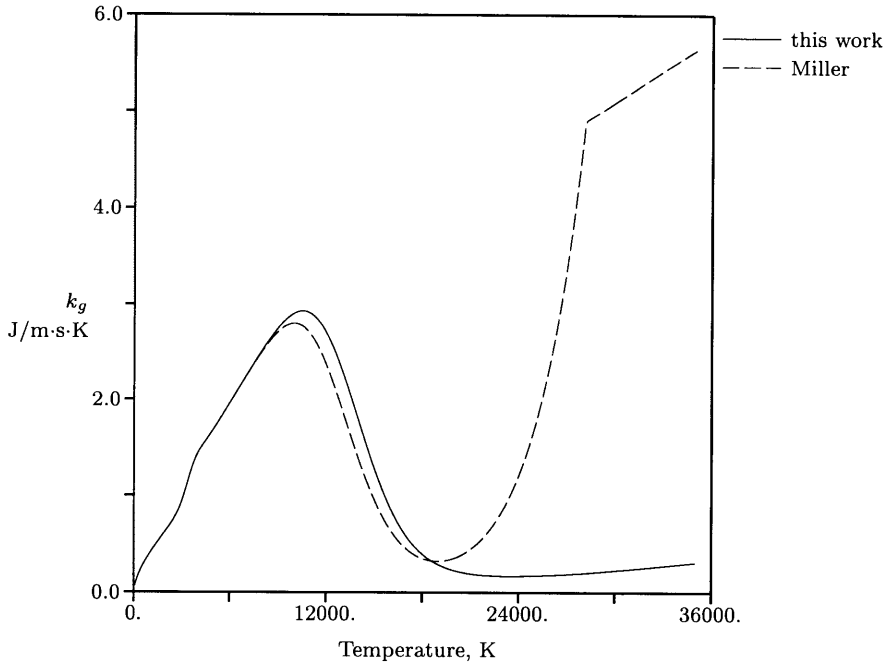

Figure 4-9: *Comparison of Calculated Heavy Species Thermal Conductivity of Hydrogen, p = 1 atm*

4.1.3 Diffusion Fluxes

Perhaps a larger error in the physics has to do with the formulation of the diffusion velocities of the different species. In Miller's formulation, ambipolar diffusion dominates, and the diffusion velocities of the atomic and molecular species were taken to be equal for simplicity. This is a gross simplification that can have dramatic effects on the energy and mass transport within the arcjet, especially from the hot arc core to the cooler outer regions. In addition, the diffusion term due to the current flow was neglected. In regions where the current density is not very high, this is a valid assumption. In the cathode tip region, where the current densities are very high, the current term may be of the same order of magnitude as the other flux terms.

Illustrative Example

In illustrating these defects, it is helpful to do an example. Let us assume that hydrogen gas is initially at rest and in a semi-infinite container, with a wall at x=0 and another wall at x=1. The length units are not important. At one instant of time, the gas has the temperature distribution as shown in Figure 4-10. To demonstrate the differences between

the methods as formulated by Miller and the methods used in this research, it is helpful to calculate values of the species densities, diffusive mass fluxes, and diffusive energy fluxes according to both methods at this instant of time and compare the two. As will be seen, the outcomes are quite different.

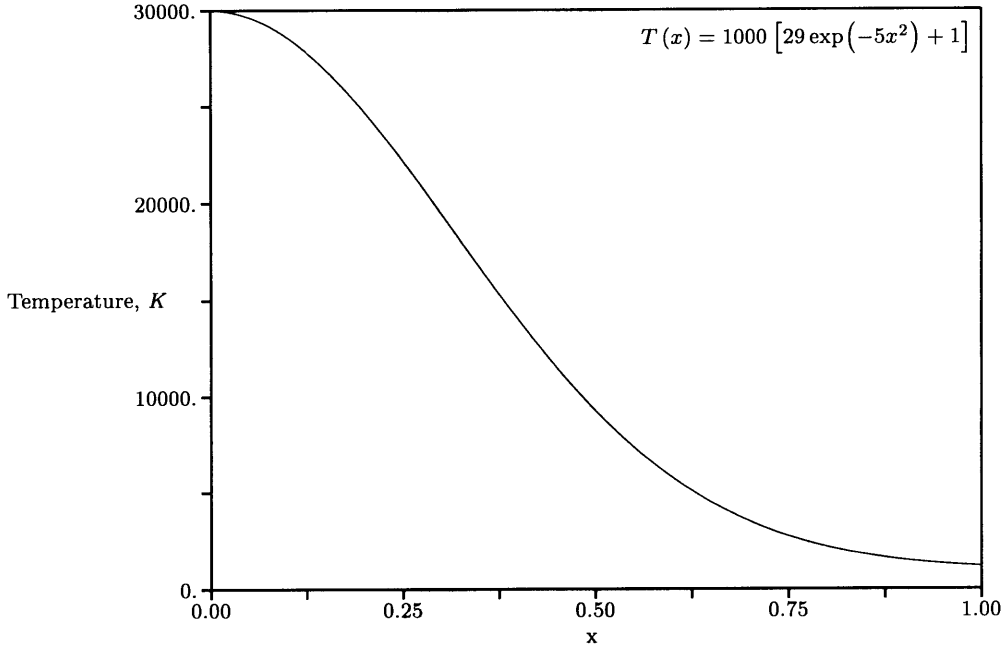

Figure 4-10: *Example: Temperature Distribution*

The total mass density distribution and the density distribution of the various species due to the temperature distribution is shown in Figure 4-11. The gradients in the different species will cause a transport of mass and energy. If the mean mass velocity is zero, then the *net* transport of mass is zero, as is implied by Equation 2.28. However, the net transport of energy may not necessarily be zero, as particles of different species carry different amounts of energy with them.

Figure 4-12 compares Miller's ambipolar diffusion coefficient with the ambipolar, effective atomic hydrogen, and effective diatomic hydrogen diffusion coefficients as calculated by this research for the present example. The ambipolar diffusion coefficients are comparable in regions of lower temperature, but diverge in the high temperature region, due to the use of MacDonald's collision integrals based on the attractive screened Coulomb potential and effective diffusion coefficient formulation. In addition, due to the smaller $H_2 - e$ collision integral, the effective diatomic hydrogen diffusion coefficient is quite high.

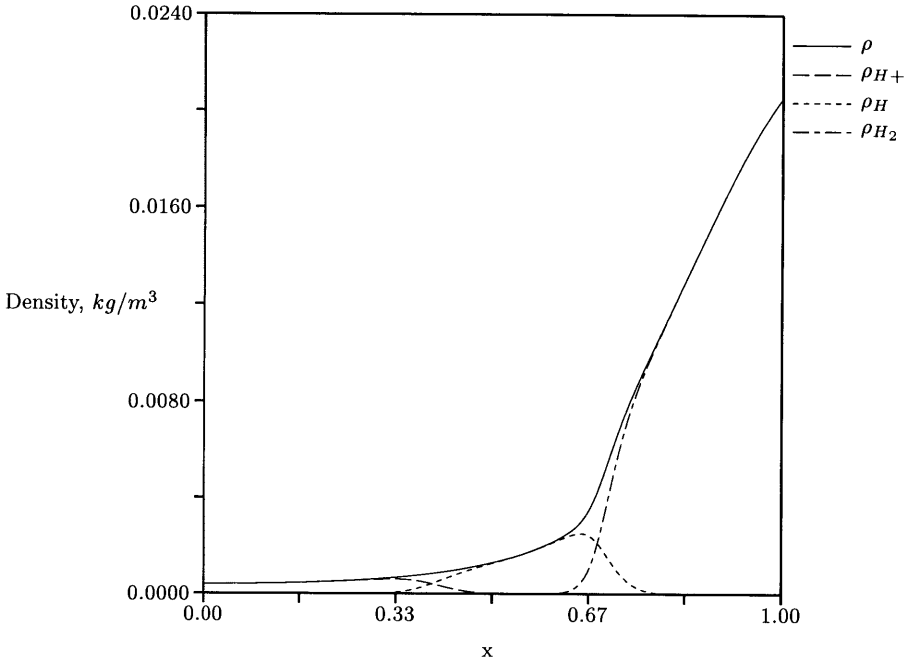

Figure 4-11: *Example: Mass Density Distribution*

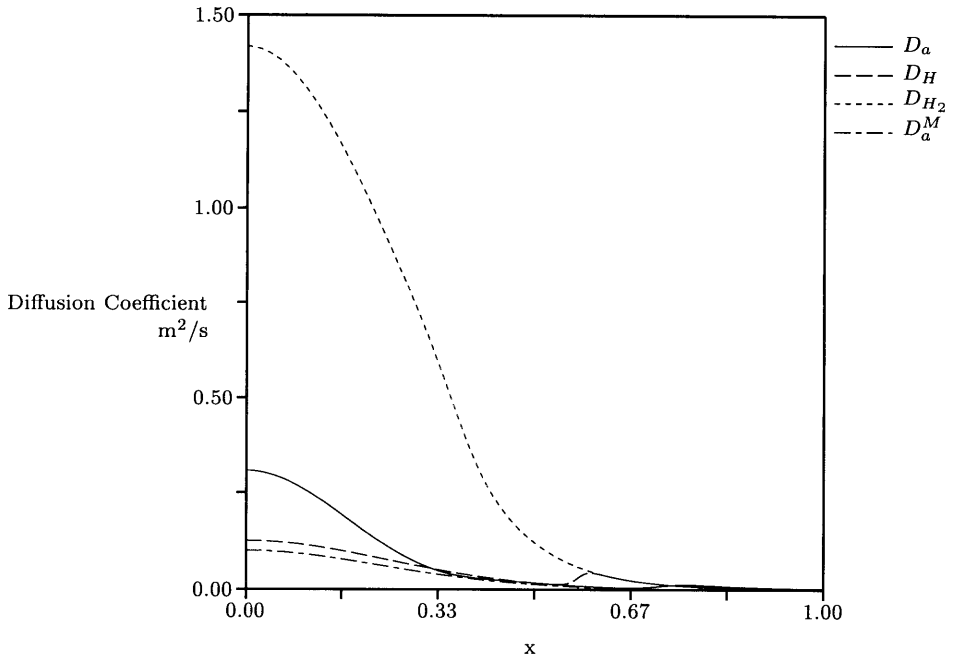

Figure 4-12: *Example: Comparison of Diffusion Coefficients*

The diffusive mass fluxes as used by Miller are

$$\rho_{H+}\vec{V}_{H+}\Big|_M = -D_a^M \frac{m_H}{m_e}\nabla\rho_e \tag{4.5}$$

for the ion species,

$$\rho_H\vec{V}_H\Big|_M = \left(1+\frac{\rho_{H_2}}{\rho_H}\right)^{-1} D_a^M \frac{m_H}{m_e}\nabla\rho_e \tag{4.6}$$

for the atomic species and

$$\rho_{H_2}\vec{V}_{H_2}\Big|_M = \left(1+\frac{\rho_H}{\rho_{H_2}}\right)^{-1} D_a^M \frac{m_H}{m_e}\nabla\rho_e \tag{4.7}$$

for the molecular species, where D_a^M is Miller's ambipolar diffusion coefficient as described above in Section 4.1.2. As can be seen, in Miller's formulation, the diffusive fluxes are all dependent on the electron (or ion) density gradients only. This method can yield dramatically different results than the method as described in Section 2.4.2.

Figure 4-13 shows the diffusion fluxes as calculated by Miller's method for the present example. A positive flux denotes diffusion towards the x=1 boundary, while a negative flux denotes diffusion towards the x=0 boundary. From this figure, it can be seen that the molecular mass diffusion term in Miller's formulation is negligible. This is due to the molecular density being very high in the region of low ion density gradients, while being small in the region of high ion density gradients. Therefore, the atomic diffusive mass flux exactly balances the ion diffusive mass flux.

As mentioned in Section 2.4.2, the method of effective diffusion coefficients is a very crude approximation to the more accurate multicomponent diffusion components. This is evident from the plots in Figure 4-14. This figure shows the diffusive mass flux of each species calculated explicitly according to

$$\rho_s\vec{V}_s = -D_s\nabla\rho_s\,, \tag{4.8}$$

where D_s is the effective diffusion coefficient of species s. The sum of the fluxes is shown, as well (solid line). As can be seen, the sum of the fluxes is not identically zero, as it should be. Because of this, one species must be relegated to "taking up the slack" in the calculation of the mass fluxes. After investigating, it was found that relegating the atomic species to this role provided the best results. If this done, the ion, atomic, and molecular

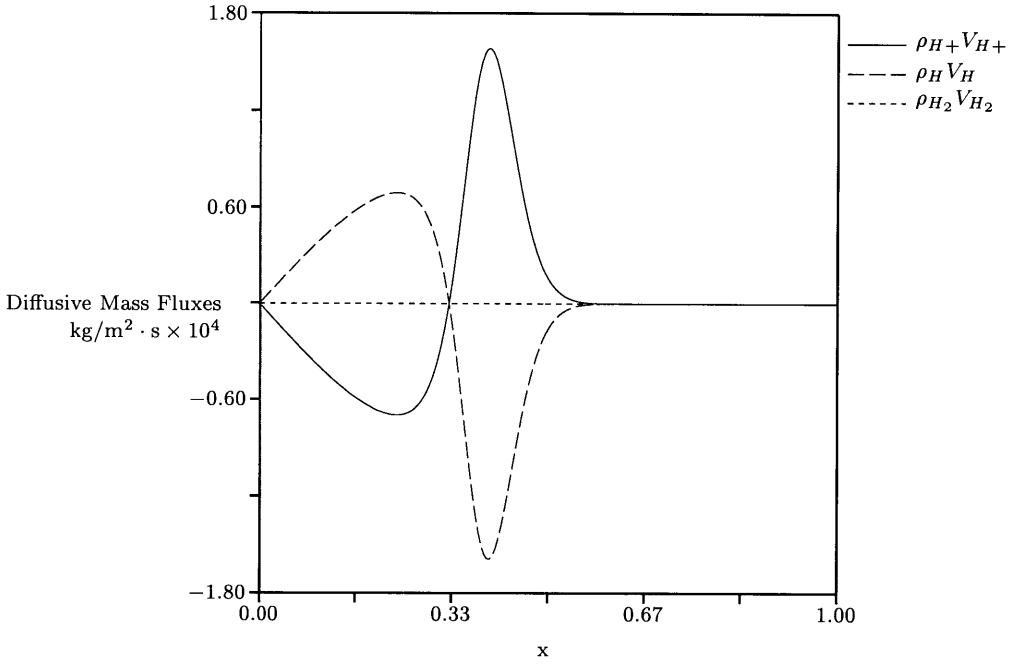

Figure 4-13: *Example: Diffusive Mass Fluxes, Miller's Formulation*

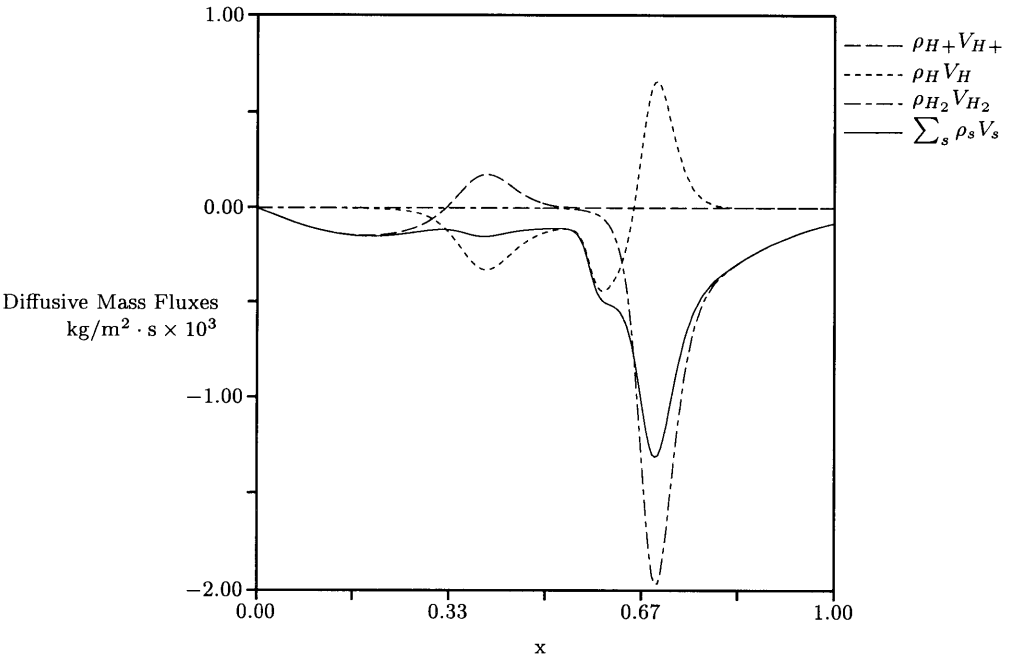

Figure 4-14: *Example: Diffusive Mass Fluxes, This Research, Each Species Calculated Explicity*

diffusive mass fluxes are calculated according to

$$\rho_{H+}\vec{V}_{H+} = -D_a \frac{m_H}{m_e}\nabla\rho_e, \tag{4.9}$$

$$\rho_H\vec{V}_H = \frac{m_e}{e}\vec{j} + D_a\frac{m_H}{m_e}\nabla\rho_e + D_{H_2}\nabla\rho_{H_2}, \tag{4.10}$$

and

$$\rho_{H_2}\vec{V}_{H_2} = -D_{H_2}\nabla\rho_{H_2}, \tag{4.11}$$

respectively, where D_{H_2} and D_a are given by Equations 2.159 and 2.163, respectively. For the present example, the current flow is assumed to be zero for simplicity. For comparison, if the multicomponent diffusion coefficients were used, the sum of the fluxes would be nearly zero, as the gradients in the flow properties are implied in the matrix solution. Figure 4-15 shows the diffusive mass fluxes of the various species, using the equations above. as calculated by this work. The ion mass flux is similar to the ion flux in Figure 4-13, but has a different magnitude due to the higher value of the ambipolar diffusion coefficient (see Figure 4-12). In addition, there is a large negative spike in the molecular mass flux due to a large diatomic species gradient. Since the ion mass density is negligible in the region of the spike, the atomic diffusive flux compensates with a large positive spike.

The calculation of the diffusion coefficients in this work (through more accurate collision integrals and the method of effective diffusion coefficients) combined with a different formulation of the diffusion fluxes paint a much different picture than the one painted by the work of Miller. Nowhere is this more evident than in the calculation of the net energy transport. The net heavy species energy flux due to diffusive transport in one dimension is

$$E_{net} = \rho_{H+}V_{H+}h_{H+} + \rho_H V_H h_H + \rho_{H_2}V_{H_2}h_{H_2}, \tag{4.12}$$

where

$$h_H = h_{H+} = \frac{5}{2}R_H T_g - \frac{7}{4}R_H T_f \tag{4.13}$$

and

$$h_{H_2} = \frac{7}{2}R_{H_2}\left(T_g - T_f\right) + \frac{R_{H_2}\theta_v}{e^{\frac{\theta_v}{T_g}} - 1}. \tag{4.14}$$

With respect to the example problem at hand, Figure 4-16 compares the net energy transport due to mass diffusion of Miller's methods to the present research. As can be seen,

the net transport of energy due to mass diffusion is negligible in the formulation of Miller. Looking back at Figure 4-13, this result is made obvious. The atoms and ions both carry the same energy per unit mass with them. If the molecular diffusion is negligible, then the only energy being transported is due to mass diffusion of ions and atoms. Since molecular diffusion is negligible, the atoms and ions diffuse in different directions to make the net mass diffusion zero. Therefore, there is no net energy transport. With the above example, it is clearly demonstrated that method of calculation of the diffusive mass fluxes, by either the methods of Miller or the methods of this research, is insufficient to accurately predict the mass and energy transport characteristics of a multispecies flow. Clearly, more work is needed in this area.

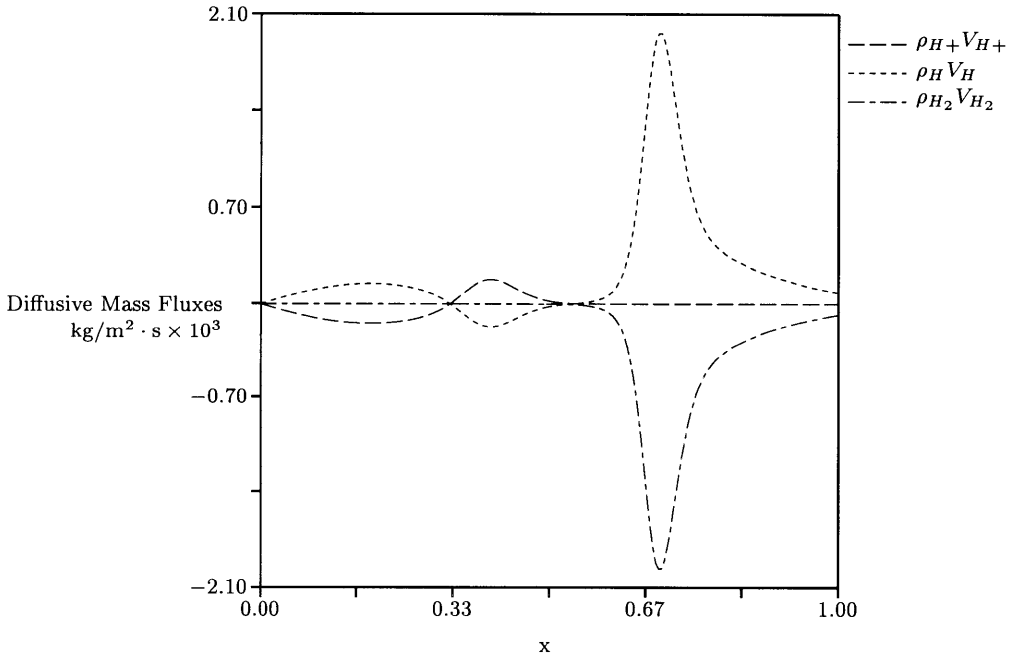

Figure 4-15: *Example: Diffusive Mass Fluxes, This Research,* $\rho_{H+}V_{H+}$ *and* $\rho_{H_2}V_{H_2}$ *Calculated Explicity*

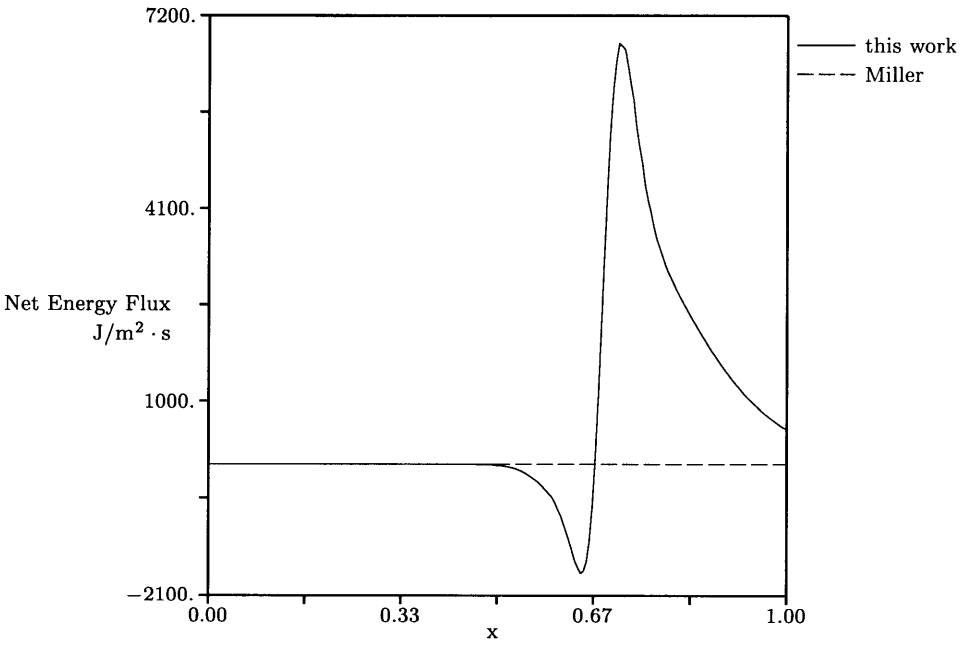

Figure 4-16: *Example: Comparison of Net Energy Fluxes*

4.2 Numerics

4.2.1 General

Scott Miller originally wrote a FORTRAN code to model viscous and diffusive effects in magnetoplasmadynamic flows for his Master's thesis [33]. In doing his doctoral research, he modified the code that he created for his Master's research to take into account electrons and nonequilibrium chemistry and temperatures, thereby resulting in a code which can calculate the flow through an electrothermal arcjet thruster. In the modification, he added many modules to his Master's code. As a result, the code as inherited contained 25 modules and over 7500 lines of code. Miller integrated the electron equations and heavy species equations separately, using global time steps for both subsets of equations. Since the calculated maximum allowable time steps were so small for both the electron and heavy species equations ($\Delta t \approx 10^{-10}\, s$), the real time necessary for calculating a fully converged flow was on the order of a seven to fourteen days on a workstation such as a DEC Alpha.

From the outset, attempts were made to improve the efficiency and reduce the computational effort necessary to obtain a converged flow solution. To this end, all of the collision integrals used were curve fitted to simple polynomials. Since the basic numerical scheme (MacCormack's method) was not to be changed, efforts were made to enable the code to use local time stepping, that is, the ability to step each node at its maximum allowable time step. In addition, a majority of the code was rewritten to reduce the number of function calls and `if then` statements, which require more computational effort than simple math operations. The modifications in the physics as mentioned in the previous section were implemented, as well. Finally, the modules used in the calculations were modified to enable calculations on any general grid structure, and not just on the grid types as Miller used. In the resulting code, the equations governing the flow of electrons were incorporated into the modules used for calculating the heavy species equations. The final code contains 19 modules and less than 5800 lines of code. Although the final version of the code seems to run faster than the code of Miller, accurate numbers could not be found, as the code could never be made to work properly.

4.2.2 Formulation of MacCormack's Method

In Miller's doctoral thesis, he mentions that he tried a number of ways to implement the governing equations numerically. In the first attempt, the grid metrics in $\xi_z - \xi_r - \eta_z - \eta_r$ form were left outside the fluxes in a non-conservative manner, and were calculated using second order central differences. He reported that the central differences were causing smoothing of the grid points, thereby reducing the accuracy of the solution. In the second attempt, the metrics were brought inside the fluxes in the $z_\xi - z_\eta - r_\xi - r_\eta$ form, and differenced centrally. Again he reported smoothing of the grid lines, although it was not as prevalent. In the final attempt, the metrics were moved outside of the fluxes again, but differenced in one direction in accordance with either the predictor or corrector step. This seemed to alleviate the problem.

In reconstructing the code, many things were rewritten, since it was simply easier to rewrite whole sections of the code than to reconstruct little pieces. In the end, to be consistent with the differencing of MacCormack's method, both one-sided and centrally differenced metrics in $z_\xi - z_\eta - r_\xi - r_\eta$ form were used, with the metrics moved inside the fluxes for a conservative formulation. The metrics multiplying the various flux terms were used to maintain second order accuracy throughout. For example, take the flux term in ξ:

$$\frac{\partial \tilde{\mathbf{F}}}{\partial \xi} = \mathbf{F} r_\eta - \mathbf{G} z_\eta. \tag{4.15}$$

Since the flux differencing is in the ξ direction, the r_η, z_η metrics are differenced centrally, for both the predictor and corrector steps. The complications in dealing with correctly differenced grid metrics occur when dealing with the viscous terms in $\mathbf{F}$ and $\mathbf{G}$. Within the $\mathbf{F}$ flux vector, the z-momentum term in the radial momentum equation, rewritten in natural coordinates, becomes

$$\begin{aligned} F_4 &= \left[\rho u_r u_z - \mu\left(\frac{\partial u_r}{\partial \xi}\xi_z + \frac{\partial u_r}{\partial \eta}\eta_z + \frac{\partial u_z}{\partial \xi}\xi_r + \frac{\partial u_z}{\partial \eta}\eta_r\right)\right] r \\ &= \left[\rho u_r u_z - \mu\left(\frac{\partial u_r}{\partial \xi}\frac{r_\eta}{J} - \frac{\partial u_r}{\partial \eta}\frac{r_\xi}{J} - \frac{\partial u_z}{\partial \xi}\frac{z_\eta}{J} + \frac{\partial u_z}{\partial \eta}\frac{z_\xi}{J}\right)\right] r\,. \end{aligned} \tag{4.16}$$

When the metrics within the parentheses were all differenced centrally, the smoothing of the grid points was observed as Miller had stated. The problem was fixed when all of the derivatives in ξ, including the derivatives implied within the Jacobian, J, were differenced

according to the requirements of the predictor or corrector step. Since the metrics and Jacobians of the transformation were all calculated once and for all at the beginning of each run, this meant calculating z_ξ, r_ξ, z_η, and r_η in the forward, backward, and central directions. The Jacobians can be handled in two ways. In the first method, the Jacobians can be calculated as the fluxes are calculated, using the appropriately differenced metrics. In the second method, all of the possible permutations of the Jacobians (five) can be calculated and stored in memory at the beginning of each run. With regards to computational effort versus required memory, either method could be performed, since the extra computational effort required by the first method and the extra memory required by the second method are minimal. In this work, the latter method was chosen, as it made the modules performing the flux calculations much simpler and easier to read.

4.2.3 Boundary Conditions

As mentioned in the previous chapter, the methods for calculated the boundary conditions were changed, so as to allow a more generic grid to be used, rather than the simple grids of Miller (see Section 4.2.4). These methods utilize the calculated grid metrics in the calculations, thereby reducing the overall number of calculations. When the boundary value calculations are performed, they must be calculated consistently with the grid metrics calculations. For example, if the grid metrics on the boundary are calculated as first order accurate one-sided, then the boundary values must be calculated according to first order accurate one-sided differences. If not, it was found that the boundary values would cause errors in the solution which would propagate into the flow, sometimes causing the solution to "blow up." In this work, first order one-sided differences were used, as second order one sided differences were found to be less stable than first order. In addition, the first order one-sided differences were easier to implement.

In Section 2.2.1, it was stated that the wall boundaries were not treated as wall boundaries at all, but as sheath boundaries. By Equation 3.125, the ion species reach this boundary with a finite velocity. However, in Miller's research, the diffusion fluxes (velocities) of all species were set to zero in the z, r, and θ directions, effectively making the normal velocities zero at these boundaries, which is inconsistent with the sheath boundary assumption. If a nonzero normal ion mass flux occurs at the sheath boundary, then the atomic and molecular mass fluxes must compensate with a net flux in the opposite direction, so as to maintain

the no-slip condition on the mass-averaged velocity. In the present code, this situation was amended. When this fix was first implemented, it was found that it was causing significantly erroneous results in the cathode tip region. It was these erroneous results that first prompted the inclusion of the axial diffusive mass flux terms in the heavy species energy equation. This improved the situation a bit. The key was including the current density in the calculation, as well, according to Equation 2.166. Due to the very high current density in the cathode tip region, the current density term can be the same order of magnitude as the other diffusive flux terms. Including the current density stabilized the cathode tip region.

The final change in the boundary conditions came at the inlet boundary. In Miller's work, an integration was performed at the end of each predictor step so that the total mass flow rate was conserved. Although this procedure does conserve the total mass flow rate, this type of boundary condition was highly reflective. Any disturbance downstream of the inlet was never allowed to propagate upstream and into the subsonic inlet. As a result, divergent waveforms would be produced which would cause errors in the macroscopic quantities, affecting the solution. For this reason, the method of Riemann invariants was implemented at the inlet as well as in the subsonic portions of the nozzle exit.

4.2.4 Grid Generation

In his research, Miller studied only one arcjet shape, which was that of the German TT1 low power arcjet. In generating the grid, he took grid lines of constant ξ to be constant in z as well. The grid lines of constant η were allowed to float in the r direction, so that the grid points would be smoothly distributed throughout the discretized domain. In general, it is desirable to keep the grid lines perpendicular to the boundaries, as this reduces the magnitude of the truncation error of the discretized equation for viscous flow calculations [38]. Due to the arcjet geometry, the vertical grid lines of Miller intersect the boundaries at an angle, incurring more error than is necessary. Initially, it was hoped that generating a new set of grids would alleviate this annoyance. It was was soon discovered that generating new, smooth grids with lines perpendicular to the boundaries was a very difficult task. In the end, the plan was abandoned, as it was felt that the improvement in the solution did not warrant the time and effort that was needed to generate the orthogonal grids. Therefore, all new grids generated for this research retain the same style as used by Miller.

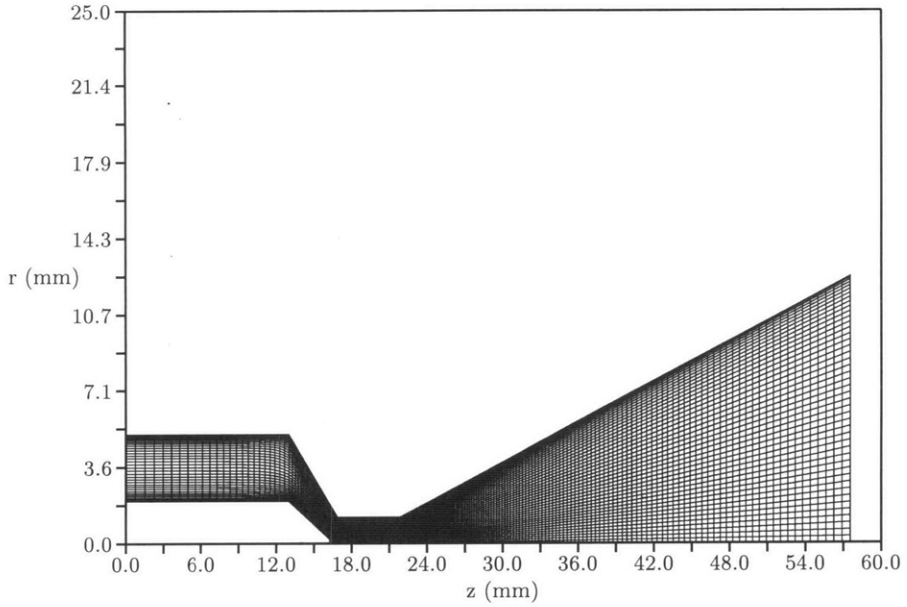

Figure 4-17: *Computational Grid for Fluid Calculations for the German TT1 Thruster*

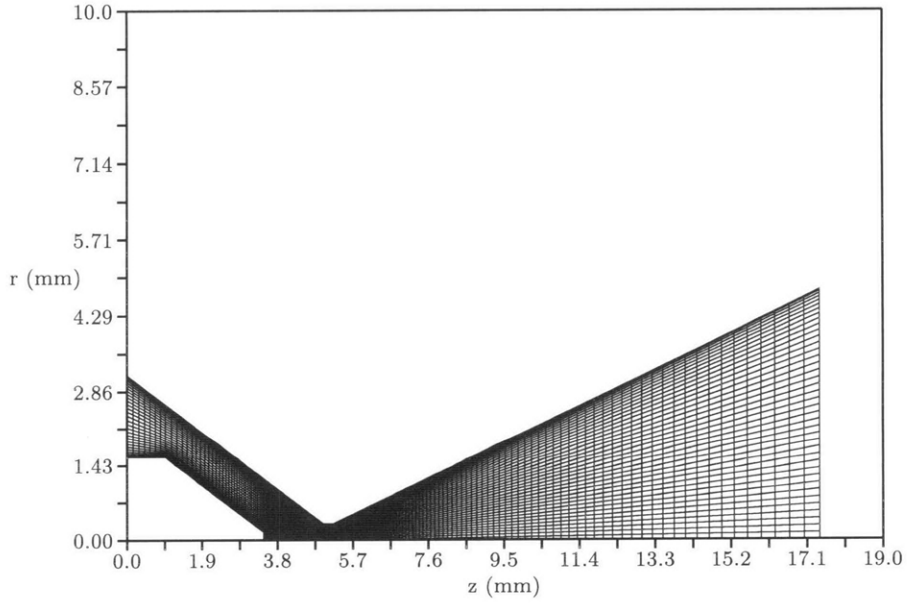

Figure 4-18: *Computational Grid for Fluid Calculations for the NASA Lewis Thruster*

In this research, two arcjet thrusters were modeled, the German TT1 and the NASA Lewis thrusters. Both have similar geometries. The major difference between the two thrusters is size. Figures 4-17 and 4-18 show the computational grids for the TT1 and NASA Lewis thrusters, respectively. As can be seen, the German thruster is much larger than the NASA thruster, in both length and radius. Another difference of note is the large length of the constrictor region in the TT1 and the comparatively large distance between cathode and anode in the Lewis thruster. As can be seen, the old grid generation style of Miller was used in generating these grids.

As mentioned in Section 3.4, the way in which the grids are utilized in this research is similar if not identical to the way they are utilized in Miller's work. In summary, the potential calculation is performed on a grid different from the fluid grid in the cathode tip region, with the calculation transitioning to the fluid grid just downstream of the constrictor entrance. The quantities which are calculated on the finer potential grid are then interpolated onto the fluid grid. When this research was first initiated, it was soon discovered that the grids used by Miller produced errors at the interface of the potential and fluid grids due to a grid discontinuity. Figure 4-19 shows the potential grid as used by Miller superimposed on the fluid grid, with the obvious discontinuity just downstream of the constrictor inlet.

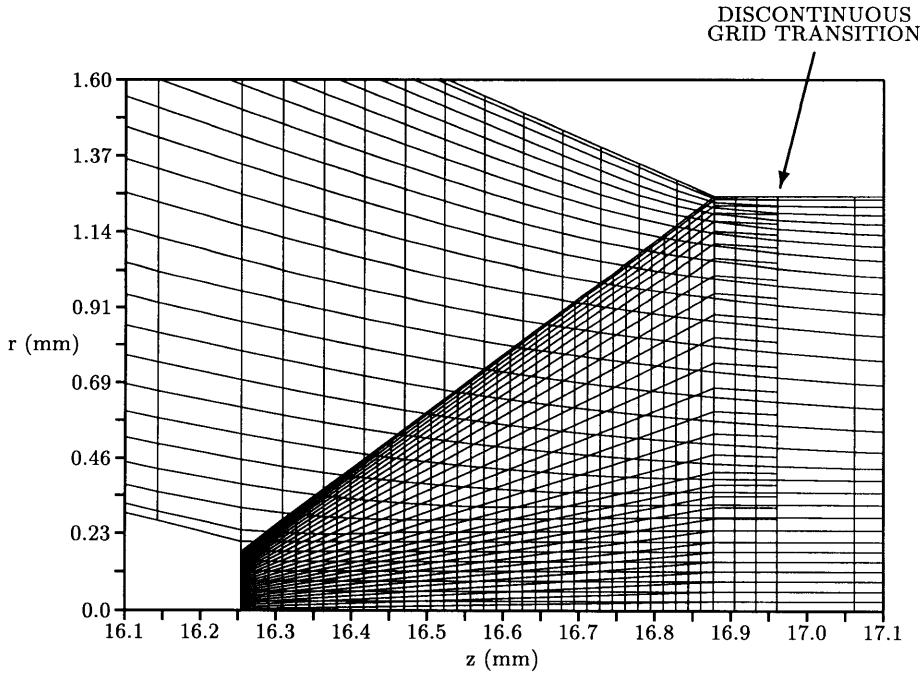

Figure 4-19: *Overlapping Fluid and Potential Grids as Used by Miller: TT1 Thruster*

This error was resolved by generating a new set of grids for the TT1 thruster. The fluid grid is shown in Figure 4-17. The new potential grid which was generated is shown in Figure 4-20 superimposed on the new fluid grid, with the view also encompassing some of the detail of the constrictor region. As can be seen the transition between the potential grids is much smoother, so that interpolation is more accurate. Another feature of the new grids is a refinement in the mesh near the cathode tip. The lines of constant ξ are brought closer together. When the new potential grid was generated, these points were used. The result is less interpolation between the potential and fluid grids, since they overlap exactly with respect to z. Interpolation need only be performed with respect to the r direction.

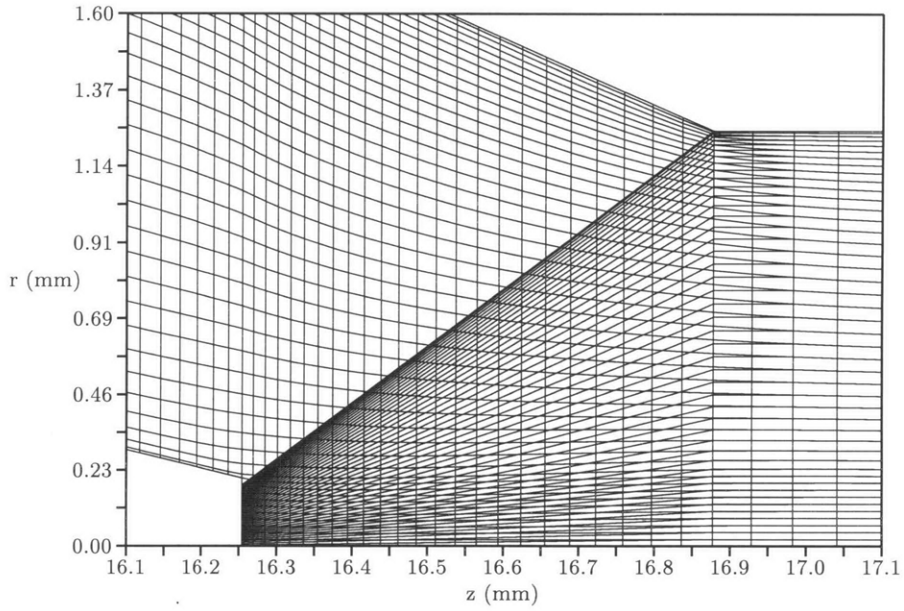

Figure 4-20: *Overlapping Fluid and Potential Grids as Used in This Research: TT1 Thruster*

4.3 Observations

Although no significant numerical results were generated from this research, observations were made during the course of the investigations. The first concerns the coupling of MacCormack's method for solution of the fluid equations with the coupling of SOR for solution of the electrical potential equation. Miller, in his original subroutine for the electrical potential calculation, inadvertently set the electron mobility to zero before the electrical potential calculation was performed. When the error was fixed, the coupled fluid-potential

equations became unstable when used with Successive-Overrelaxation. As a result, a relaxation factor (ω) of less than one had to be used so that the fluid equations would converge. Therefore, under-relaxation, and not over-relaxation, had to be used when a solution was attempted. This further increased the convergence time of the solution, as more iterations were necessary for the potential to relax a steady state solution.

In general, it seemed that all of the numerical problems encountered during this research involved, to some extent, the coupling of the fluid and potential equation. One of the largest concerned the new formulation of the diffusive mass fluxes. In the nozzle exit area, the electrical potential equation, due to the reformulation of the boundary conditions, became notorious for diverging. As a result, high current densities were being calculated in the exit plane of the thruster, which, in turn, affected the diffusive mass fluxes, which then affected the flow equations. In addition, the high current densities drove the electron temperature very high, as a higher current density manifests itself as a source term $\left(\frac{j^2}{\sigma}\right)$ on the right hand side of the energy equation. In the end, it was instabilities like this one which proved to be a hurdle which could not be overcome.

4.4 Conclusions and Recommendations

Numerical modeling of arcjet thrusters is a difficult task, for a number of reasons, the largest being its multicomponent nature. For a simple mixture consisting of diatomic molecules, atoms, ions, and electrons, eight fluid equations must be coupled with the electric potential equation to find a solution. Without the assumption of quasi-neutrality, the number of equations increases by one. Simply getting the set of highly nonlinear partial differential equations to behave nicely is, in itself, a daunting task.

The choice of numerical scheme can have a large effect on the solvability of the equations, as well. In general, the simpler the numerical scheme, the more easily gettable a solution. However, due to the viscous nature of arcjet flows, Euler solvers are ruled out immediately. Therefore, one is left to solving some set of modified form of the Navier-Stokes equations. Although computer power and ability is much cheaper, it still takes a good amount of computational effort to solve, say, the viscous flow over a flat plate. In addition, as discussed in Chapter 3, the viscous nature rules out types of grids which would facilitate a simpler solution, namely unstructured grids.

Therefore, one is left to solving a form of the Navier-Stokes equations on a structured mesh of some short. Scott Miller mentioned in his doctoral thesis that, due to the complex nature of the arcjet flow and its corresponding boundary conditions, an explicit method would be the easiest to implement. This statement is probably true. However, in this author's opinion, it might be worth the extra effort to use an implicit numerical scheme to solve the set of equations, perhaps a time accurate Beam and Warming scheme. One could still perform unsteady calculations, if need be, without the burden of a time stability criterion. However, it is unclear how much time would be saved by using an implicit scheme over an explicit scheme. The time consuming calculations needed for iterations in an explicit scheme might be replaced by equally time consuming calculations for the different matrix elements in an implicit scheme. But, since the stability criterion is removed, both the heavy species and electron equations could be integrated together, without fear of the solution blowing up, and arriving at just as valid a solution.

Another difficulty in solving the flow within an arcjet might be removed if the electrical potential equation was rewritten as a diffusive equation, in the form of the fluid equations. The need for using an elliptic solver to solve for the electric potential, and then calculating the current density could be avoided. Indeed, if this could have been done, many of the numerical difficulties encountered within this work could have possible been avoided. In this case, due to the unsteady term, the electric field, and not the electric potential, must be solved. Since a time varying electric field implies a magnetic field, an equation accounting for the magnetic field field must be included, as well. If the electric and magnetic field vectors are contained within the state vector of the governing equations, the whole set could then be solved at once and for all, using a single numerical scheme.

Appendix A

Fundamental Constants

Boltzmann constant	$k = 1.3807 \times 10^{-23}$	JK^{-1}
Planck's constant	$h = 6.6261 \times 10^{-34}$	$J\,s$
Stefan-Boltzmann constant	$\sigma_{SB} = 5.6705 \times 10^{-8}$	$Wm^{-2}K^{-4}$
Avogadro's number	$N_A = 6.0221 \times 10^{23}$	mol^{-1}
Universal gas constant	$\hat{R} = N_A k = 8.3145$	$JK^{-1}mol^{-1}$
Elementary charge	$e = 1.6022 \times 10^{-19}$	C
Permittivity of vacuum	$\epsilon_0 = 8.8542 \times 10^{-12}$	Fm^{-1}
Permeability of vacuum	$\mu_0 = 4\pi \times 10^{-7}$	Hm^{-1}
Atomic mass unit	$m_u = 1.6605 \times 10^{-27}$	kg
Gravitational acceleration	$g_e = 9.81$	$m\,s^{-2}$
Electron mass	$m_e = 9.1094 \times 10^{-31}$	kg
Hydrogen atomic mass	$m_H = 1.6737 \times 10^{-27}$	kg
Nitrogen atomic mass	$m_N = 2.3258 \times 10^{-26}$	kg
Dissociation energy (H_2)	7.236×10^{-19}	J
Dissociation energy (N_2)	1.570×10^{-18}	J
Ionization energy (H)	2.179×10^{-18}	J
Ionization energy (N)	2.329×10^{-18}	J
Energy of 1 Kelvin	$k/e = 8.6174 \times 10^{-5}$	eV
Temperature of 1 eV	$e/k = 1.1604 \times 10^{4}$	K
Atmospheric pressure	$p_0 = 1.0133 \times 10^{5}$	Pa
Monatomic specific heat ratio	$\gamma = 1.667$	
Diatomic specific heat ratio	$\gamma = 1.400$	

Appendix B

Equilibrium Constants

Table B.1: *Equilibrium Constants for the Hydrogen and Nitrogen Dissociation Reactions (from JANAF Thermochemical Tables)*

Temperature (K)	$\log K_p$	
	$\frac{1}{2}H_2 \rightleftharpoons H$	$\frac{1}{2}N_2 \rightleftharpoons N$
200	-54.325	-120.419
400	-25.876	-58.710
600	-16.335	-38.084
800	-11.538	-27.746
1000	-8.644	-21.530
1200	-6.705	-17.377
1400	-5.313	-14.407
1600	-4.264	-12.175
1800	-3.446	-10.437
2000	-2.788	-9.045
2200	-2.249	-7.905
2400	-1.798	-6.954
2600	-1.415	-6.148
2800	-1.087	-5.457
3000	-0.801	-4.857
3200	-0.551	-4.332
3400	-0.330	-3.867
3600	-0.133	-3.455
3800	0.044	-3.085
4000	0.203	-2.751

Table B.1: *continued*

Temperature (K)	$\log K_p$	
	$\frac{1}{2}H_2 \rightleftharpoons H$	$\frac{1}{2}N_2 \rightleftharpoons N$
4200	0.347	-2.449
4400	0.478	-2.175
4600	0.598	-1.923
4800	0.708	-1.693
5000	0.809	-1.480
5200	0.902	-1.283
5400	0.989	-1.101
5600	1.069	-0.931
5800	1.144	-0.773
6000	1.213	-0.625

Appendix C

Collision Cross Sections

Table C.1: *Total Collision Cross Sections for Electron Collisions*

Temperature (K)	Q_{ij} ($\mathring{A}^2$)			
	$e - H_2$	$e - N_2$	$e - H$	$e - N$
1000	10.1	5.05	-	-
2000	11.3	7.70	-	30.7
3000	12.6	8.85	26.01	21.8
4000	13.4	9.50	24.54	19.3
5000	14.2	9.85	23.20	17.7
6000	14.8	10.1	21.96	16.7
7000	15.5	10.2	20.83	16.3
8000	15.9	10.2	19.80	15.9
9000	16.4	10.0	18.86	15.5
10000	16.9	9.90	17.99	15.3
11000	17.3	9.80	17.18	15.0
12000	17.6	10.0	16.44	14.8
13000	17.8	10.5	15.76	14.7
14000	18.0	10.8	15.11	14.6
15000	18.2	11.2	14.52	14.4
16000	18.3	11.5	13.96	14.3
17000	18.4	11.9	13.43	14.2
18000	18.5	12.4	12.93	14.0
19000	18.5	13.1	12.47	13.8
20000	18.4	13.8	12.02	13.7

Table C.1: *continued*

Temperature (K)	Q_{ij} ($\mathring{A}^2$)			
	$e - H_2$	$e - N_2$	$e - H$	$e - N$
21000	18.3	15.7	-	13.5
22000	18.2	18.9	-	13.3
23000	18.0	24.8	-	13.1
24000	17.8	26.8	-	13.0
25000	17.6	27.9	-	12.8
26000	17.4	28.9	-	-
27000	17.2	29.5	-	-
28000	17.0	29.8	-	-
29000	16.7	30.0	-	-
30000	16.4	29.8	-	-
31000	16.3	29.1	-	-
32000	16.0	27.8	-	-
33000	15.7	25.4	-	-
34000	15.4	23.0	-	-
35000	15.2	21.0	-	-

Appendix D

Collision Integrals

Table D.1: *Diffusion Collision Integrals for Hydrogen Interactions*

Temp (K)	$\langle \Omega_{ij}^{(1,1)} \rangle$ $(\mathring{A}^2)$					
	$H_2 - H_2$	$H_2 - H$	$H_2 - e$	$H - H$	$H - H+$	$H - e$
1000	5.21	4.16	3.81	5.24	-	-
2000	4.37	3.27	4.58	4.13	-	-
3000	3.79	2.80	4.99	3.57	-	-
4000	3.42	2.49	5.23	3.23	-	-
5000	3.14	2.27	5.33	3.03	27.7	6.85
6000	2.93	2.09	5.35	2.88	27.0	6.29
7000	2.75	1.94	5.30	2.76	26.4	5.82
8000	2.60	2.37	5.21	2.62	26.0	5.43
9000	2.47	2.25	5.09	2.48	25.5	5.09
10000	2.36	2.14	4.95	2.36	25.2	4.80
11000	2.26	2.04	4.81	2.25	24.8	4.54
12000	2.17	1.95	4.67	2.15	24.5	4.31
13000	2.09	1.87	4.52	2.07	24.2	4.11
14000	2.02	1.80	4.37	1.99	24.0	3.92
15000	1.95	1.74	4.23	1.92	23.7	3.76
16000	-	-	4.10	-	23.5	3.61
17000	-	-	3.97	-	23.3	3.47
18000	-	-	3.85	-	23.1	3.34
19000	-	-	3.73	-	22.9	3.23
20000	-	-	3.62	-	22.8	3.12

Table D.1: *continued*

Temp (K)	$\langle \Omega_{ij}^{(1,1)} \rangle$ $(\mathring{A}^2)$					
	$H_2 - H_2$	$H_2 - H$	$H_2 - e$	$H - H$	$H - H+$	$H - e$
21000	-	-	3.51	-	22.6	3.03
22000	-	-	3.41	-	22.4	2.94
23000	-	-	3.32	-	22.3	2.86
24000	-	-	3.23	-	22.1	2.79
25000	-	-	3.14	-	22.0	2.72
26000	-	-	3.06	-	21.9	2.66
27000	-	-	2.99	-	21.8	2.60
28000	-	-	2.92	-	21.6	2.55
29000	-	-	2.85	-	21.5	2.51
30000	-	-	2.79	-	21.4	2.46
31000	-	-	2.73	-	21.3	2.43
32000	-	-	2.67	-	21.2	2.39
33000	-	-	2.62	-	21.1	2.36
34000	-	-	2.56	-	21.0	2.33
35000	-	-	2.51	-	21.0	2.31

Table D.2: *Diffusion Collision Integrals for Nitrogen Interactions*

Temp (K)	$\langle\Omega_{ij}^{(1,1)}\rangle$ $(\mathring{A}^2)$			
	$N_2 - N_2$	$N_2 - N$	$N - N$	$N - N+$
1000	9.13	8.21	6.46	34.3
2000	7.55	6.84	5.36	31.4
3000	6.76	6.10	4.83	30.0
4000	6.24	5.60	4.48	29.0
5000	5.87	5.22	4.21	28.3
6000	5.59	4.93	4.00	27.7
7000	5.34	4.68	3.82	27.3
8000	5.16	4.48	3.68	26.9
9000	5.00	4.30	3.52	26.5
10000	4.86	4.15	3.43	26.2
11000	4.73	4.01	3.33	25.9
12000	4.62	3.88	3.24	25.7
13000	4.52	3.77	3.15	25.4
14000	4.43	3.67	3.06	25.2
15000	4.35	3.58	2.99	25.0
16000	-	-	2.92	24.8
17000	-	-	2.85	24.6
18000	-	-	2.79	24.5
19000	-	-	2.74	24.3
20000	-	-	2.69	24.2
21000	-	-	-	24.0
22000	-	-	-	23.9
23000	-	-	-	23.8
24000	-	-	-	23.7
25000	-	-	-	23.6
26000	-	-	-	23.5
27000	-	-	-	23.4
28000	-	-	-	23.3
29000	-	-	-	23.2
30000	-	-	-	23.1
31000	-	-	-	23.0
32000	-	-	-	22.9
33000	-	-	-	22.8
34000	-	-	-	22.7
35000	-	-	-	22.6

Table D.3: *Viscosity Collision Integrals for Hydrogen Interactions*

Temp (K)	$\langle\Omega_{ij}^{(2,2)}\rangle$ $(\mathring{A}^2)$					
	$H_2 - H_2$	$H_2 - H$	$H_2 - e$	$H - H$	$H - H+$	$H - e$
1000	6.00	5.13	4.18	5.95	-	-
2000	5.33	4.10	4.94	4.74	-	-
3000	4.73	3.55	5.31	4.12	-	-
4000	4.29	3.35	5.44	3.74	-	-
5000	3.97	2.91	5.42	3.50	13.6	5.81
6000	3.71	2.69	5.30	3.28	12.5	5.27
7000	3.50	2.52	5.13	3.06	11.6	4.83
8000	3.32	2.37	4.92	2.88	10.8	4.47
9000	3.17	2.25	4.71	2.73	10.2	4.15
10000	3.03	2.14	4.49	2.60	9.60	3.89
11000	2.91	2.04	4.28	2.50	9.10	3.65
12000	2.81	1.95	4.08	2.42	8.66	3.44
13000	2.71	1.87	3.89	2.34	8.26	3.27
14000	2.62	1.80	3.71	2.25	7.90	3.11
15000	2.54	1.74	3.55	2.18	7.57	3.00
16000	-	-	3.39	2.09	7.27	2.84
17000	-	-	3.25	2.02	6.99	2.73
18000	-	-	3.12	1.96	6.74	2.63
19000	-	-	3.00	1.89	6.50	2.54
20000	-	-	2.89	1.84	6.27	2.46
21000	-	-	2.79	1.78	6.07	2.40
22000	-	-	2.70	1.73	5.87	2.33
23000	-	-	2.61	1.68	5.69	2.27
24000	-	-	2.54	1.63	5.51	2.23
25000	-	-	2.46	1.59	5.35	2.19
26000	-	-	2.40	1.55	5.19	2.15
27000	-	-	2.33	1.51	5.04	2.12
28000	-	-	2.27	1.48	4.90	2.10
29000	-	-	2.22	1.45	4.77	2.08
30000	-	-	2.17	1.42	4.64	2.06
31000	-	-	2.12	1.39	4.52	2.05
32000	-	-	2.07	1.36	4.41	2.04
33000	-	-	2.03	1.34	4.30	2.04
34000	-	-	1.99	1.31	4.19	2.04
35000	-	-	1.95	1.29	4.09	2.04

Table D.4: *Viscosity Collision Integrals for Nitrogen Interactions*

Temp (K)	$\langle\Omega_{ij}^{(2,2)}\rangle$ $(\mathring{A}^2)$			
	$N_2 - N_2$	$N_2 - N$	$N - N$	$N - N+$
1000	10.4	9.82	7.24	13.3
2000	8.86	8.27	5.97	10.5
3000	8.07	7.43	5.36	9.15
4000	7.55	6.85	4.96	8.33
5000	7.17	6.42	4.70	7.74
6000	6.87	6.08	4.46	7.26
7000	6.64	5.80	4.28	6.85
8000	6.43	5.56	4.14	6.48
9000	6.26	5.36	4.01	6.15
10000	6.11	5.17	3.89	5.84
11000	5.98	5.01	3.79	5.56
12000	5.86	4.87	3.70	5.31
13000	5.75	4.73	3.61	5.07
14000	5.65	4.61	3.53	4.86
15000	5.56	4.50	3.45	4.66
16000	-	-	3.38	4.48
17000	-	-	3.32	4.31
18000	-	-	3.26	4.15
19000	-	-	3.20	4.00
20000	-	-	3.14	3.87
21000	-	-	-	3.74
22000	-	-	-	3.62
23000	-	-	-	3.52
24000	-	-	-	3.41
25000	-	-	-	3.32
26000	-	-	-	3.24
27000	-	-	-	3.16
28000	-	-	-	3.07
29000	-	-	-	2.99
30000	-	-	-	2.91
31000	-	-	-	2.85
32000	-	-	-	2.79
33000	-	-	-	2.73
34000	-	-	-	2.67
35000	-	-	-	2.61

Table D.5: *Non-dimensional Collision Integrals for Charged Particle Interactions*

$\psi_{i,j}$	$F_{Paq}^{(1,1)}$	$F_{Paq}^{(2,2)}$	$F_{Mac}^{(1,1)}$	$F_{Mac}^{(2,2)}$
-7.0	-6.051	-5.102	-5.532	-4.887
-6.8	-5.897	-4.947	-5.372	-4.725
-6.6	-5.745	-4.792	-5.212	-4.563
-6.4	-5.593	-4.638	-5.053	-4.401
-6.2	-5.442	-4.485	-4.894	-4.238
-6.0	-5.292	-4.332	-4.734	-4.074
-5.8	-5.142	-4.181	-4.573	-3.911
-5.6	-4.994	-4.030	-4.410	-3.749
-5.4	-4.846	-3.881	-4.245	-3.588
-5.2	-4.700	-3.732	-4.077	-3.430
-5.0	-4.554	-3.584	-3.906	-3.276
-4.8	-4.409	-3.437	-3.733	-3.126
-4.6	-4.265	-3.291	-3.558	-2.980
-4.4	-4.123	-3.146	-3.382	-2.840
-4.2	-3.981	-3.002	-3.206	-2.704
-4.0	-3.840	-2.859	-3.030	-2.572
-3.8	-3.700	-2.717	-2.855	-2.443
-3.6	-3.561	-2.576	-2.683	-2.316
-3.4	-3.422	-2.436	-2.514	-2.189
-3.2	-3.285	-2.297	-2.348	-2.063
-3.0	-3.149	-2.158	-2.187	-1.934
-2.8	-3.013	-2.011	-2.029	-1.803
-2.6	-2.878	-1.884	-1.876	-1.669
-2.4	-2.743	-1.748	-1.727	-1.531
-2.2	-2.609	-1.612	-1.582	-1.390
-2.0	-2.475	-1.477	-1.441	-1.246
-1.8	-2.341	-1.341	-1.305	-1.098

Table D.5: *continued*

$\psi_{i,j}$	$F_{Paq}^{(1,1)}$	$F_{Paq}^{(2,2)}$	$F_{Mac}^{(1,1)}$	$F_{Mac}^{(2,2)}$
-1.6	-2.207	-1.205	-1.171	-0.9478
-1.4	-2.071	-1.069	-1.041	-0.7956
-1.2	-1.935	-0.9320	-0.914	-0.6418
-1.0	-1.797	-0.7940	-0.7880	-0.4865
-0.8	-1.657	-0.6524	-0.6640	-0.3299
-0.6	-1.514	-0.5084	-0.5406	-0.1718
-0.4	-1.366	-0.3605	-0.4171	-0.01189
-0.2	-1.213	-0.2074	-0.2926	0.1504
0.0	-1.053	-0.04749	-0.1657	0.3160
0.2	-0.8833	0.1209	-0.03529	0.4858
0.4	-0.7026	0.2999	0.1003	0.6612
0.6	-0.5078	0.4920	0.2427	0.8435
0.8	-0.2960	0.6996	0.3940	1.034
1.0	-0.06429	0.9251	0.5563	1.235
1.2	0.1900	1.170	0.7315	1.445
1.4	0.4680	1.435	0.9213	1.667
1.6	0.7686	1.715	1.127	1.898
1.8	1.087	2.006	1.347	2.137
2.0	1.416	2.297	1.582	2.380
2.2	1.741	2.580	1.827	2.625
2.4	2.049	2.848	2.078	2.869
2.6	2.330	3.100	2.330	3.108
2.8	2.588	3.338	2.579	3.343
3.0	2.829	3.567	2.821	3.571

Bibliography

[1] Anderson, Dale A., John C. Tannehill, and Richard H. Pletcher. *Computational Fluid Mechanics and Heat Transfer.* Series in Computational and Physical Processes in Mechanics and Thermal Sciences. Hemisphere Publishing Corporation, 1984.

[2] Anderson, John D., Jr. *Modern Compressible Flow with Historical Perspective.* McGraw-Hill, New York, 2nd edition, 1990.

[3] Belov, V.A. "Viscosity of Partially Ionized Hydrogen". *High Temperature*, 5:31–6, 1967.

[4] Bittencourt, J. A. *Fundamentals of Plasma Physics.* Pergamon Press, New York, 1986.

[5] Burke, P. G., K. A. Berrington, M. Le Dourneuf, and Vo Ky Lan. "The $^3P^e$ Resonance in the Low-energy Scattering of Electrons by Atomic Nitrogen". *Journal of Physics B*, 7(18):L531–L535, 1974.

[6] Capitelli, M. and M. DiLonardo. "Nonequilibrium Vibrational Populations of Diatomic Species in Electrical Discharges: Effects on the Dissociation Rates". *Chemical Physics*, 24:417–427, 1977.

[7] Chapman, Sydney and T. G. Cowling. *The Mathematical Theory of Non-Uniform Gases.* Cambridge University Press, Cambridge, 3rd edition, 1970.

[8] Chase, Jr., M. W. et. al. *Journal of Physical and Chemical Reference Data Supplement No. 1: JANAF Thermochemical Tables*, volume 14. American Chemical Society and American Institute of Physics for the National Bureau of Standards, Washington D.C., 3rd edition, 1985.

[9] Chen, Francis F. *Introduction to Plasma Physics and Controlled Fusion; Volume 1: Plasma Physics.* Plenum Press, New York, 2nd edition, 1984.

[10] Cubley, S. J. and E. A. Mason. "Atom-molecule and Molecule-molecule Potentials ans Transport Collision Integrals for High-temperature Air Species". *Physics of Fluids*, 18(9):1109–1111, September 1975.

[11] Daybelge, U. "Transport Coefficients of Two-Temperature Partially Ionized Gases". Stanford University Institute for Plasma Research Report Number 263, December 1968.

[12] Devoto, R. S. "Transport Properties of Ionized Monatomic Gases". *Physics of Fluids*, 9(6):1230–40, June 1966.

[13] Devoto, R. S. "Transport Coefficients of Partially Ionized Hydrogen". *Journal of Plasma Physics*, 2:617–31, 1968.

[14] Drawin, H. W. and P. Felenbok. *Data for Plasmas in Local Thermodynamic Equilibrium.* Gauthier-Villars, Paris, 1965.

[15] Foutter, Richard R. A Numerical Investigation of Weak Shock Wave Effects in Reacting Nozzle Flows. Master's thesis, Massachusetts Institute of Technology, 1995.

[16] Grier, Norman T. *Calculation of Transport Properties of Ionizing Atomic Hydrogen.* Technical Report TN D-3186, NASA, April 1966.

[17] Heimerdinger, D. J. *Fluid Mechanics in a Magnetoplasmadynamic Thruster*, Doctoral thesis. Massachusetts Institute of Technology, 1988.

[18] Hill, Philip G. and Carl R. Peterson. *Mechanics and Thermodynamics of Propulsion.* Addison-Wesley, Reading, Mass., 1965.

[19] Hinnov, Einar and Joseph G. Hirschberg. "Electon-Ion Recombination in Dense Plasmas". *Physical Review*, 125(3):795–801, February 1, 1962.

[20] Hirsch, C. *Numerical Computation of Internal and External Flows, Volume 2: Computational Methods for Inviscid and Viscous Flows.* John Wiley and Sons, Inc., New York, 1988.

[21] Hirschfelder, Joseph O., Charles F. Curtiss, and R. Byron Bird. *Molecular Theory of Gases and Liquids.* John Wiley and Sons, Inc., New York, 1954.

[22] Itikawa, Y. "Momentum-Transfer Cross Sections for Electron Collisions with Atoms and Molecules ". *Atomic Data and Nuclear Data Tables*, 21(1):69–75, January 1978.

[23] Janev, R. K., W. D. Langer, K. Evans Jr., and D. E. Post Jr. *Elementary Processes in Hydrogen-Helium Plasmas.* Springer-Verlag, New York, 1987.

[24] Krier, Herman, Rodney L. Burton, T. W. Megli, S.A. Bufton, and N.T. Tiliakos. *Arcjet Plasma Modeling with Experimental Validation.* Technical Report UILU-ENG 94-4011, University of Illinois at Urbana-Champaign, Department of Mechanical and Industrial Engineering, 1994.

[25] Kutler, P., L. Sakell, and G. Aiello. "On the Shock-On-Shock Interaction Problem". AIAA 74-524, AIAA 7th Fluid and Plasma Dynamics Conference, June 1974.

[26] Langan, W. T., J. D. Cresswell, and W. G. Browne. "Effect of Ablation Products on Ionization in Hypersonic Wakes". *AIAA Journal*, 3(12), December 1965.

[27] MacCormack, Robert W. "The Effect of Viscosity in Hypervelocity Impact Cratering". AIAA 69-354, AIAA Hypervelocity Impact Conference, April 30 - May 2 1969.

[28] MacCormack, Robert W. "Numerical Solution of the Interaction of a Shock Wave with a Laminar Boundary Layer," Proceedings from the Second International Conference on Numerical Methods in Fluid Dynamics. In *Lecture Notes in Physics*, pages 151–63. Springer-Verlag, New York, 1971.

[29] MacCormack, Robert W. and B. S. Baldwin. "A Numerical Method for Solving the Navier-Stokes Equations with Application to Shock-Boundary Layer Interactions". AIAA 75-1, AIAA 13th Aerospace Sciences Meeting, January 1975.

[30] MacDonald, James. "Accurate Collision Iintegrals for the Attractive Static Screened Coulomb Potential with Application to Electrical Conductivity ". *Astrophysical Journal Supplement Series*, 76:369–382, May 1991.

[31] Maecker, Heinz M. "Principles of Arc Motion and Displacement". *Proceedings of the IEEE*, 59(4):439–449, 1971.

[32] Martinez-Sanchez, M. "Arcjet Modeling: Status and Prospects". AIAA 94-2653, 25th AIAA Plasmadynamics and Lasers Conference, June 20-23 1994.

[33] Miller, Scott A. Viscous and Diffusive Effects in Magnetoplasmadynamic Flows. Master's thesis, Massachusetts Institute of Technology, 1990.

[34] Miller, Scott A. *Multifluid Nonequilibrium Simulation of Arcjet Thrusters*, Doctoral thesis. Massachusetts Institute of Technology, 1994.

[35] Mitchner, M. and Charles H. Kruger, Jr. *Partially Ionized Gases.* John Wiley and Sons, Inc., 1973. Reprints available from authors.

[36] Oyerokun, F. and M. Martinez-Sanchez. "A Study of Alkali-Seeded Hydrogen Arcjet Performance". IEPC 95-236, 26th International Electric Propulsion Conference, September 1995.

[37] Paquette, C., C. Pelletier, G. Fontaine, and G. Michaud. "Diffusion Coefficients for Stellar Plasmas". *Astrophysical Journal Supplement Series*, 61:177–95, May 1986.

[38] Peraire, J. Private communication, October 1994.

[39] Peraire, J. Class notes, "16.160: Computational Fluid Dynamics". Massachusetts Institute of Technology, Spring 1994.

[40] Perez de la Cruz, Carmen. Arc Rate Predictions and Flight Data Analysis for the Solar Array Module Plasma Interactions Experiment (SAMPIE). Master's thesis, Massachusetts Institute of Technology, 1995.

[41] Pfender, E. "Electric Arcs and Arc Gas Heaters". In M. N. Hirsch and H. J. Oskam, editors, *Gaseous Electronics*, volume 1, chapter 5. Academic Press, 1978.

[42] Pipkin, A. C. "Electrical Conductivity of Partially Ionized Gases". *Physics of Fluids*, 4(1):154–58, January 1961.

[43] Press, William H., Saul A. Teukolsky, William T. Vetterling, and Brian P. Flannery. *Numerical Recipes in Fortran.* Cambridge University Press, New York, 2nd edition, 1992.

[44] Rainwater, James C., Louis Biolsi, Kevin J. Biolsi, and Paul M. Holland. "Transport Properties of Ground State Nitrogen Atoms". *Journal of Chemical Physics*, 79(3):1462–1468, August 1983.

[45] Richtmyer, R. D. and K. W. Morton. *Difference Methods for Initial-Value Problems.* Interscience Publishers, Wiley, New York, 2nd edition, 1967.

[46] Rogers, R. C. and C. J. Schexnayder Jr. "Chemical Kinetic Analysis of Hydrogen-Air Ignition and Reaction Times". NASA Technical Paper 1856, 1981.

[47] Sheppard, Eric J. *Nonequilibrium Ionization in Electromagnetic Accelerators*, Doctoral thesis. Massachusetts Institute of Technology, 1994.

[48] Stallcop, James R., Harry Partridge, and Eugene Levin. "Resonance Charge Transfer, Transport Cross Sections, and Collision Integrals for $N^+(^3P)-N(^4S^0)$ and $O^+(^4S^0)-O(^3P)$ Interactions". *Journal of Chemical Physics*, 95(9):6429–6439, November 1991.

[49] Sutton, G. W. and A. Sherman. *Engineering Magnetohydrodynamics.* McGraw-Hill, New York, 1965.

[50] Sutton, George P. *Rocket Propulsion Elements, An Introduction to the Engineering of Rockets.* John Wiley and Sons, Inc., New York, 6th edition, 1992.

[51] Thompson, J. F., F. C. Thames, and C. W. Mastin. "Automatic Numerical Generation of Body-Fitted Curvilinear Coordinate System for Field Containing Any Number of Arbitrary Two-dimensional Bodies". *Journal of Computational Physics*, 15:299–319, 1974.

[52] Vanderslice, J.T., Stanley Weissman, E.A. Mason, and R.J. Fallon. "High-Temperature Transport Properties of Dissociating Hydrogen". *Physics of Fluids*, 5(2):155–64, February 1962.

[53] Vincenti, Walter G. and Charles H. Kruger, Jr. *Introduction to Physical Gas Dynamics.* Robert E. Krieger Publishing Co., Inc., Malabar, Florida, 1965.

[54] Von Braun, Wernher and Frederick I. Ordway III. *Space Travel.* Harper and Row, New York, 1985.

[55] Wang, Joseph Jiong. *Electrodynamic Interactions Between Charged Space Systems and the Ionospheric Plasma Environment*, Doctoral thesis. Massachusetts Institute of Technology, 1991.

[56] Yun, K. S. and E. A. Mason. "Collision Integrals for the Transport Properties of Dissociating Air at High Temperatures". *Physics of Fluids*, 5(4):380–386, April 1962.